AC LOSSES IN SUPERCONDUCTING NIOBIUM

Fahad A. Al-Huseini

A Thesis Submitted for the Degree of PhD
at the
University of St Andrews

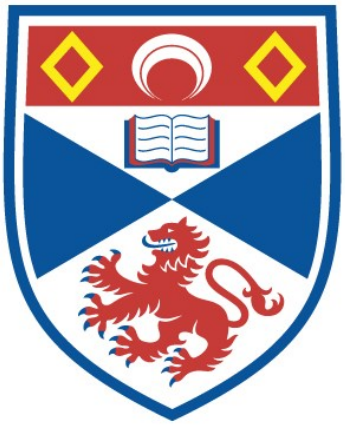

1973

AC LOSSES IN SUPERCONDUCTING NIOBIUM

A Thesis

Presented by

Fahad A. Al-Huseini, B.Sc.

to the

University of St. Andrews

in application for the Degree

of Doctor of Philosophy.

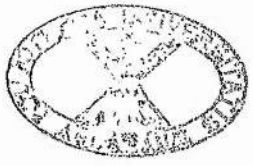

ProQuest LLC.
789 East Eisenhower Parkway
P.O. Box 1346
Ann Arbor, MI 48106 – 1346

Th 7030

DECLARATION

I hereby certify that this thesis has been composed by me, and is a record of work done by me, and has not previously been presented for a higher degree.

This research was carried out in the Physical Science Laboratory of St. Salvator's College, in the University of St. Andrews, under the supervision of Dr. I.M. Firth.

Fahad A. Al-Huseini

CERTIFICATE

I certify that F.A. Al-Huseini, B.Sc., has spent nine terms at research work in the Physical Science Laboratory of St. Salvator's College, in the University of St. Andrews, under my direction, that he has fulfilled the Conditions of Ordinance No. LXXIX (St. Andrews No. 16) and that he is qualified to submit the accompanying thesis in application for the Degree of Doctor of Philosophy.

Research Superviser

CAREER

In 1965 I received the degree of Bachelor of Science in Physics and Geology, Riyad University, Saudi Arabia. In 1965-1966 I was appointed Assistant Lecturer in the Faculty of Education, Jeddah University, Saudi Arabia. In October 1966 I was admitted as a research student in the Department of Physics of St. Andrews University and since then I have been engaged upon the research of which this thesis is the record, under the supervision of DR. I.M. FIRTH.

ACKNOWLEDGEMENTS

The author wishes to express his gratitude to Dr. I.M. Firth for his patient guidance and encouragement during this work.

He is particularly grateful to Professor J.F. Allen, F.R.S. for discussions and invaluable encouragement. He thanks Mr. J. McNab for skilful technical assistance.

Finally He is indebted to those who have helped in the preparation of this thesis, Mrs. P. Cooper for her proficient typing; and to Mr. T. McQueen for the copying.

ABSTRACT

This thesis is concerned with measurements of alternating field losses in cylindrical rods of niobium in its superconducting state. Six samples have been investigated each with a different surface condition.

Magnetization measurements of the samples have been studied which show the effect of the surface condition on the first critical magnetic field H_{c_1}. The effect of the surface on flux pinning are discussed. Power losses have been studied experimentally for single crystal niobium and for polycrystalline niobium each with three different surface conditions in order to study the effect of the surface properties on these ac losses. A wattmeter technique was developed for measurements of power losses in the samples. Experiments were conducted over a range of applied fields at 50 Hz and at 4.2 K. This technique will be described together with the experimental results. The results will be compared with predictions from a modified critical state theory and their significance discussed. The critical current density has been measured for each sample using a method based on the measurements of the power dissipation in a small modulating field, in the presence of a steady bias field. The technique will be described together with experimental results.

The shielding field ΔH in the mixed state has been studied for the samples. The technique and the results will be discussed for each sample.

CONTENTS

LIST OF ILLUSTRATIONS

LIST OF SYMBOLS

T_c	Superconducting transition temperature
H_c	Thermodynamic critical magnetic field strength
H_o	Critical magnetic field strength at OK
H_a	Applied magnetic field strength
V_s	Velocity of superelectrons
E	Electric field strength or energy
J_s	Super-current density, or surface current density
n_s	Number of superelectrons per unit volume
B	Magnetic flux density ($B = n\phi_o$)
J_n	Normal current density
σ	Electrical conductivity
λ_L	London penetration depth ($\lambda_L = \left(\frac{m}{\mu_o n_s e^2}\right)^{\frac{1}{2}}$)
λ_o	Penetration depth at OK
ξ	Coherence length
ξ_o	Coherence length for pure metal
l_e	Electron mean free path
g_n	Gibbs free energy per unit volume of the normal phase
g_s	Gibbs free energy per unit volume of the superconducting phase
ρ	Electrical resistivity
C_n	Specific heat of normal phase
C_s	Specific heat of superconducting phase
C_{el}	Electronic contribution to specific heat
C_{latt}	Lattice contribution to specific heat
Δ	Surface energy parameter ($\Delta = \xi - \lambda$)
H_{c_1}	Lower critical field of Type II superconductor
H_p	Magnetic field, in which the critical current may be induced to flow through the entire sample ($H_p = \frac{2}{5}\pi J_c R$)
k	Ginzburg-Landau parameter ($k = \frac{\lambda}{\xi}$)
k_o	Ginzburgh-Landau parameter in pure metal

ϵ	Kinetic energy of electron ($\epsilon = P^2/2_m$)
ϵ_f	Fermi energy
E_g	Energy gap of superconductor ($E_g = 2\Delta$)
$\Delta(o)$	Half energy gap at OK
ϕ	Magnetic flux
ϕ_o	Quantum of magnetic flux ($\phi_o = \frac{ch}{2e}$)
d	Distance between the flux lines
b	Size of the pinning centre
F_p	Pinning force
J	Current density
J_c	Critical current density
$\propto$	Proportionality or threshold value of the critical state ($\propto = \frac{BJ}{C}$)
W_v	Energy loss per unit volume per cycle ($W_v = \frac{1}{4\pi} \oint$ HdB)
f	Frequency
S	Length of the perimeter of the sample ($S = 2\pi r$)
e(t)	Penetration voltage ($e(t) = -N \frac{d\phi}{dt} \times 10^{-8}$)
V_p	Output of the multiplier
K_c	Scale factor of the multiplier
P_s	Power loss per unit surface area
ΔH	Shielding field

CHAPTER I

INTRODUCTION

We shall discuss briefly the basic properties of superconductivity. The difference between the two kinds of superconductivity, type I and type II will be clear when we refer to the surface energy. These include[1-6]; (1) occurance of superconductivity, (2) basic electric and magnetic properties, (3) surface energy, (4) thermodynamic properties, (5) microscopic theory, and (6) some applications of superconductivity.

1. Occurance of superconductivity

The most outstanding property of superconductivity is the complete disappearance of electrical resistivity at some low tempearture T_c which is characteristic of the material. So far twenty six elements have been shown to be superconducting, and also many alloys and compounds have been found to be superconducting. The highest value of T_c for an element is 9.2 K for niobium, and the lowest value of T_c so far found is for tungsten at 0.01 K. The highest[7] value of T_c known for an alloy is 20.0 K for Nb ($Al_{0.8}$-$Ge_{0.2}$) alloy followed closely by Nb_3Sn with T_c = 18 K. It is found that the transition temperature T_c is not very sensitive to small amounts of impurity but the more pure the sample the sharper is the transition.

Matthias[8] pointed out that there are certain conditions which favour the appearance of superconductivity;. most superconducting metals or alloys have an average of between 2 and 8 valence electrons per atom, and also high transition temperatures occur in the transition group elements close to 5 and 7 valence electron per atom.

It has been found that superconductivity can be associated with a change in the properties of the crystal lattice[9], and also that the transition temperature T_c varies for isotopes of most superconductors according to the relation

$$T_c = K M^{-\frac{1}{2}}$$ where K is a constant, and where M is the atomic mass of the isotope. This is in agreement with the BCS microscopic theory based on the interaction between electrons (pairs) and the crystal lattice. This theory shows that an attractive interaction between pairs of electrons arises below a certain critical temperature and causes superconductivity. This process occurs in the poor metallic conductors like tin, lead and tantalum, but not in good conductors such as copper, silver and gold because they have a weak electron-phonen interaction.

2. Electric and Magnetic Properties

The word superconductivity was coined to describe the tremendous increase in electrical conductivity which arises as a material is cooled below its transition temperature, an effect which was first observed in mercury by Kamerlingh Onnes in 1911. Onnes measured the electrical resistance of frozen mercury wire as a function of temperature, and observed the total disappearance of resistance between 4.3 K and 4.2 K. Three years later he found that the resistance of superconductors could be restored to its value for the normal state by applying a sufficiently large magnetic field. This magnetic transition occurs quite sharply in many pure metals, the transition field value being known as the critical field H_c which varies with temperature according to the approximate relationship

$$H_c(T) \simeq H_o\left(1 - \frac{T^2}{T_c^2}\right) \qquad \text{I 2.1}$$

where H_o is the value of the magnetic field at zero temperature.

In 1933 Meissner and Ochsenfeld[1] measured the flux distribution outside tin and lead samples which had been cooled below their transition temperatures, while in a magnetic field $H_a < H_c$. They found that the samples became perfectly diamagnetic. The perfect diamagnetism arises because there are screening currents circulating on the surface of the sample which create a flux density equal in magnitude and opposite in direction to the flux density due to the applied magnetic field.

Before the discovery of the Meissner effect, Becker, Heller and Souter[10] (1933) described the electrodynamic properties of a zero resistance material. They pointed out that under the influence of an electric field E the conduction elections of mass m and charge e would be accelerated indefinitely according to the equation

$$m\dot{V}_s = eE \qquad \text{I 2.2}$$

where V_s is the velocity of superelectrons.

The supercurrent density is given by

$$J_s = n_s e V_s$$

where n_s is the number of superelectrons per unit volume, moving with velocity V_s.

Substituting this into equation (I 2.2) we obtain

$$\dot{J}_s = \frac{n_2 e^2}{m} E \qquad \text{I 2.3}$$

Forming curl E, and using Maxwell's equations for a region where $\mu = 1$

$$\text{and} \qquad \text{curl } E = -\dot{B}$$
$$\text{curl } H = J + \dot{D}$$

where $\dot{D}$ is the displacement current. In superconductors the currents flowing in the metal affect B but not H, so that within the superconductor

$$\text{curl } B = \mu_o (J_s + \dot{D})$$

and Maxwell's equations can be written in the form

$$\dot{B} = - \text{curle } E \qquad \text{I 2.4}$$

$$\text{curle } B = \mu_o J_s \qquad \text{I 2.5}$$

The Meissner effect shows that inside the superconductor the flux density is always zero. F. and H. London (1935) suggested that the magnetic behaviour of a superconducting metal might be correctly described if B replaced $\dot{B}$, therefore substituting equation (I 2.3) into equation (I 2.4)

$$B = - \frac{m}{n_s e^2} \text{ curle } \dot{J}_s \qquad \text{I 2.6}$$

Equations I 2.6 and I 2.3 describing the electrodynamics of the superconducting current are known as the London equations. Equations (I 2.3) and (I 2.6) describe the zero resistance and the Meissner effect respectively.

In the most general case where the total current is the sum of the normal current and supercurrent,

$$J = J_n + J_s$$

According to Ohm's law $J_n = \sigma E$ where is the conductivity associated with the normal electrons and is a function of temperature. Hence the special equations which apply to a superconducting metal are

$$J = J_n + J_s \qquad \text{I 2.7a}$$

$$J_n = \sigma (T) E \qquad \text{I 2.7b}$$

$$\text{Curl } J_s = - \frac{1}{\mu_o \lambda_L^2} B \qquad \text{I 2.7c}$$

$$\dot{J}_s = \frac{1}{\mu_o \lambda_L^2} E \qquad \text{I 2.7d}$$

where $\lambda_L = \left(\frac{m}{\mu_o n_s e^2} \right)^{\frac{1}{2}}$ is the London penetration depth, describing the depth of the superconductor to which supercurrents penetrate. In the steady state, when fields and currents are not changing with time,

the only current flowing is the supercurrent i.e. $J_n = 0$, then, equations (I 2.7c) and (I 2.7d) lead to

$$\nabla^2 B = \frac{1}{\lambda_L^2} B \qquad \text{I 2.8}$$

Equation (I 2.8) can be used to find the distribution of flux density within any superconducting body by applying to the solution of this equation boundary conditions imposed by the shape of the body and the form of the applied magnetic field. The simplest case is that of a plane surface of semi-infinite superconductor, if B_a is the magnetic induction outside the sample and $B(\chi)$ the induction a distance χ inside, equation (I 2.8) reduces to

$$\frac{d^2B}{d\chi^2} = \frac{B(\chi)}{\lambda_L^2} \qquad \text{I 2.9}$$

As $\chi \longrightarrow \infty$, $B \longrightarrow 0$, the solution for $\chi > 0$ is

$$B(\chi) = B_a e^{-\chi/\lambda_L} \qquad \text{I 2.10}$$

Thus the field falls off exponentially within the superconductor and this decrease is characterized by the penetration depth λ_L.

For a sheet of thickness 2a whose surfaces at $\chi = \pm a$ with B_a parallel to the surfaces

$$B(\chi) = \frac{B_a}{\cosh (a/\lambda_L)} \cosh (\chi/\lambda_L) \qquad \text{I 2.11}$$

The penetration depth is the thickness within which the screening currents flow at the surface of the superconducting sample. These surface currents screen inside from the applied magnetic field.

The penetration depth is of the order of 10^{-5} cm, although the exact value varies for different metals. It increases rapidly and approaches infinity as the temperature approaches the transition

temperature T_c. The variation of penetration depth with temperature is found to fit the relation

$$\lambda_{(T)} = \lambda_{(o)}\left[(1 - (\frac{T}{T_c})^4\right]^{-\frac{1}{2}} \qquad \text{I 2.12}$$

where $\lambda_{(o)}$ is the penetration depth at OK.

3. The surface energy

In 1935 H. London suggested that the total exclusion of an external magnetic field does not lead to a state of lowest energy for a superconductor unless at the boundary a surface free energy exists. In the presence of an external magnetic field H, the energy of the superconductor increases by $\frac{1}{2}\mu_o H_c^2 = g_n - g_s$.

Pippard[12] (1953) pointed out that in the two-fluid model the number of superelectrons n_s changes gradually from the normal region with a distance which he called the coherence length ξ. This distance depends on the impurity of the superconducting metal where ξ increases with the electron m.f.p. (l_e) according to the expression

$$\frac{1}{\xi} = \frac{1}{\xi_o} + \frac{1}{\alpha l_e} \qquad \text{I 3.1}$$

where ξ_o is the range of the coherence length for pure metal, and α is a constant of order unity.

In the case of very impure samples, which are characterized by short electron m.f.p., the coherence length becomes approximately equal to l_e, $\xi \simeq l_e$. Pippard suggested that the surface free energy between the superconducting and normal regions in a superconducting sample depends directly on the relative magnitude of the coherence length (ξ) and penetration depth (λ). Hence the surface free energy, the difference between the Gibbs free energy for the normal and superconducting regions ($g_n - g_s$), is given approximately by

$$g_n - g_s = \tfrac{1}{2}\mu H_c^2 \, \Delta$$

where $\Delta = \xi - \lambda$, which has the dimension of length and is of the same order of magnitude as the boundary thickness. It is found that Δ has the same temperature dependence as the penetration depth

$$\Delta(T) = \Delta(o)\,[(1 - (\frac{T}{T_c})^4]^{-\frac{1}{2}} \qquad \text{I 3.2}$$

In materials where $\xi > \lambda$ the total energy is increased close to the boundary, i.e. there is a positive surface energy (Figure I·1). This type of superconductor shows a sharp transition at magnetic field H_c, and has been designated as type I. If $\xi < \lambda$ (Figure I·2) the surface energy contribution is negative, and for a given value of the applied magnetic field the free energy may be reduced by allowing flux penetration and the formation of normal-superconducting boundaries. Materials belonging to this class are called type II superconductors. In this class are found a few metals and elements (Nb, Ta), but generally alloys in which enhanced electron scattering results in a reduction of the coherence length ξ, and the preferential formation of normal-superconducting surfaces which show a negative surface energy.

At low magnetic fields, both type I and type II materials exhibit a perfect Meissner effect but as the magnetic field is increased surface free-emergy effects become important for type II superconductors and partial flux penetration occurs abruptly at a value of magnetic field H_{c_1} (first critical magnetic field). This state of partial flux penetration, called the mixed state persists until the applied field is raised to equal to the second critical field, H_{c_2}, at which value magnetic flux fully penetrates the sample Fig I.3.

A little earlier than Pippard's suggestion Landau and Ginsburg (1950)[13], starting from quantum mechanical consideration concluded that the order parameter at the superconductive-normal interface cannot change rapidly. Their theory led to results concerning the value and sign of the surface

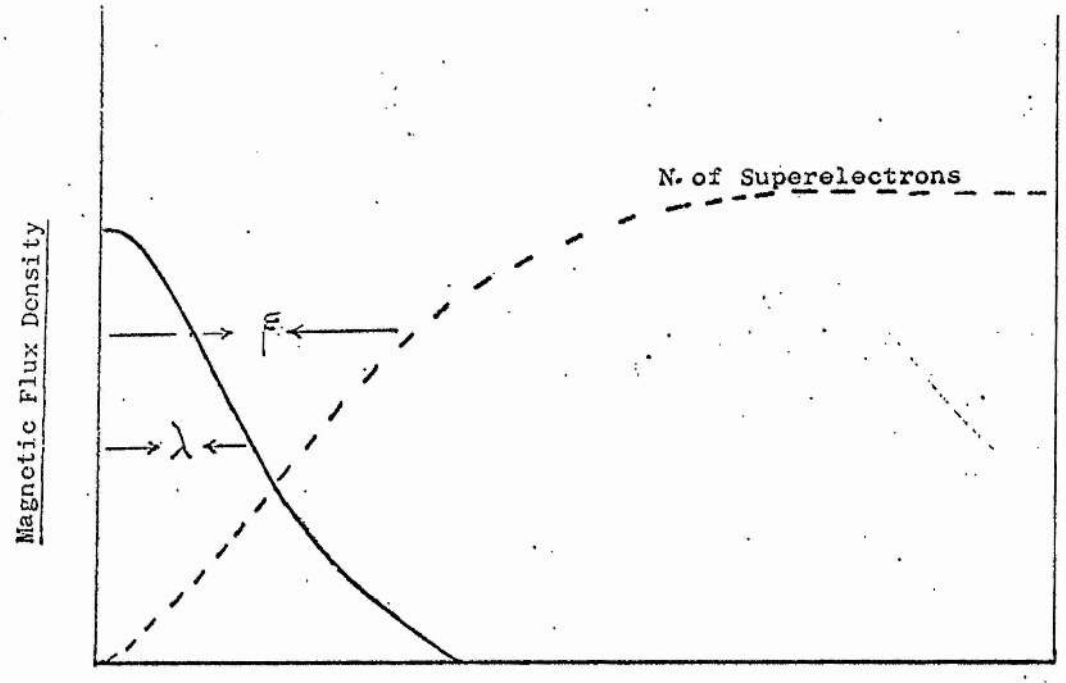

(a) Penetration Depth and Coherence Range at Boundary

(b) Total Free energy

Positive Surface Energy (Type I)

FIGURE I.1

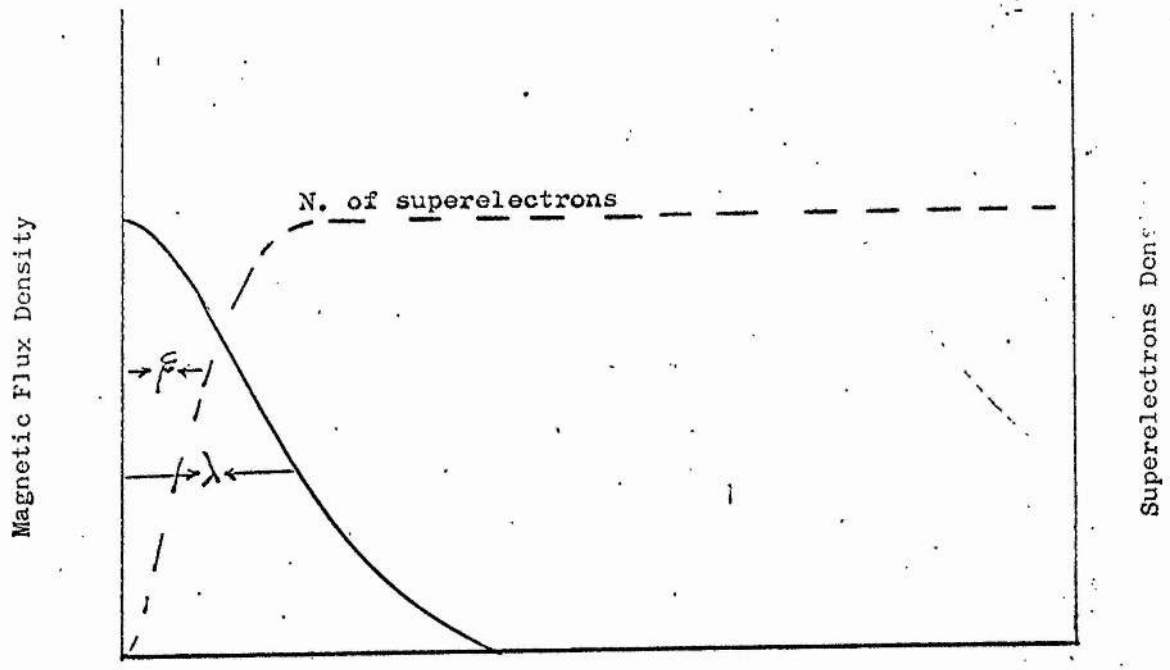

(a) Penetration Depth and Coherence Range at Boundary

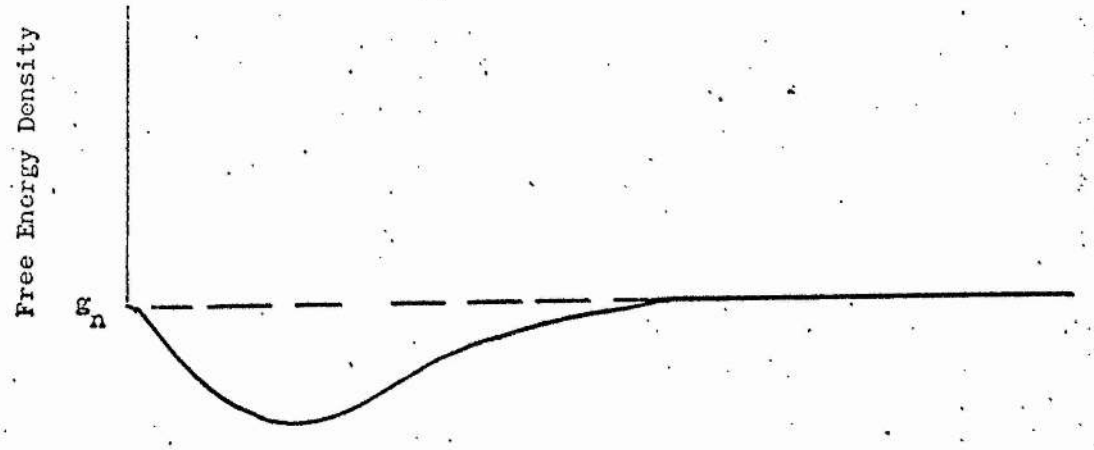

(b) Total Free Energy

Negative Surface Energy (Type II)

FIGURE I.2

tension $\Delta = (\xi - \lambda)$ which are similar to those of Pippard. Ginzburg and Landau found that the properties of a superconductor could be characterized by a constant,

$$k = \frac{2\sqrt{2}\,\lambda e H_c}{\hbar c} \qquad \text{I } 3.3$$

where k is a nondimensional parameter. The value of this parameter is very important and the sign of the surface energy depends, strictly, on whether k is less or greater than $1/\sqrt{2}$. It is found that if $k > 0.71$ the surface energy is negative (type II).

Gorkov[14] (1959) calculated the effect on k when the electronic m.f.p. is much smaller than the intrinsic coherence length ξ_o, he found that

$$k_o \simeq 0.96 \frac{\lambda(o)}{\xi_o} \qquad 3.4$$

where k_o is the value of k in a pure material.

For strongly alloyed materials Goodman (1962) suggested that

$$k = k_o + 7.5 \times 10^3\, y^{\frac{1}{2}} \rho$$

where y is the Sommerfeld electronic specific heat constant in $erg/cm^3/deg^2$ and ρ is the residual resistivity in ohm-cm. Abrikosov[15] (1957) used the G-L theory to analyze the magnetic behaviour of type II superconductors. He showed that for $H_{c_1} < H_a < H_{c_2}$ the material is neither in the perfect super-conducting nor in the normal phase, but it existed in what he described as the mixed state, which was first shown to exist experimentally by Shubnikov et al. (1937) in lead alloys. Abrikosov also predicted that the magnetization curve of type II superconductors (Figure I·3) vanishes entirely at an applied magnetic field, H_a, which is given by

$$H_a = H_{c_2} = \sqrt{2}\, kH_c$$

The theory predicts no hysteresis in the magnetization curve.

The collective theories of Ginzburg, Landau, Abrikosov and Gorkov

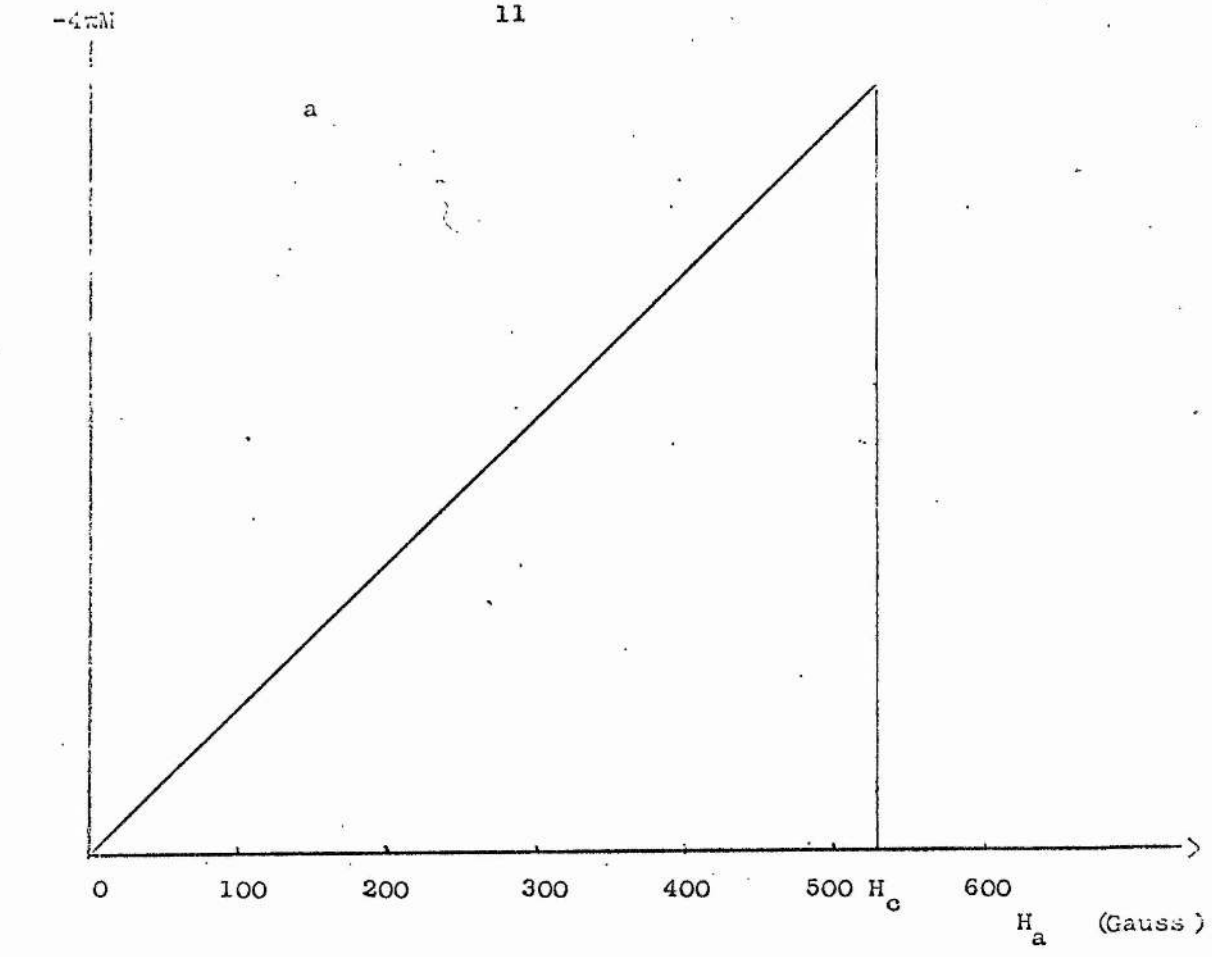

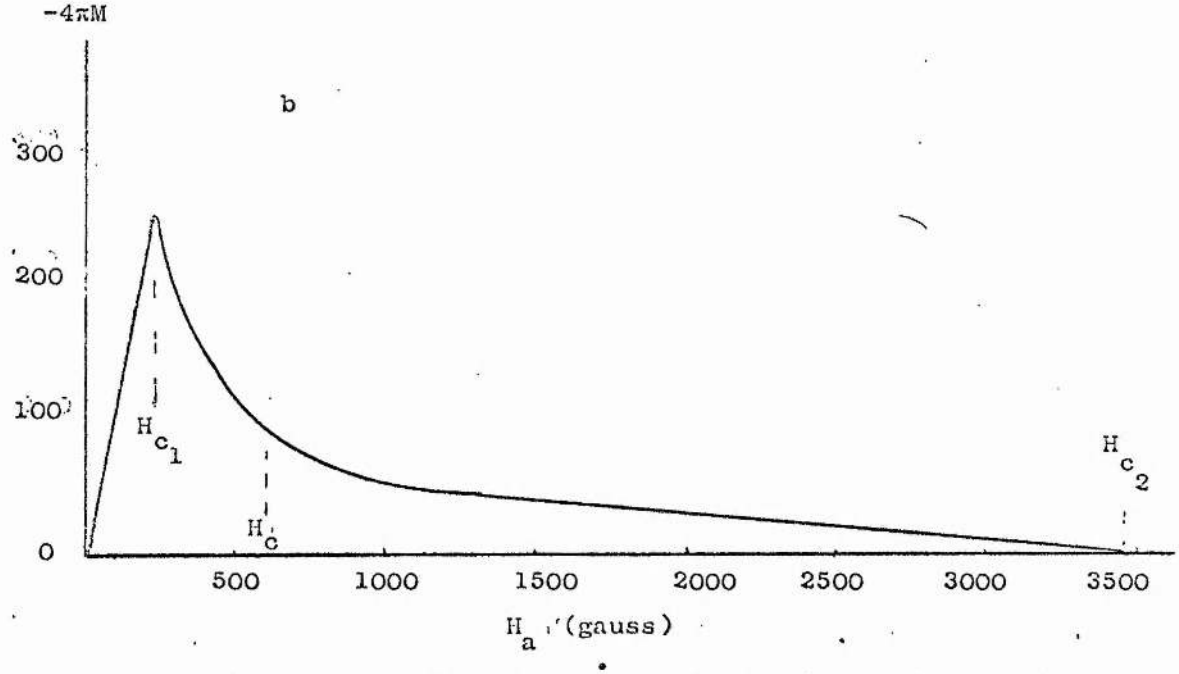

FIGURE I.3. a. Magnetization Curve of Lead (Type I), H_c = 530 gauss.
b. Magnetization Curve of Type II Lead Indium Alloy (85% Lead - 15% Indium), H_{c_1} = 240 G, H_c = 580 H_{c_2} = 3450 G.

are the firm basis of the description of type II superconductors. Together the theories are known as the GLAG theory.

According to GLAGtheory the mixed state consists of a regular alloy of normal cores of radius equal to the coherence length ξ surrounded by a superconducting matrix. The normal cores contain magnetic field in quantum unit of 2×10^{-7} gauss cm^2, but the field penetrates into the matrix around each core with characteristic length λ. The flux density due to the magnetic field has maximum value at the normal cores and falls over distance about λ away from the cores (Figure I.4).

Abrikosov[15] (1957) predicted that in the mixed state the vortex lines form a square array at all fields except near H_{c_1}. Kleiner et al[16] (1964) have shown that for $k > 1$ a triangular array has a lower energy throughout the mixed state than the square lattice. Kramer[17] (1966) predicted that for small k the free energy of the triangular lattice near H_{c_1} is higher than that of the square lattice. The direct experimental observation of the mixed state was not achieved until 1967 by Essmann and Trauble[18], when they observed the triagular lattice in a Pb-In alloy and in Nb, by depositing small ferromagnetic particles onto the surface of the superconducting sample and observing the resulting pattern by use of an electronmicroscope, Obst[19] (1969) using the Essmann and Trauble[18] technique, observed the square flux line lattice near H_{c_1} for pb-Ti alloys where $k > 1$ which confirms Kramer's[17] prediction.

4. Thermodynamic Properties

The thermodynamic theory concerns the relationship between the magnetic and thermal properties of a superconductor at the phase transition. The free energy of a material arises from its thermodynamic state, and thus the material's temperature, entropy, pressure and magnetization are the parameters involved. The increase in the Gibb's free energy of a superconductor due to its magnetization is given by

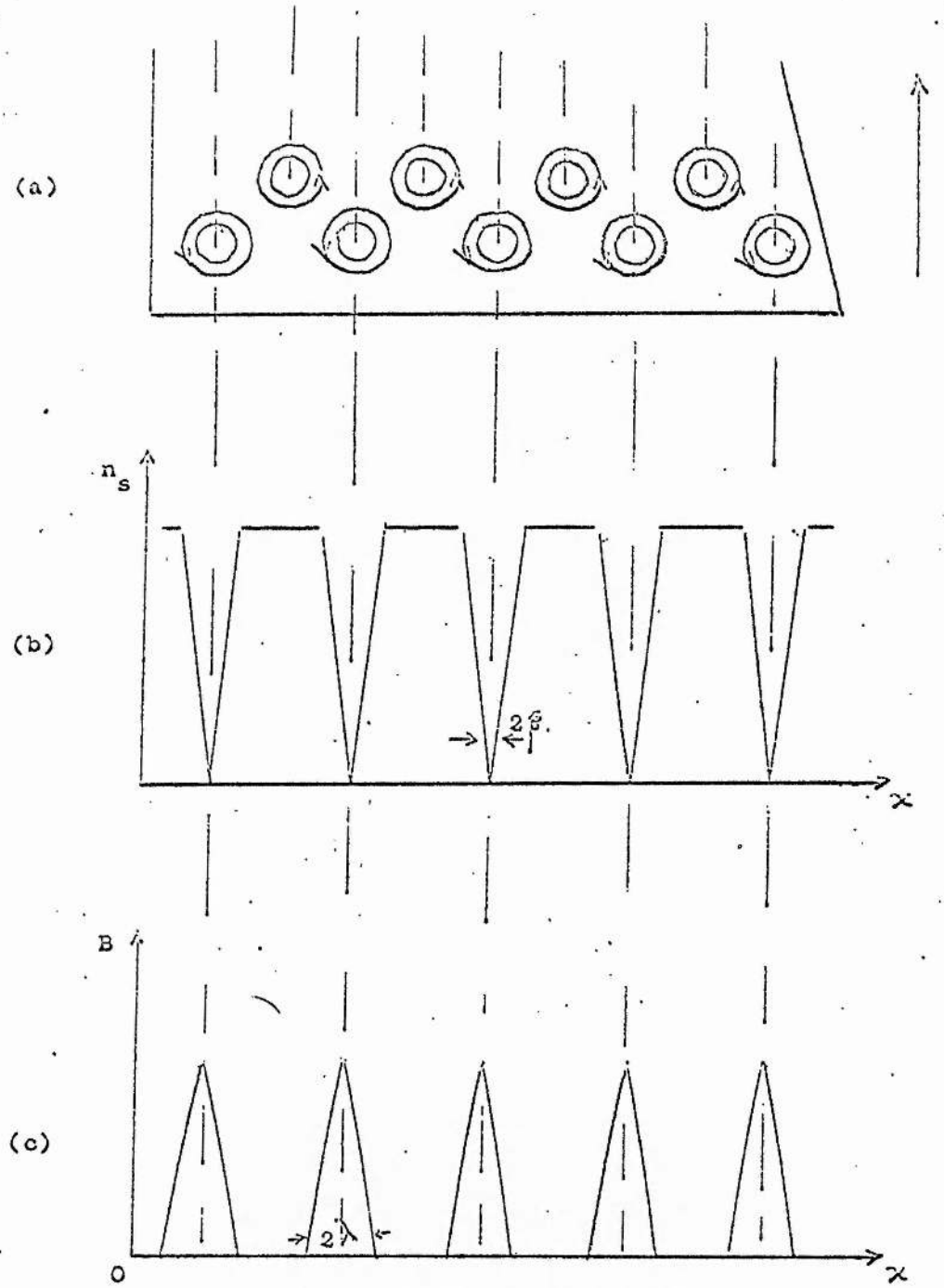

Mixed State in Applied Magnetic Field of Strength Just Greater than H_{c_1}. (a) Lattice of Cores and Associated Vortices. (b) Variation with Position of Concentration Superelectrons. (c) Variation of Flux Density. (Schematic only)

FIGURE I.4

$$\Delta g_s = \int_0^H \mu_o M dH = \tfrac{1}{2}\mu_o H^2 \qquad \text{I 4.1}$$

At the critical field H_c the increase in free energy is obviously $\frac{1}{2}\mu_o H_c^2$.

The energy difference between the superconducting and normal states at a given temperature T in the absence of any field is

$$g_n - g_s = \tfrac{1}{2}\mu_o H_c^2 \qquad \text{I 4.2}$$

where g_n and g_s are the free energies of the normal and superconducting phases respectively.

The entropy difference between the superconducting and normal states in the absence of field is given by

$$S_n - S_s = -\frac{d\Delta g}{dT} = -\mu_o H_c \frac{dH_c}{dT} \quad . \qquad \text{I 4.3}$$

Since the entropy is a measure of the disorder of a system, this indicates that the superconducting state is one of greater order than the normal state. The entropy difference is given by the relationship

$$Q = T(S_n - S_s) = \mu_o T H_c \frac{dH_c}{dT} \qquad \text{I 4.4}$$

This shows that in the presence of a magnetic field a latent heat is associated with the transition, on passing from the superconducting to normal under the influence of an increasing field, a superconductor absorbs heat.

The difference in specific heat between the two phases follows from

$$C = T\frac{ds}{dT}$$

$$C_n - C_s = \mu_o \left[TH_c \frac{d^2H_c}{dT^2} + T\left(\frac{dH_c}{dT}\right)^2\right] \qquad \text{I 4.5}$$

when $T = T_c$, $H_c = o$ and

$$(C_s - C_n)_{T_c} = \tfrac{1}{2}\mu_o T_c \left(\frac{dH_c}{dT}\right)^2_{T_c} \qquad \text{I 4.6}$$

This is known as Rutgers formula and it predicts the discontinuity in the specific heat of a superconductor at the transition temperature.

The specific heat of any conductor is due to the contribution of both the lattice ions and the conduction electrons and has the form

$$C_n = C_{latt} + C_{el}$$

$$= A\left(\frac{T}{\Theta}\right)^3 + yT$$

where A is a constant with the same value for all metals, Θ is the Debye temperature of the lattice and y Sommerfeld constant.

The lattice specific heat is found to be unchanged in the superconducting state, so the difference between the specific heat values in the superconducting and normal states arises only from the change in the electronic specific heat.

The electronic specific heat of a metal in the superconducting state is given by

$$(C_{el})_s = yT_c\, e^{-b/KT} \qquad \text{I 4.7}$$

where a and b are constants. Such an exponential variation suggests that as the temperature is raised electrons are excited across an energy gap above their ground state. If the gap of width 2ϵ lies below the lowest available excited state, the number of thermally excited electrons is proportional to $e^{-2\epsilon/2KT}$, where K is Boltzmann constant- the factor of 2 arises because every excitation creates two independent particles, an electron and a hole. According to the microscopic theory (BCS) of superconductivity, the energy gap depends on both temperature and field strength, where the energy gap has its maximum value at OK and decreases to zero at $T = T_c$, so the parameter b in equation (I 4.7) can be given by

$$b = \frac{\epsilon(T)}{KT_c}$$

It is now appropriate to comment breifly on present concepts of the microscopic theory.

5. Microscopic theory

An early step in the search for a microscopic theory came in 1950 when Fröhlich and a little later Bardeen (1950) described a mechanism of interaction between electrons and phonons. An attractive interaction may arise from processes in which an electron emits a virtual phonon which is absorbed by another electron in such a way that they behave as if there is direct interaction between them. This type of electron interaction produces a lowering of energy. The next step towards a microscopic theory of superconductivity was taken by Cooper[20] (1956) who discussed what happens when two additional electrons are added to a metal at absolute zero. He was able to show that if there is an attraction between them, however weak, they are able to form a bound state so that their total energy is less than $2\epsilon_F$ (ϵ_F is the Fermi energy). This indicates that there could be an electron ground state which is lower than that for free electrons, the attractive interaction between electrons creating pairs which have opposite momentum and spin ($Pi^{\uparrow}$, $-Pi^{\downarrow}$) so that a pair of electrons behaves as quqsi-particle of zero spin.

The great step forward towards a microscopic theory of superconductivity came in 1957 when Bardeen, Cooper and Schrieffer[21] succeeded in linking the two ideas (Fröhlich and Cooper) showing that bound electron pairs of opposite spin and momentum would form, provided that the attraction arising from the virtual phonon process exceeded any repulsive coulomb interaction. The phonons emitted by the electrons of a pair interact with other electrons within the coherence length in such a way that an attractive interaction exists between the electrons of the pair. All electron pairs have the same momentum, if no magnetic field is present; the momentum of all pairs is zero.

By the attractive process the energy of pairs is lower relatively than the mean energy [Fermi energy ϵ_F] of unpaired electrons. In order

to break a pair of electrons (by raising the temperature or the magnetic field) a minimum amount of energy 2ϵ is required to accelerate the electrons from the ground state to the first available state which is equal to the height of the energy gap. According to the BCS theory, the minimum energy required to break up a pair so as to produce two free electrons with momentum P_i and P_j is given by

$$E = E_i + E_j = [(\epsilon_i - \epsilon_F)^2 + \Delta^2]^{\frac{1}{2}} + [(\epsilon_j + \epsilon_F)^2 + \Delta^2]^{\frac{1}{2}} \qquad \text{I 5.1}$$

where $\epsilon_i = P_i^2/2m$ and the positive square root is taken, 2Δ has the dimensions of energy and is given by

$$2\Delta = 4h\gamma \exp\,[-[N(\epsilon_F)V]^{-1}]$$

γ is the average phonon frequency, -V is the matrix element of the scattering interaction and $N(\epsilon_F)$ is the density of states at the Fermi surface in the normal metal.

The BCS theory predicts the energy gap with temperature can be expressed approximately by

$$E_g = 3.2\ KT_c\ (1 - \frac{T}{T_c})^{\frac{1}{2}} \qquad \text{I 5.2}$$

This has been confirmed experimentally. At temperatures below 0.6 T_c the energy gap is substantially independent of temperature. The theory predicts that the critical temperature is related to the energy gap at absolute zero by

$$E_g = 2\Delta(o) = 3.5\ KT_c \qquad \text{I 5.3}$$

The magnitude of $2\Delta(o)$ can be characterized by a frequency γ_g such that $h\gamma_g = 2\Delta(o)$ where γ_g is about $10^{11} - 10^{12}$ Hz. The values of $\Delta(o)$ were obtained experimentally by Richards and Tinkham[22] (1960) from infrared absor tion measurement for some superconducting elements, and are close to the BCS theoretical value.

The BCS theory predicts further that at temperature T, the number of pairs which are broken is proportional to $e^{-\Delta(o)/KT}$. This leads to an

electronic specific heat which is proportional to $e^{-\Delta_{(o)}/KT}$. As the temperature T rises close to T_c the specific heat rises more rapidly because $\Delta(T)$ becomes smaller. Above T_c the electrons behave as in the normal metal, all pairs being broken.

Also the BCS theory predicts the magnetic dependence of the energy gap. The ciritcal magnetic field required to cause a transition between the normal and superconducting states is given by

$$\tfrac{1}{2}\mu_o H_c^2 = g_n - g_s$$

At T = o the critical magnetic field in the BCS theory obtained by setting the diamagnetic energy of superconductor equal to the condensation energy.

$$\tfrac{1}{2}\mu_o H_o^2 = (g_n - g_s)_{T=o} = \tfrac{1}{2}N(\epsilon_F)\,\Delta^2(o) \qquad \text{I 5.4}$$

where $N(\epsilon_F) = \frac{3}{2}\gamma\left(\pi^2 K^2\right)^{-1}$

Using the value of $2\Delta(o) = 3.5\ KT_c$, we obtain

$$\frac{H_o^2}{T_o^2} = \frac{0.47\gamma}{\mu_o} \qquad \text{I 5.5}$$

where γ is the coefficient of T in the expression for the specific heat in the normal state.

6. Some applications of superconductivity

There are two features in type II superconductors, its high critical current densities and high field strengths in which type II superconductors operate. These characteristics of superconductors can lead to a wide variety of potential applications. The most advanced application of superconductors is in the generation of high magnetic fields, where the first application for superconductive magnets are in the nuclear accelerator field.

The unique property of zero resistance of superconductors can be

exploited to allow the construction of superconducting motors[23], transformers[24] and generators[25], with advantages in weight, size and performance over a wide range of ratings, which in some cases are cheaper than the conventional machines, and which present an exciting challenge to the power industry.

The promise of the superconductor is that power losses can be reduced to essentially zero (for dc) or to a very small level (for ac) and thus mitigate the heat dissipation problem. Furthermore, the ability of superconductors to operate at very high current densities makes the superconducting cable system[26-29] a likely candidate for high capacity underground service. The a.c. losses in most superconductors are not negligible, but should the losses prove sufficiently small, a.c. superconducting cables should be readily and economically integratable into utility systems.

Recent studies of small diameter wires and foils of superconducting niobium have indicated that this material exhibits very low a.c. losses and thus may very well be the desired material for use in superconducting power transmission systems.

The work of this study is to examine the effect of the surface on a.c. losses measurements for cylindrical rods of single crystal and polycrystalline Nb at different surface conditions. This study is divided into magnetization measurements, ac losses at 50 Hz, critical current measurements and shielding field for both single crystal and polycrystalline Nb at different surface treatments.

REFERENCES

1. Superconductivity, by E. Lynton, Methuen and Co. Ltd.,(1964).
2. Applied Superconductivity, by V. Newhouse, John Wiley and Sons, (1964).
3. Low Temperature Solid State Physics, by H. Rosenberg, Oxford,(1965).
4. Experimental Physics at Low Temperature, by L. Mackinnon, Wayne State University Press, (1966).
5. Introduction to Superconductivity, by A. Rose-Innes and E.H. Rhoderick, Pergamon Press,(1969).
6. Superconductivity and its Application by J.E.C. Williams, Pion Limited,(1970).
7. Science 156, 645,(1967).
8. Matthias, B.T., Chapter V, Progress Low Temperature Physics, Vol II, New York, Interscience,(1957).
9. Phillips, J.C., Phys.Rev.Lett., 26, 543,(1971).
10. Becker R., Heller G., and Sauter F., Z.Phys. 85, 772,(1933).
11. London F., and London H., Proc.Roy.Soc. A149, 71,(1935); London F., and London H., Physica 2, 341,(1935).
12. Pippard A.B., Proc.Roy.Soc., A216, 547,(1953).
13. Ginzburg V.L., and Landau L.D., J.E.T.P., 20, 1064, (1950).
14. Gorkov L.P., J.E.T.P., 36, 1918,(1954).
15. Abrikosov A.A., J.E.T.P., 32, 1442,(1957).
16. Kleiner W.H., Roth L.M., Autler S.H., Phys.Rev., 133, 1226,(1964).
17. Kramer L., Phys.Lett., 23, 619,(1966).
18. Essmann U., and Trauble H., Phys.Lett. 24A, 526,(1957).
19. Obst B., Phys.Lett., 28A, 662,(1969).
20. Cooper L.N., Phys.Rev., 104, 1184,(1956).
21. Bardeen J., Cooper L.N., and Schrieffer J.R., Phys.Rev., 108, 1172, (1957).

22. Richards P.L., and Tinkham M., Phys.Rev., 119, 557, (1960).

23. Appleton A.D., and MacNab R.B., Conference on Low Temperatures and Electric Power, p. 112, (1969).

24. Lorch H.O., Cryogenics, 9, 354, (1969).

25. Harrowell R.V., Nature, 222, 598, (1969).

26. Rogers E.C., and Edwards D.R., Electrical Review, 348, 8th Sept, (1967).

27. Rogers E.C., Conference on Low Temperatures and Electric Power, p.83, (1969).

28. Minich S.H., and Fox G.R., Cryogenics, 9, 165, (1969).

29. Snowden P.D., Scientific American, 226, Number 4, 84, (1972).

CHAPTER II

SAMPLES

In this study on ac losses two different samples of niobium have been investigated. The surface conditions of each sample have been altered by electropolishing and mechanically polishing to give three distinct surface features to each. The first sample is a single crystal in the form of a cylindrical rod 65 mm long and 4 mm diameter, with 110 orientation. This was cut from the central position of a rod 125 mm long which had been electron-beam, zone refined by Dr. D.W. Jones, Centre for Materials Science, University of Birmingham.

The second sample is polycrystalline niobium supplied as a centreless ground rod by Murex Limited. The chemical analysis of the ingot from which the rod was made showed impurities less than the normal limits for common elements (O_2, H, N_2, C, Si, Fe, Cr, Mo, W, Ta, Ti, Ni) and very low for Tantalum (75 ppm). It is expected that after swaging from the ingot the gaseous impurities would be larger, and the number of crystaline defects in the material would be very high. The rod investigated had similar dimensions to the single crystal, and was cut from the centre of a long rod.

1. Electropolishing

By electropolishing the sample its surface changes responding to the chemical solution and its effect on the impurities on the surface of the sample, i.e. new surface may be added which might be different from the real surface of the superconducting sample, or material might be removed from the surface. It is noted that the surface plays an important role in our experimental measurements.

The electrolyte used consists of 98.8% sulphuric acid and 40% hydrofluoric acid in the ratio of 90:10 by volume. The bath voltage is 4.5 volts and the mean current density is about 10 $m\text{A}/cm^2$. The cathode is cylindrical platinum foil, 10 cm long and 3 cm diameter. The sample, used as the anode, is connected to a nylon holder, and is rotated by a small low speed motor. The sample is kept in the chemical solution under the above conditions for about three hours.

The electropolishing solution (H_2SO_4-HF) has been used by De Blis[1] et al. and others[2,3,4,5] for Nb samples.

2. Mechanical Polishing

After electropolishing treatment, the samples have been mechanically polished. The single crystal Nb was polished using fine polishing powder (cerium oxide). Polycrystalline Nb was mechanically polished using series of emery papers and finally with cerium oxide.

3. Single Crystal Nb

Figure II.1[ab] shows the single crystal Nb surface as received (Sample A) taken by a scanning electron microscope with magnification of 5500, the picture shows different surface scratches resulting from the electron beam zone refining.

Figure II.2[ab] shows the same surface after electropolishing (Sample B). By electropolishing the surface a new thin surface due to the reaction between the surface and the chemical solution may be added, the surface may look smooth, but the scrath es on the original surface have not been fully removed.

Sample B has been polished (Sample C) by fine polishing powder. The surface of this sample is shown in Figure II.3[ab]. In this sample the surface has become smooth, which shows that the visible scratches

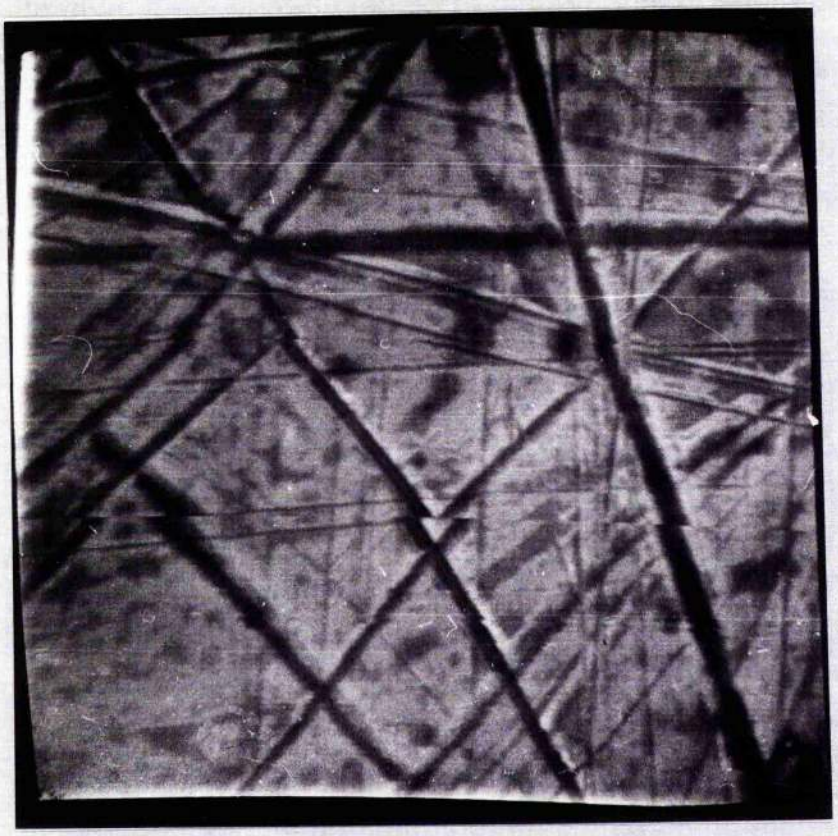

a

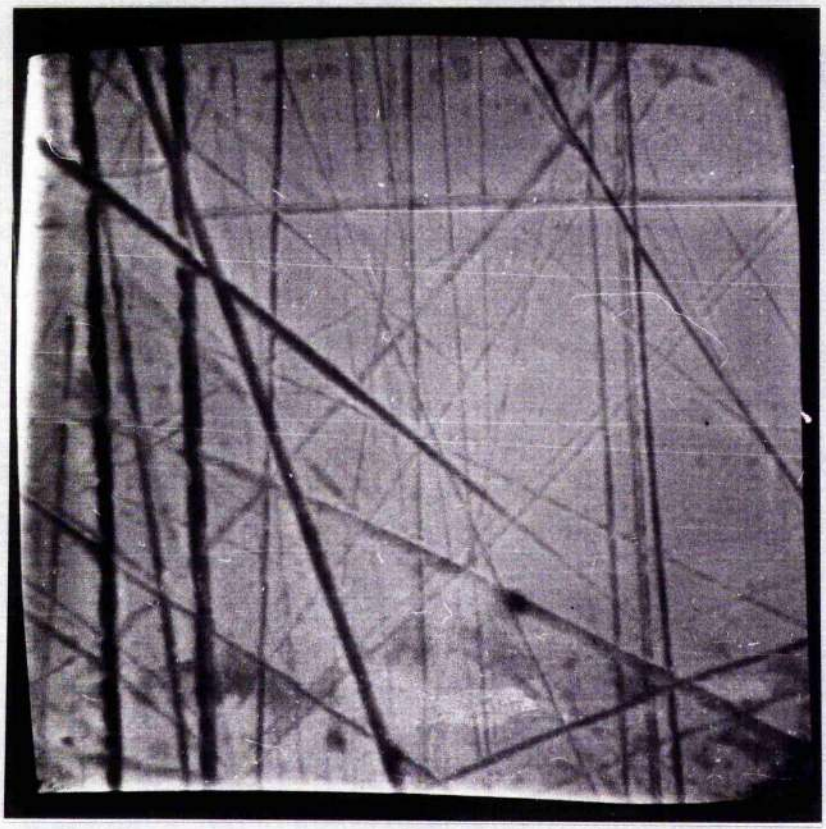

b

Figure II.1 (ab)

Surpace of Single Crystal Niobium as

received, magnification 5500

a

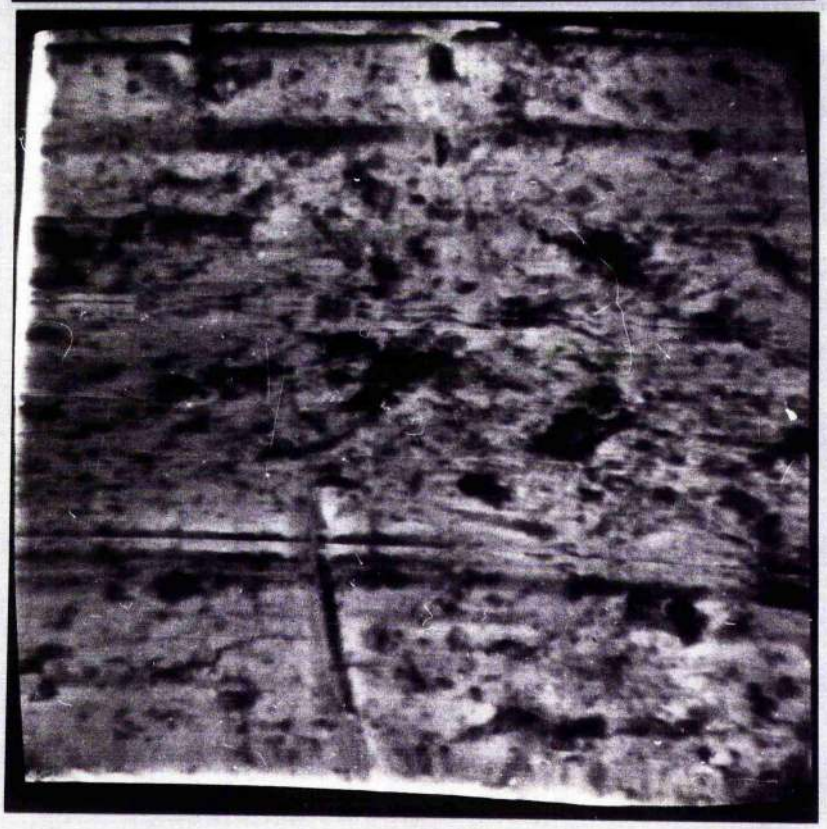

b

Figure II.2 (ab)

Surface of electropolished single crystal Nb, Magnification 5500

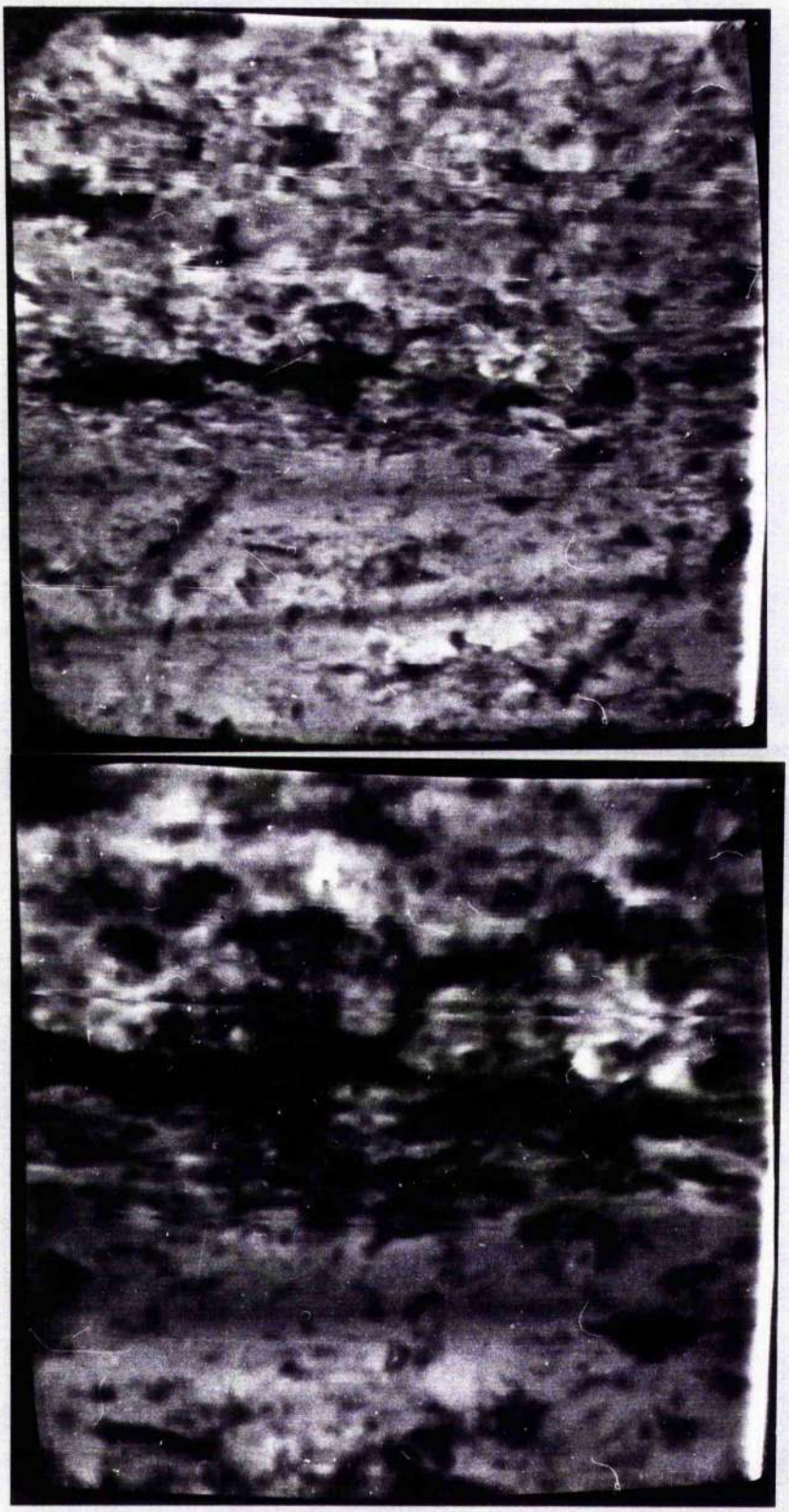

a

b

Figure II.3 (ab)

Surface of Mechanically Polished Single Crystal Nb

a. Magnification 5500

b. Magnification 22000

seen in Figures II.1, II.2 have been largely eliminated. It is worth noting that in its superconducting state the initial flux penetration H_{c_1} occurs at a higher field than in both samples A and B (See Section III).

4. Polycrystalline Nb

A chemical assay of the material of the large ingot from which the rod was swaged is shown in table 1, where it can be seen that major metallic impurity is roughly 75 parts per million (ppm) tantalum..

Table 1

Typical chemical analysis for Polycrystalline Nb

Impurity	O	H	N	C	Si	Fe	Cr	Mo	W	Ta	Ti	Ni
Assay (ppm)	16	4	45	40	15	<30	10	<50	<50	75?	50	5

Annealing.

The sample was heated in furnace under a vacuum in order to reduce the chemical and physical defects. The sample was kept in the furnace at a temperature of about 900-1000 C for almost 60 hours in a vacuum of about 10^{-5} mm Hg. The temperature was then reduced gradually to room temperature while maintaining the same vacuum.

Annealing has great effect on polycrystalline Nb. The major effect is to reduce the degree of irreversibility in the magnetization curve of the superconducting state because of a decrease in the number of flux pinning sites provided by dislocations and impurities. The second effect is to increase the value of k (Ginzburg-Landau parameter).

The effect of annealing on both the critical fields H_{c_1} and H_{c_2} has been reported by De Sorbo[6] (1964) in magnetization measurements of Nb containing dissolved gases (oxygen and nitrogen), where H_{c_1} and H_{c_2} are controlled by amount of the gases the sample contained. Berlincourt[7]

(1959) found that after annealing Nb, H_{c_2} was reduced from 7.65 Kg to 5.0 Kg.

After annealing the surface of the polycrystalline sample (Sample D) is shown in Figure II.4ab, an SEM photograph with magnification of 5500. Figure II.5ab shows the surface of polycrystalline sample after electropolishing (Sample E), it can be clearly seen that the surface has become rougher than sample C, this is because the electropolishing has left the impurities on the surface untouched. Figure II.6ab represents the surface of Sample E after a series of mechanical polishings (Sample F), the irregularities have been removed, so that the surface has become smooth.

The conclusion we note is that, in polycrystalline Nb the electropolishing appears to leave the imperfections relatively untouched which cause irregularities on the surface, while mechanical polishing smooths out all irregularities on the surface. In the case of the single crystal Nb the surface has been smoothed relatively by electropolishing due to the absence of impurities. In both samples mechanical polishing reduced roughness of the surface to a minimum.

In this study only two rods of niobium have been investigated. One was a single crystal, the other one of polycrystalline material. The surface of each rod was altered twice by polishing. Hence three separate samples each with a distinct surface were available from each rod for the investigation of the dependence of ac losses on surface state. The designation of these samples is listed in Table 2.

Table 2

Sample	Designation of surface	
	Single crystal	polycrystalline
A	as received	
B	sample A Electropolished	
C	sample B Mechanically polished	
D		as received, after annealing
E		sample D Electropolished
F		sample E Mechanically polished

For each sample, measurements were taken of (i) its magnetisation (ii) ac power loss in 50 Hz field, (iii) J_c, as obtained from ac loss measurements -- see Section VI.4 , and (iv) ΔE, as mentioned in section III and VI. Once these measurements had been made in full on each sample as small piece 0.7 cm long was cut from the end of the rod, and the remaining part of the rod was polished to produce a new surface state, and hence a new sample for further investigation. (The ends, which were taken to be representative of the surface of the whole rod, were later viewed by SEM. Photographs were taken of the roughest and smoothest parts of each end piece.)

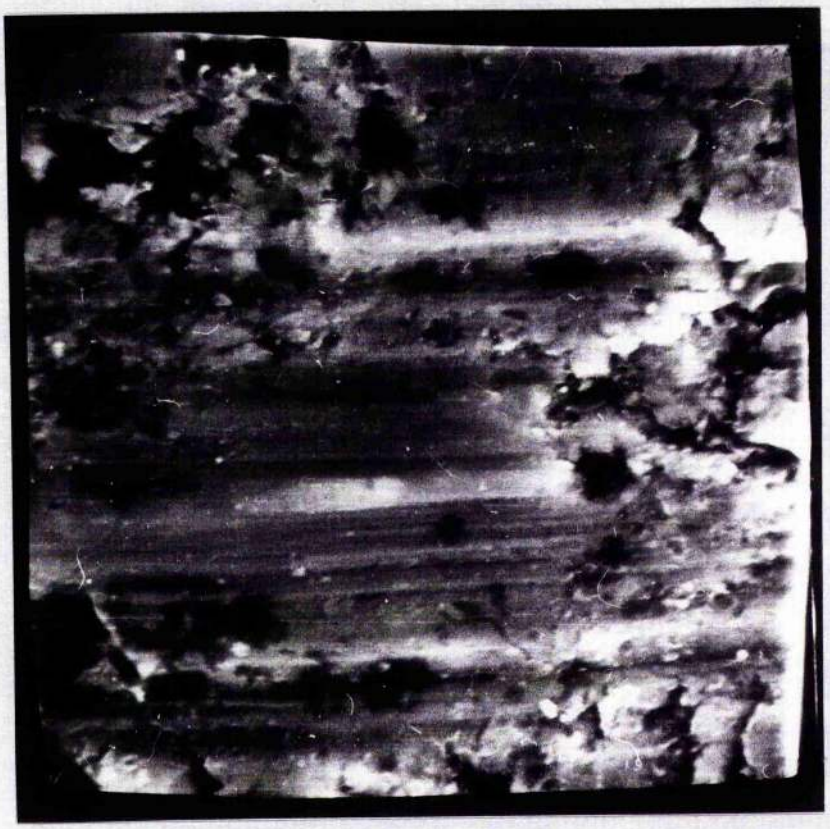

a

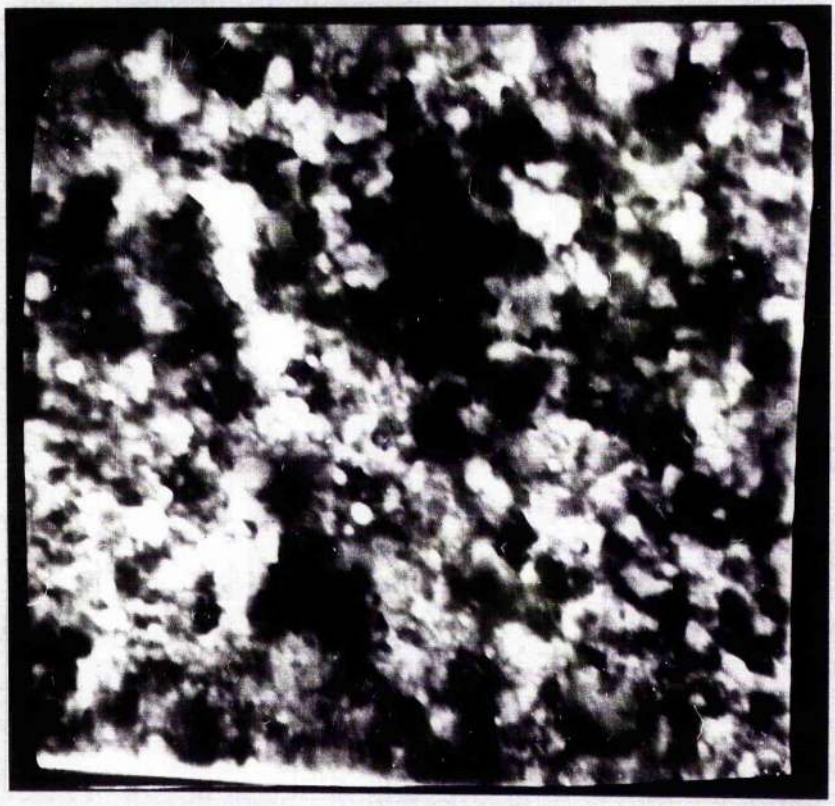

b

Figure II.4 (ab)

Surface of Polycrystalline Nb after Annealing,
Magnification 5500

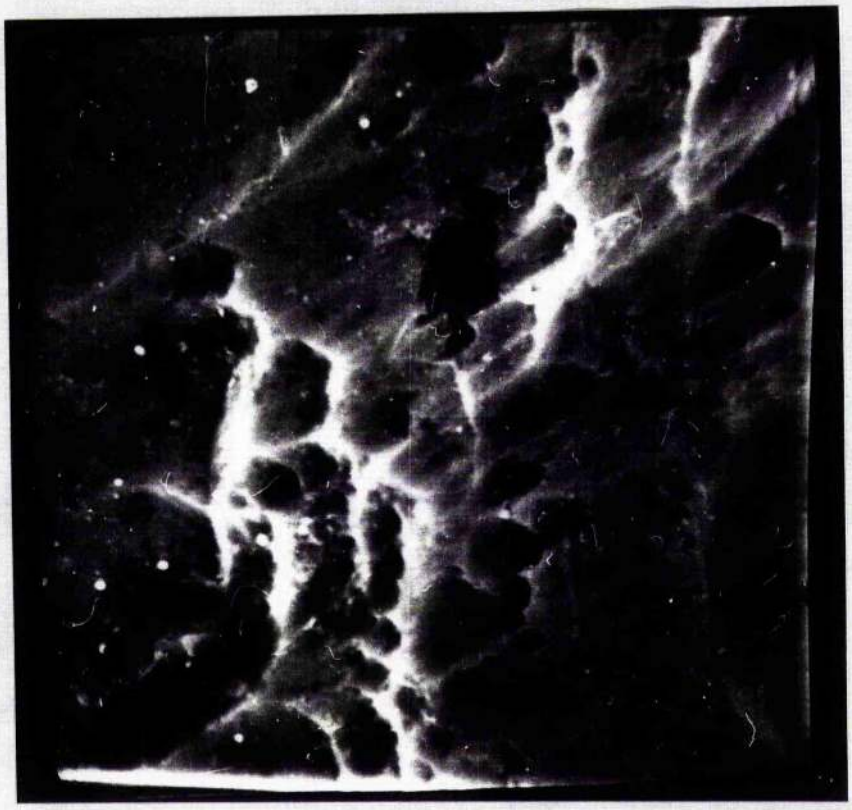

a

b

Figure II,5 (ab)

Surface of Electropolished Polycrystalline Nb,
Magnification 5500.

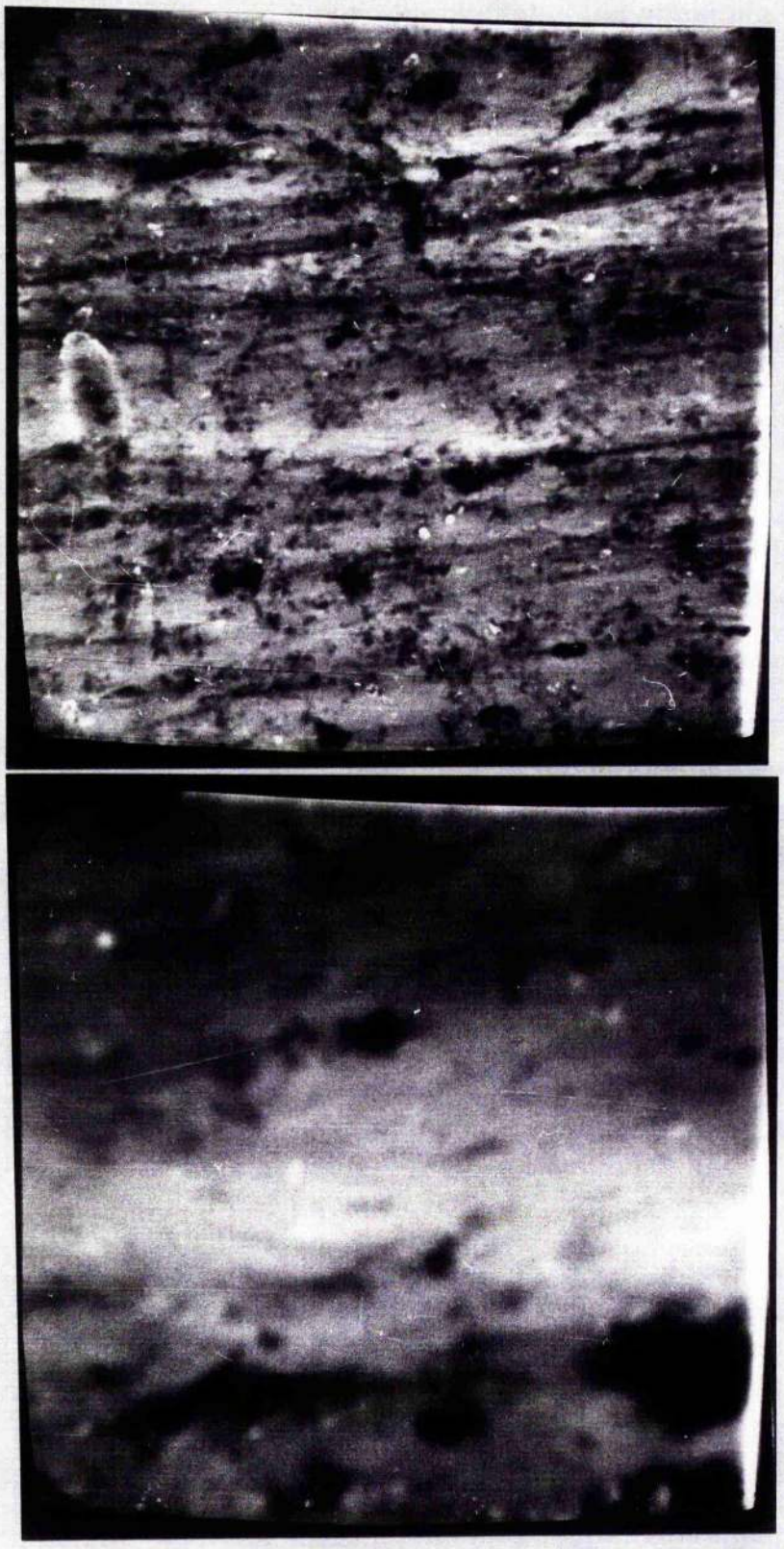

a

b

Figure II.6 (ab)

Surface of Mechanically Polished Polycrystalline Nb

a. Magnification 5500

b. Magnification 22000

REFERENCES

1. De Balis, R.W., and DeSorbo, W., Phy Rev.Lett. 12, 494 (1964).
2. Miller, G.L., Tantalum and Niobium, London, Butterworths Scientific Publications (1959).
3. Rocher, Y.A., and Septfonds, J., Cryogenics, 7, 99 (1967).
4. Diepers, H., Schmidt, O., Martens, H. and Sun, F.S., Physics Lett. 37A, Number 2, 139 (1971).
5. Narbiker, A.V., and DewHughes, D., Phys.Stat.Soli., 6, 385 (1964).
6. Desorbo, W., Phys.Rev., 134, A1119 (1964).
7. Berlincourt, T.G., Phys.Rev., 114, 969 (1959).

CHAPTER III

MAGNETIZATION MEASUREMENTS

We report the magnetization curve measurements of cylinders of Niobium, both single crystal and polycrystaline, each with different surface condition, at applied magnetic field H_a, $H_{c_1} < H_a < H_{c_2}$, at temperature 4.2 K. It has been found that the surface plays a major role in determining H_{c_1} and also the hysteresis of the magnetization.

1. Magnetization Models

They are two theoretical models which have been used to describe the magnetic behaviour of type II superconductors.

1.1 Abrikosov[1] and Goodman's[2] Model. This model, based on the negative surface energy in type II materials, applies to homogeneous strain-free material. The magnetic field penetrates into the sample at value H_{c_1}, where $H_{c_1} < H_c$ [H_c is the thermodynamic critical field], and a complete penetration occurs at H_{c_2}. Between H_{c_1} and H_{c_2} (mixed state), there is a uniform distribution of current particles, or fluxoids, whose density increases as the applied field increases. The model predicts a reversible magnetization curve.

1.2 Bean's[3] Model. This model deals with an inhomogeneous superconductor in which it is argued that the reversibility in the magnetization curve is related to the shielding currents carried by filaments, the critical current of the filaments is proportional to the size of the sample. This argument leads directly to the magnetization being size-dependent. According to this model, the change in magnetization, $\Delta(4\pi M)$, between increasing and decreasing curves in the hysteresis loop is proportional to the specimen radius R, and to the critical current density J_c.

The essential difference between the two models lies in the fact that Bean's model predicts a size-dependent magnetization, and the other reversibility in the magnetization.

2. Apparatus

The magnetic field is produced by a superconducting magnet (bore 1.6 cm, length 20 cm (made by BOC) homogeneity over the central region of 8 cm is 0.09% measured at 20 K gauss, producing 349 gauss Amp^{-1}. The power supply for the magnet delivers up to 60 Amps, and by means of a sweep unit current, can be raised and lowered at various constant rates. In these measurements the magnetic field was swept at 58, 29 or 11.6 gauss/sec. The current delivered to the magnet was measured by observing the voltage over a 0.1 ohm standard resistance (0.1%) by a digital voltmeter, and in these experiments this voltage was also used to drive the χ-axis of an χ-y plotter. The sample holder for the niobium rods was placed inside the magnet bore. The holder is a perspex rod which makes a good fit within the bore (length 20 cm, diameter 1.5 cm). The Nb sample rests on a shoulder in a hole drilled axially in the perspex, so that the sample is placed centrally in the magnet. A hole to the base of the perspex allows liquid helium to circulate freely.

To measure the magnetization of the sample two pickup coils are required; one is wound directly onto the surface of the sample (in the central portion) with one layer comprising 200 turns of 48 S.W.G. This is the penetration coil and it detects the flux within the sample. The other coil is wound on a small perspex rod with the same diameter as the sample, placed on the top of the sample and has 200 turns. This coil is the bucking coil detecting only the flux due to the external magnet. By means of the bucking coil the flux due to the external field in the penetration coil can be cancelled so that only the net flux due to the

sample is detected. On integration with respect to time the signal from the coils represents the magnetization of the sample. The connections between the coils and the external circuit are made outside the superconducting magnet, in order to avoid any e.m.f. generated from the solder connections with external leads, the leads being taken up, far outside the magnetic region and are connected to the external leads, and outside the cryostat are connected to the rest of the circuit as shown in Figure III-1.

The two coils are wound in opposite senses, and the voltage from the bucking coil is divided across a potentiometer before being added to that from the penetration coil to obtain compensation of the externally swept field. In order to get an accurate compensation, the potentiometer should be adjusted just before transferring liquid helium i.e. when the coils are cold. This is done by passing a small ac current through the magnet and adjusting the potentiometer for the zero output across the coils.

During the run, when sweeping the applied magnetic field an e.m.f. is developed across each coil, which is proportional to the rate of change of the magnetic flux threading it. Since one coil contains the superconducting sample and the other does not, and since they are balanced in series opposition, the net e.m.f. across the two coils is proportional to the rate of change of magnetization of the sample, $\mathcal{E} \alpha \frac{dI}{dt}$. This e.m.f. is amplified by a milli-microvoltmeter (Keithly model 149) with a gain of about 10^5, and its output is fed to an electronic integrator Figure III 1. The output of the integrator $V\alpha \int \mathcal{E}\, dt$ where $V\alpha \int \frac{dI}{dt}\, dt = I$ is proportional to the magnetization of the sample. This voltage is fed to the y-axis of the χ-y plotter, where χ-axis displays the applied magnetic field H_a.

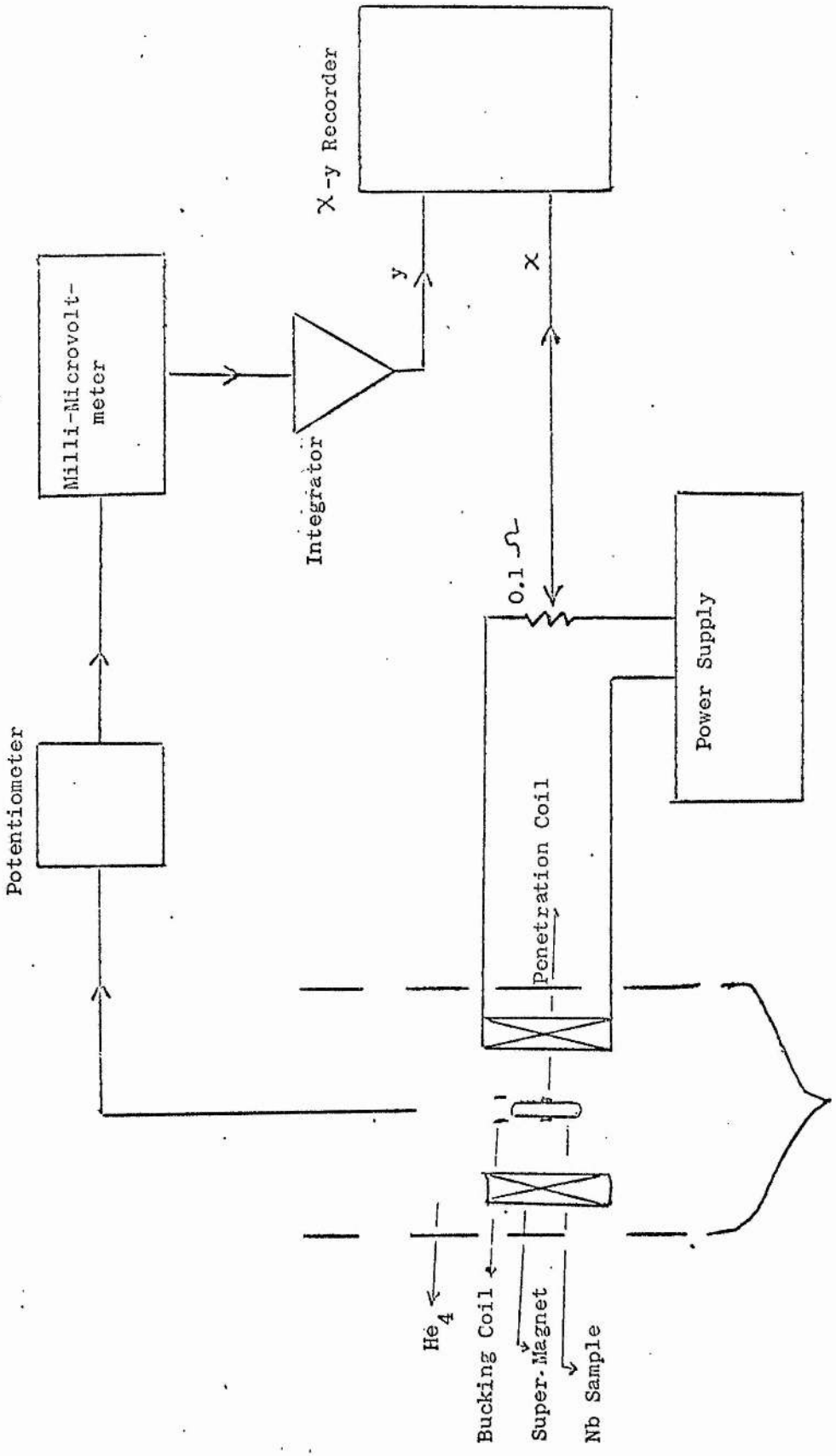

Expcrimental Arrangement

FIGURE III.1

In this method plots of I against H_a are taken for each sample.

3. The Results

At applied magnetic field $-H_{c_1} < H_a < H_{c_1}$, each sample displays diamagnetic behaviour with a slope $H_a = -4\pi M$, but when the magnetic field $H_a > H_{c_1}$, there is nonlinearity of the magnetization, which is due to flux penetrating into the sample, and the transition to the mixed state. In our measurements, once the external magnetic field exceeds the first critical field H_{c_1}, the magnetization curve is no longer reversible, where the reverse path falls below the initial magnetization curve and leads to a hysteresis loop. The transition to the mixed state is not sharp, which is due probably to local flux gradient at the surface of the sample. This has been noticed also by Finnmore[5] (1966), on a single crystal of Nb. The average internal field in the sample $\langle B \rangle$ with irreversible magnetization curve is equal the vertical distance between the extension of the initial diamagnetic and the magnetization curve Figure III-2. Also the remanent value of $4\pi M$ in zero field, gives the value of the trapped flux remaining indefinitely in the sample.

The irreversibility in the magnetization curve is due to dislocations, impurities or deformations in the sample which provide trapping centres for the penetrating flux-lines.

3-1 Magnetization curves for the single crystal Nb.

In a pure single crystal which is uniform in composition and which does not have therefore Mendelssohn[7] sponge-structure there should be no barriers to trap flux. In such a homogeneous sample the normal channels

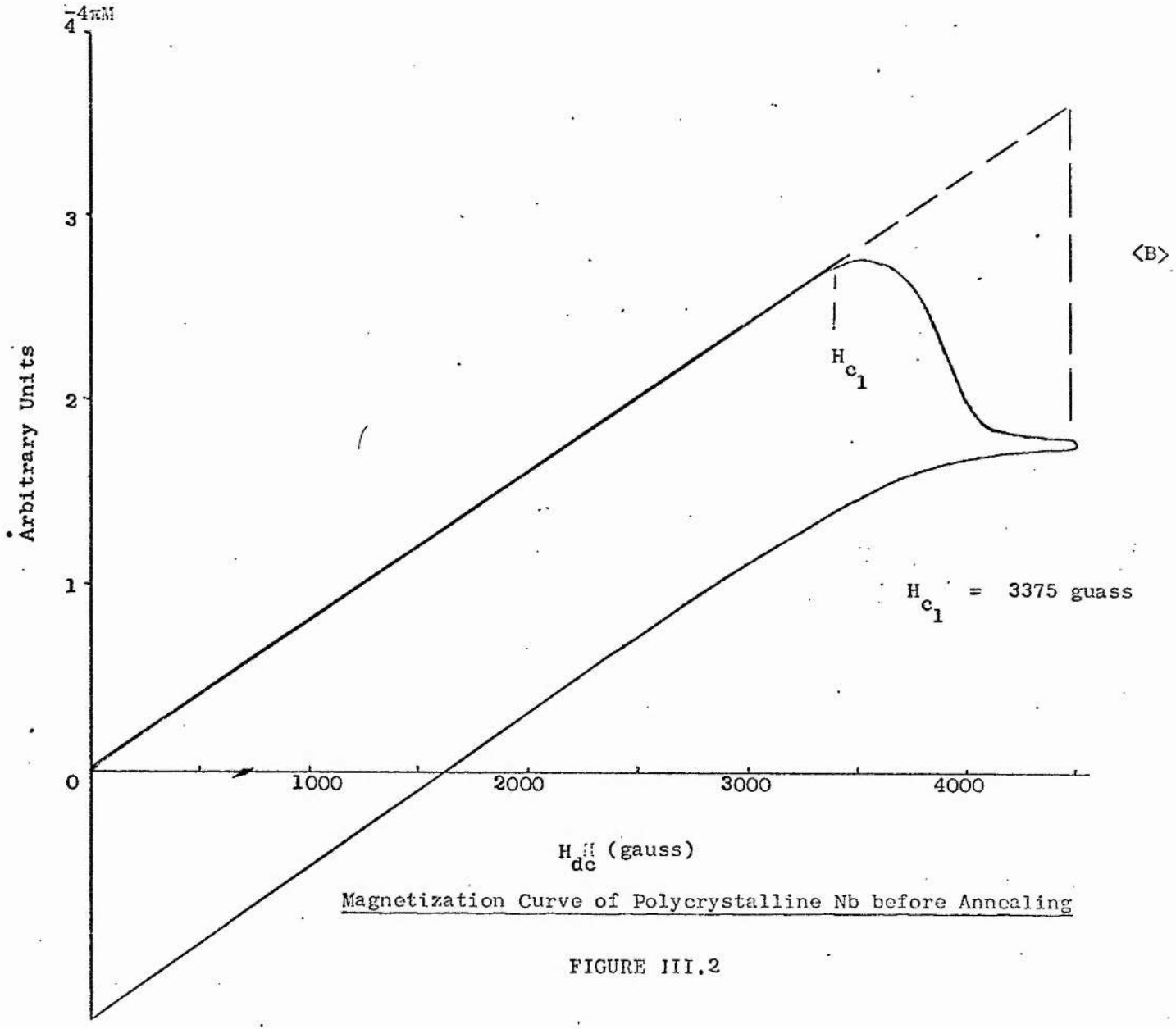

Magnetization Curve of Polycrystalline Nb before Annealing

FIGURE III.2

containing flux can migrate easily to the surface and expel the flux so that there should be no hysteresis in the magnetization.

Figure III.3, shows the magnetization curve for a single crystal Nb as it was received (Sample A) with H_{c_1} = 1330 gauss, where $H_{c_1} < H_a < H_{c_2}$, the minor hysteresis loop. (in case of major hysteresis loop, the magnetic field sweeps from 0 $\longrightarrow$ H_{c_2} and then back from H_{c_2} $\longrightarrow$ 0) obtained is probably caused by the dislocations in the sample. Such hysteresis loops were observed by Pippard[8], on single crystal of Sn-In, but on annealing the sample, it showed a reversible magnetization curve, because annealing swept the lattice clean of grain boundaries. French[9], found that the magnetization curves of single crystals Nb-Ta and Nb-Mo, are reversible which agrees with the Abrikosov[1] prediction. The reversibility of the magnetization curves such as Nb-Ta, and Nb-Mo alloys, where there are possibly great impurity concentrations and there are no regions with properties sufficiently different from the bulk of the material to act as barriers, suggests that a single atom does not act as barrier. Hence it may be expected that the dimensions of the barrier sites are at least as large or larger than the coherence length .

Figure III.4 shows the magnetization curve after the sample has been electropolished (Sample B), where H_{c_1} went up to about 1355 gauss, also the curve shows a sharper transition at H_{c_1} than Figure III.3.

Figure III.5 shows the magnetization curve for the same electropolished sample after the surface was polished, using fine polishing powder (Sample C). H_{c_1} increased to 1550 gauss and also the curve shows a sharper transition in the first critical field than before, which supports Bean and Livingston's prediction. They predicted for materials $\lambda \gg \xi$ (by considering the effects of attractive image forces experienced by flux lines near a surface) that plane surfaces can provide

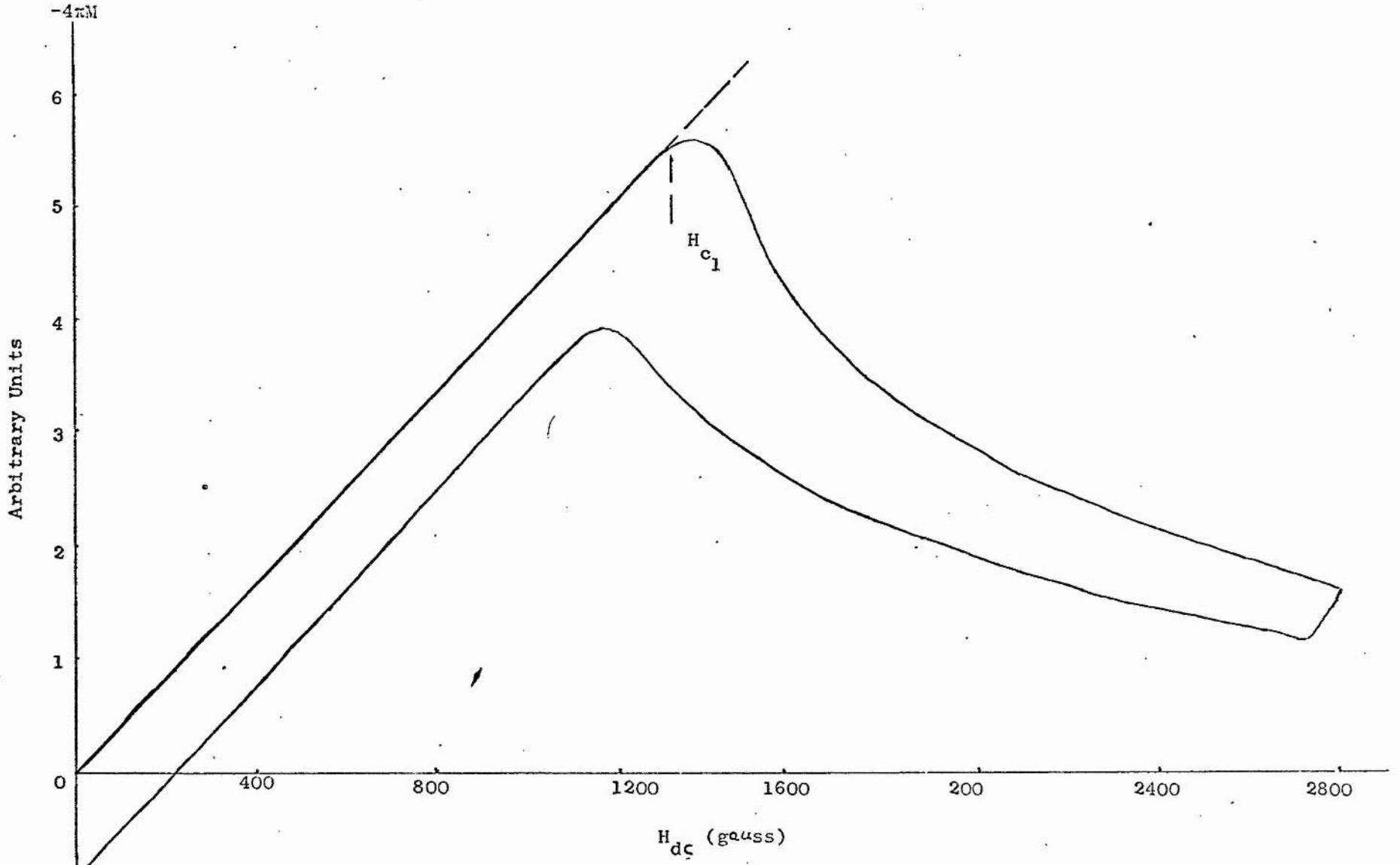

Magnetization Curve for Single Crystal Nb as Received

FIGURE III.3

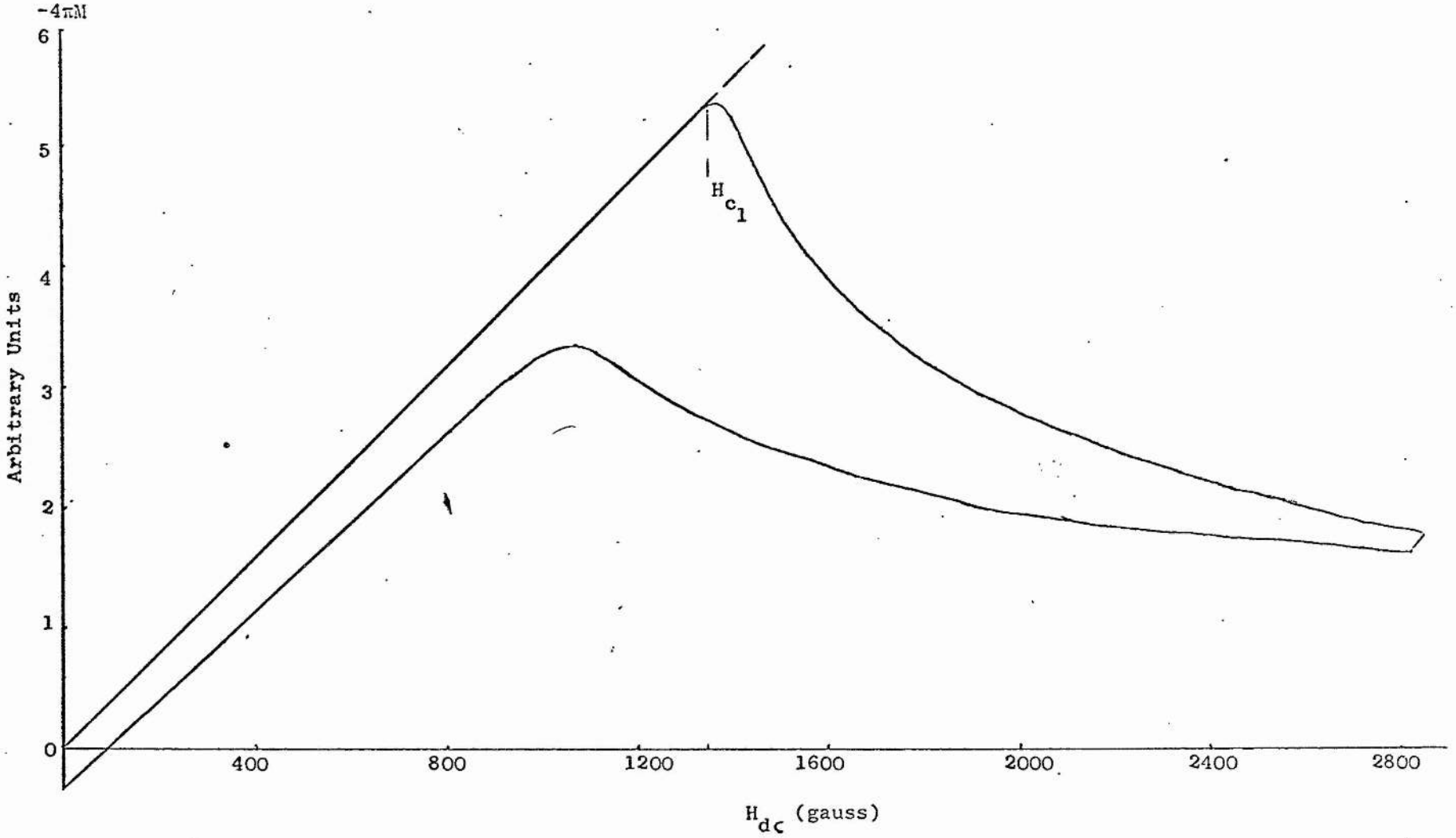

Magnetization Curve for Electropolished Single Crystal Nb

FIGURE III.4

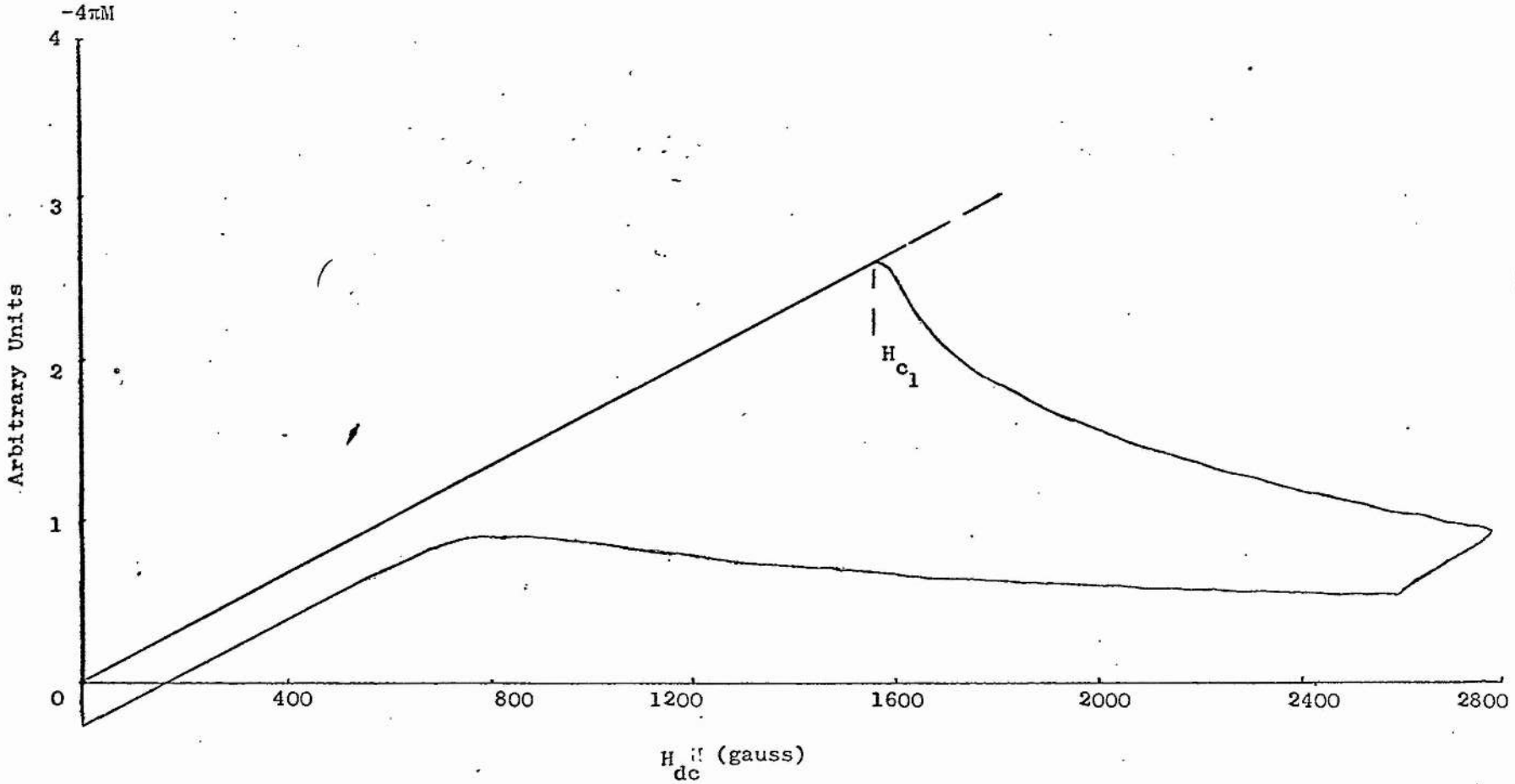

Magnetization Curve for Electropolished and Polished Single Crystal Nb

FIGURE III.5

an energy barrier to flux lines motion into or out of the sample. They pointed out that the flux line concentrations at surface irregularities and voids may create local fields less than H_{c_1} of the bulk of the sample, which are then sufficient to overcome the surface barriers, so that flux spreads into the rest of the sample at a low field. According to our magnetization curves, H_{c_1} is well controlled by the surface properties, which is related to the critical shielding currents which are higher in a smooth surface than the rough ones (See Section VI.4). By reducing the magnetic field, shielding currents at a smooth surface delay the expulsion of the flux which has been trapped by dislocations in the sample. In the same sample the area of the hysteresis loop is larger for smooth surfaces than for rough (Figures III.3, III.5).

3.2 Magnetization Curves of Polycrystalline Nb

Figure III.2 shows the magnetization curves of polycrystalline Nb as it was received. The first transition magnetic field was found to be 3,375 K gauss. This sample had been swaged and rolled from a large block of niobium. In order to improve the chemical and crystalline form of this niobium the sample was heated at a temperature between 900-1000 C, and at vacuum of about 10^{-5} torr for three days. At the end of the annealing period the sample was cooled slowly over two days while still under 10^{-5} torr vacuum. At the end of this treatment the magnetization curve was measured and H_{c_1} was found to have fallen to 656 gauss Figure III.6 (Sample D). This is probably the effect of degassing the material, which has been observed for Nb samples by a number of workers[10,11].

The first transition magnetic field H_{c_1} was found to be broadened over that of the single crystal, which is caused by the local flux gradients at the many impurities on the surface. When the sample was

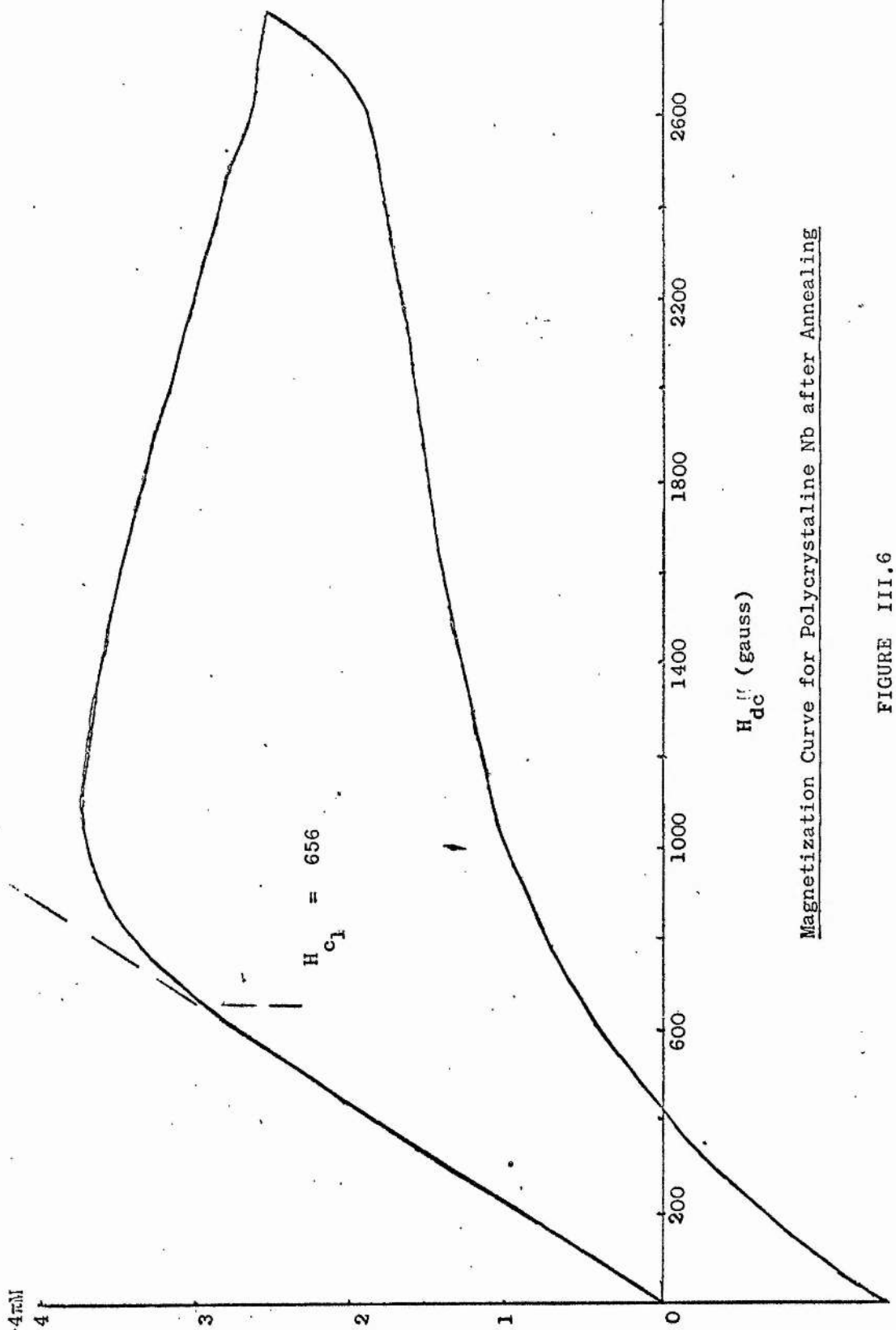

Magnetization Curve for Polycrystaline Nb after Annealing

FIGURE III.6

electropolished in the same way as the single crystal, the surface became rougher than before (Sample E). This is due to etching the impurities on the surface and exposing the crystallite boundaries. Here the flux penetrated at magnetic field H_{c_1} = 455 gauss Figure III.7a, then spread into the sample at lower magnetic field than before electropolishing.

When the sample was mechanically polished using fine emery papers and then fine polishing powder (Sample F), the magnetization curve (Figure III.7b) showed an increase in H_{c_1} to 616 gauss, but also that flux penetration to the bulk of the material is very much broaden than Figure III.7a. The enclosed area of the hysteresis loop in Figure III.7b is more than area enclosed in the hysteresis loop of the rough surface Figure III.7a.

This change between the two surface conditions gives good indication that the smooth surface has a high critical shielding current to prevent the flux lines spreading into the bulk of the sample. It has been suggested by Kwasritza and Wiker[12] from their results on Nb, that hysteresis is caused by the effects of flux trapping near the surface and by shielding current at the surface of the sample.

From the above results, for both single crystal and polycrystalline Nb magnetization curves, H_{c_1} increases with surface smoothness. This is caused by high shielding currents on the surface which prevent the flux from entering the surface of the sample. Our measurements are low field magnetization measurements, where $H_{c_1} < H_a << H_{c_2}$, which show that the surface of the sample plays a major role in determining H_{c_1}, and the hysteresis loop area.

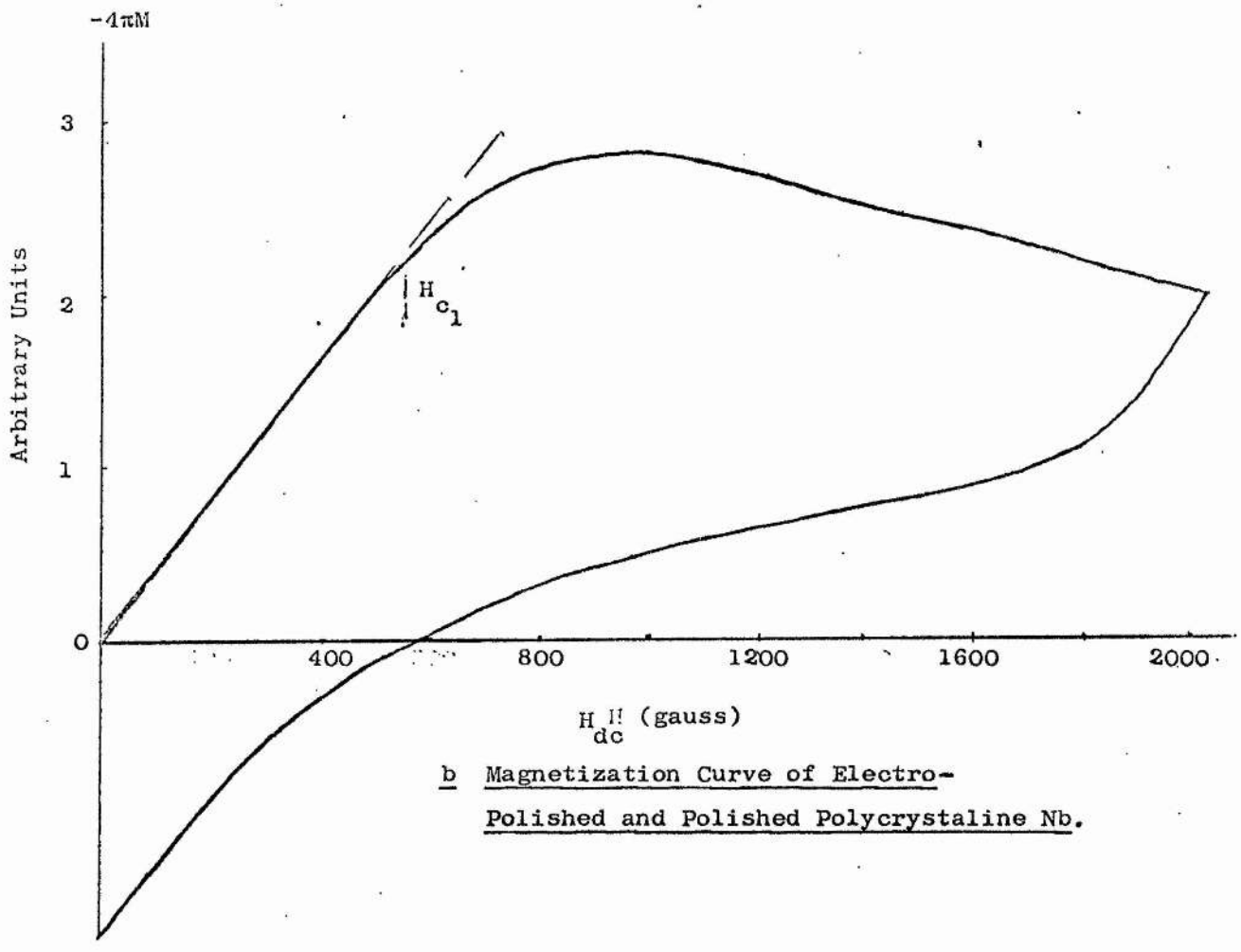

b Magnetization Curve of Electro-Polished and Polished Polycrystaline Nb.

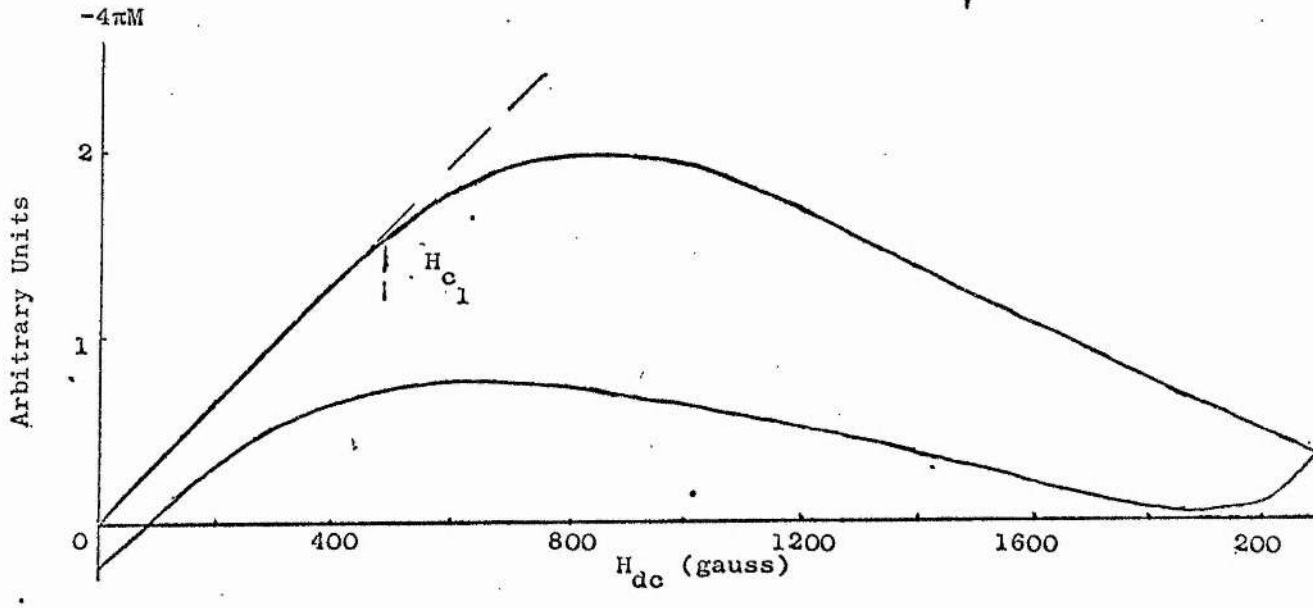

a Magnetization Curve of Electropolished Polycrystaline Nb

FIGURE III.7

References

1. Abrikosov A.A., J.E.T.P., 5, 1174 (1957).
2. Goodman B.B., Phys.Rev.Lett 6, 597 (1961); Phys.Lett. 1, 215 (1962).
3. Bean C., Phys.Rev.Lett 8, 250 (1962); Rev.Mod.Phys. 36, 31 (1964).
4. Introduction to superconductivity by Rose-Innes A.C. and Rhoderick E.H. (1969).
5. Finnemore D.K., Stromberg T.F. and Swenson C.A., Phys.Rev. 149, 231 (1966).
6. Bean C and Livingstone J.D., Phys.Rev.Lett. 12, 14 (1964).
7. Mendelsohn K., Proc.Roy.Soc., A152, 34 (1935).
8. Pippard A.B., Phil. Tran.Roy.Soc. 148A, 97 (1955).
9. French R.A., Lewel J., and Mendelsohn K., Cryogenics 7, 83 (1967).
10. De Sorbo W.T., Phys.Rev, 132, 107 (1963).
11. Beal W.T. and Meyerhoff R.W., J.Appl.Phys. 40, 2052 (1969).
12. Kwasniza K and Winkler W., Z.Physik, 227, 391 (1969).

CHAPTER IV

Flux Phenomenon

Type II superconductors are characterized by the mixed state, where the magnetic flux penetrates the material. This flux exists in the form of quantized flux lines (each line contains one quantum of flux $\phi_o = \frac{ch}{2e}$). In an ideal type II material the flux lines arrange[1] themselves in a triangular lattice. The flux line can be considered to contain a normal core which has a radius of the order of the coherance length ξ.

In the core of a flux line the superelectron concentration falls to zero, so that within the diameter of each core where the electron order decreases, there is a local increase in free energy $\sim$ $\pi \xi^2 \frac{1}{2} \mu_o H_c^2$ per unit length of the core. Each core is screened by circulating superelectrons which extend around the core out to , the penetration depth. Penetrating magnetic field is contained within the core of the flux line. The concentration of the flux lines (normal cores) increases with increasing magnetic field. At a magnetic field equal to the upper critical field H_{c_2} the cores of the flux lines overlap and superconductivity in the bulk material disappears.

Flux enters the sample as flux lines at the lower critical magnetic field H_{c_1}, and move freely, their motion being damped in perfect material only by an electromagnetic viscous friction force which is proportional to the flux line density. The motion of the flux lines is modified however in real materials because of the presence of chemical impurities, crystal defects and dislocations. Such defects act as pinning centers for flux lines. Under the action of a transport current flux lines can be dislodged from their pinning sites and move across the sample.

Such motion is reflected as an energy dissipation by the transport current.

In the next pages the effect of the surface on the flux pinning will be discussed on the light of the magnetization and the critical current measurements. Also the critical state and the flux motion will be briefly discussed.

1. The effect of the surface on flux pinning

At an applied magnetic field $H_a < H_{c_1}$ the sample exhibits total flux expulsion (Meissner effect), in this region no magnetic flux can cross the surface. The entry of the flux into the sample is governed by the same consideration and models[2,3] have been suggested which make use of a surface barrier to the entry of flux through a surface. Hence an increase in the applied field may not be accompanied by further flux penetration until the surface critical field or barrier is overcome. The presence of the surface barrier suggests that, with a perfect surface at absolute zero, flux lines may not be able to enter the surface until a higher field at which the barrier to the flux penetration has been overcome. According to the surface pinning mechanism, at magnetic fields $H_a \simeq H_{c_1}$, the flux lines which meet the surface of the sample are pinned at locations which make their free energy a minimum. Surface irregularities and surface defects can act as effective pinning sites. In these regions the electron m.f.p. is small which implies that the flux lines are attracted to such regions. Therefore the pinning force F_p, which is due to the local variation of the flux line energy ΔE_L over length δ is given by[4]

$$F_p = \Delta E_L \delta \qquad \text{(IV - 1)}$$

where

$$E_L = \frac{\phi_o}{4\pi} H_{c_1}$$

$$F_p = \frac{\phi_o \delta}{4\pi} \Delta H_{c_1} \qquad \text{(IV - 2)}$$

ΔH_{c_1} is the local decrease of H_{c_1}, which is due to the presence of a defect.

Our experimental results in both magnetization and critical current measurements show the effect of the surface in pinning flux lines. Figures III.3 and III.5 (Section III.3.1) show the magnetization curves for single crystal Nb with two different surface conditions (See SEM pictures of the two surfaces Figures II.1,3). (Section II.1), where Figure III.3 shows the magnetization curve for rough surface (Sample A) in which the flux lines enter the surface at magnetic field H_{c_1} = 1335 gauss. In Figure III.5 the magnetization curve for the same sample with a smooth surface (Sample C) is shown, and indicates that flux lines cross the surface at a higher field, H_{c_1} = 1550 gauss. This difference is due to the absence of pinning centers on the surface of the smooth sample. Here the Bean-Livingston surface barrier is larger, for the smoother the surface the harder it is to create nucleation centers from which flux lines can enter the surface. This effect can be seen also in Figure III.7[a] (Section III.3,2) which represents the magnetization curves for polycrystalline Nb, where Figure III.7[a] is the magnetization curve for the sample with rough surface (Sample E), and Figure III.7[b] is the magnetization curve for the same sample after smoothing the surface (Sample F), (See SEM pictures of the two surfaces Figures II.5,6 Section II.2). By comparing these two curves (E and F) we find that the flux enters the rough surface at lower fields than the smooth surface which indicates that the roughness acts as pinning centers.

The effect of the surface state on flux pinning can be seen in Figure VI.16 (Section VI.4) which shows that the critical current density for single crystal Nb is high with a smooth surface (Sample C) and low in the sample with rough surface (Sample A). Also in Figure VI.17 (Section VI.4) the critical current density for polycrystalline Nb is

shown, where the critical current density of the sample with rough surface (curve E) is lower than the critical current density of the same sample with a smooth surface (curve F). This fact can be explained as above, leading to the consideration that surface roughness represents an important source of pinning[5,6] sites.

At magnetic fields $H_{c_1} < H_a << H_{c_2}$ flux penetrates, and in this field range the distance between the flux lines d is large ($\lambda \sim d$). The surface nevertheless still maintains its importance, where the more smooth the surface the higher the critical current and the shielding field ΔH. Figure VI.19 (Section VI.5) shows the shielding field ΔH for single crystal Nb with three different surface conditions as stated before. The sample with smooth surface (Sample C) has higher shielding field than the sample with rough surface (Sample B). This also can be seen in Figure VI.20 (Section VI.5) which shows that the polycrystalline Nb with smooth surface (Sample F) has higher shielding field than the same sample with rough surface (Sample E). In this region of field the fluxoid lattice is relatively flexible, and fluxoids can bend to pass through many potential wells, i.e. as many pinning points as possible. The energy of one isolated vortex line is given[7] by

$$E_L = \left(\frac{\phi_o}{4\pi\lambda}\right)^2 \ln \frac{\lambda}{\xi} \qquad (IV.3)$$

where $\lambda >> \xi$, the normal core of radius ξ is very small and its contribution to the energy is neglected. But taking the contribution of the core to the line energy, the total energy is then

$$E = \left(\frac{\phi_o}{4\pi\lambda}\right)^2 \cdot (\ln \frac{\lambda}{\xi} + \varepsilon) \qquad (IV.4)$$

The numerical constant[7] ε includes the effect of the hard core and is of the order of 0.1.

When the applied magnetic field $H_{c_1} < H_a < H_{c_2}$, the state of the

surface is still important as stated above. In this range $\lambda < d$ and if the size of the pinning point b is greater than the distance between flux lines d, a number of flux lines are trapped on the same point. When $b < d$ only a fraction of possible pinning points trap flux lines. In both cases the pinning force is less than if $b \simeq d$, where one line only is pinned on each point, and the pinning force is given[8] by

$$F_p = \left(\frac{\phi}{4 \pi \lambda} \right)^2 \log \left(\frac{d}{\xi_o} \right) \qquad \text{(IV.5)}$$

$$= \frac{H_{c_1} \phi_o \log (d/\xi_o)}{4 \pi \log (\lambda/\xi_o)} .$$

$$(\lambda > d > \xi_o)$$

$$(b \sim d)$$

The measurements of the pinning forces have been reported by Ulmaier[9,10], using two methods. In the first, he calculated the pinning forces from the critical current density of the sample, and in the second one, from the magnetization curve of the sample. In both methods B and $\frac{dH}{dB}$ have to be known from the reversible magnetization curve of the same material.

2. The critical state

The superconducting sample is said to be in the critical state when the current density J or the field B is increased to a maximum value at which no vortex movement will occur and no voltage gradient in the sample arises.

If the superconducting sample is placed in an applied magnetic field $H_{c_1} \ll H_a < H_{c_2}$, because of the presence of defects in the sample, B (the magnetic induction) will not be equal to B(H) but varies from point to point over the sample volume. If we consider the variation

in the x-direction, when a macroscopic current J_y flows in y-direction, then $J_y = \frac{C}{4\pi} \frac{\partial B}{\partial x}$. Magnetic flux in regions of high line density (high B) tend to move towards regions of low density (low B) under the action of a pressure, P. This may be described in terms of pressure P in a two dimentional line system.

The force per unit volume in x-direction is $-\frac{\partial P}{\partial x}$, which is balanced by pinning force caused by structural defects. The pinning force must stay below a certain threshold value α (beyond this value superconductivity will collapse),

$$\left| \frac{\partial P}{\partial x} \right| < \alpha. \qquad \text{(IV.6)}$$

Hence the force acting on the flux lines per unit volume is

$$K_x = -\frac{\partial P}{\partial x} = -\frac{B}{4\pi} \frac{\partial H(B)}{\partial x} \qquad \text{(IV.7)}$$

where H(B) is the external field required to produce an induction B at thermal equilibrium.

As H(B) is nearly equal to B, then

$$\frac{\partial P}{\partial x} = \frac{B}{4\pi} \frac{\partial B}{\partial x} = \frac{BJ_y}{C} \qquad \text{(IV.8)}$$

Therefore the condition for the critical state may be written[7]

$$\left| \frac{B}{4\pi} \frac{\partial B}{\partial x} \right| = \left| \frac{BJ_y}{C} \right| = \alpha \qquad \text{(IV.9)}$$

3. Flux motion

According to Abrikosov's[11] notion of the quantized flux line, the smallest possible breakdown of superconductivity is the motion of a single quantum of magnetic flux through the sample. Therefore, when

a superconducting sample is in the mixed state under the action of an applied magnetic field and transport current passing through it, if the current density J or the magnetic field H_a increases beyond the critical values ($\frac{JB}{C} > \alpha$) so that the fluxoids just start to move through the material, a voltage appears across the sample indicating a new process,[12] called flux creep. This process continues so that just before complete breakdown of superconductivity movement changes to a process[13] called "flux flow" leading to linear relation between the voltage across the sample and the applied field.

3.1 Flux creep

In an inhomogeneous sample (hard superconductor) the flux lines are caught by pinning sites in the material, but when the critical value is exceeded, the flux lines to some extent bind together forming "flux bundles" by the interaction of their fields and wavefunctions. The central feature of the creep theory[12] is that flux pinned by physical irregularities present in the material can creep by thermal activation, the rate of creep being determined by relative strength of pinning forces and magnetic pressure.

It was proposed by Kim et al. (1963) that moving flux lines induced an electrical field, presumably by the induction mechanism ($\nabla \times E = -\frac{1}{c}\frac{\partial B}{\partial t}$). The presence of electric field implies power dissipation $P = E.J$ in hard superconductors.

Evetts et al.[14] (1964) reported that, by cycling the applied magnetic field from $+H_a$ to $-H_a$, where $H_a > H_{c_1}$, leads to power dissipation, where at $-H_{c_1}$ negative fluxoids can enter the sample, these will encounter positive fluxoids previously trapped in the sample, and be attracted to them. As they coalesce and annihilate their self-

energies will be released as heat.

Flux creep has been observed experimentally by Kim et al.[15] (1962) in hollow cylinders, and they[16] (1964) observed also the energy dissipation due to the flux creep in Nb-Zr wires.

Our experimental results on ac losses (Section VI.2) can be interpreted naturaley in terms of the flux-creep notion.

3.2 Flux flow

When the voltage across the superconducting sample is approximately linear in $\alpha[\alpha = \frac{JH}{C}$, where $H \simeq B = n\phi_o]$, the process is called[16] flux flow. Flux flow has been observed experimentally by otter et al.[17] (1966) in measuring the entropy carried by flux lines using an alloy of In with 40% pb. The superconducting d.c. transformer confirms the existence of flux flow.

References

1. Essmann U and Trauble H., Phys.Lett. 24A, 526 (1967).
2. Bean C.P. and Livingstone J.D., Phy.Rev.Lett., 12, 14 (1964).
3. Hart H.R. and Swartz P.S. Phy.Rev. 156, 403 (1963).
4. Van Gurp G.J., Philips Res.Report, 22, 10 (1967).
5. Joiner W.C.H. and Kulul G.E., Phy.Rev. 163, 362 (1967).
6. Mannison D and Rose R.M. Phys.Rev.Lett. 25, 356 (1970).
7. Superconductivity of Metals and Alloys by P.G. De Gennes (1966)..
8. Friedel J., De Gennes P.G. and Matricon J. Appl.Phys.Lett. 2, 119 (1963).
9. Ullmaier H., Papastalkoads K., Takacs S and Skilling W., Phys.Stat.Sol., 41, 671 (1970).
10. Ullmaier H., Phys.Stat.Sol. 17, 631 (1966).
11. Abrikosov A.A., Soviet Phys. JETP 5, 1174 (1957).
12. Anderson P.W., Phys.Rev. 9, 309 (1962).
13. Kim Y.B., Hempstead C.F., and Stranad A.R., 131, 2486 (1963); Phys.Rev. 139, 1163 (1965).
14. Evetts J.E., Campbell A.M. and Dew-Hughes D., Phil.Mag., 10, 339 (1964).
15. Kim Y.B., Hempstead C.F. and Stranad A.R., Phys.Rev.Lett. 9, 306 (1962).
16. Kim Y.B., Hempstead C.F. amd Stranad A.R., Rev.ModPhys. 36, 43 (1964).
17. Otter F.A. and Solomon P.R., Phys.Rev.Lett. 16, 681 (1966).

CHAPTER V

A.C. Losses in Superconductors

I. Introduction to ac losses

In a perfect type-1 superconductor the interior is screened by currents induced in its surface when it is placed in a magnetic field H_a. These currents penetrate the surface to a depth λ. During a change (an increase) in the applied field energy flows into this layer given by the Poynting vector S = EXH, where E is the electric field at the surface caused by the change in H_a, and this energy is stored in the increased magnetic field and partly in the additional kinetic energy of the screening current. The stored energy can be fully recovered by reducing the magnetic field. No energy losses are encountered for ac magnetic fields at moderate frequencies. At frequencies of about 10 MHz losses are produced because of the motion of normal electrons at temperatures close to critical, and in the microwave region energy losses are produced because of quantum transitions involving the superconducting energy gap.

On the other hand in perfect type-II superconductors the above behaviour occurs for $H_a < H_{c_1}$, and above this value of applied fields energy losses are encountered in ac magnetic fields. Above H_{c_1} magnetic field begins to penetrate the sample more or less uniformly finally to fully penetrate the material at H_{c_2}. Although the electrical resistance of the sample between H_{c_1} and H_{c_2} is zero measured with small currents, resistance does appear above a certain critical current density J_c. It is this feature which allows field to penetrate the material. In pure type-II materials J_c is low and nearly constant for $H_{c_1} < H_a < H_{c_2}$. A change in applied magnetic field in this region, $H_{c_1} < H_a < H_{c_2}$, is accompanied by current induced in the surface which arises so that the current density

exceeds J_c leading to resistivity ρ. The electric field ρJ so produced permits further field penetration to occur. The penetration field follows the changing applied field H_a with a constant difference, ΔH, where ΔH is the critical surface sheath screening field which must be overcome before penetration occurs.

The fact that the penetration and applied fields are "out of step" implies in ac magnetic field that an energy loss is produced in the sample over each cycle of the field; the Poynting vector at the surface of the superconductor averaged over one cycle is not zero any longer. A plot of flux penetrating the material against applied field shows a hysteresis loop, the area of which is proportional to the energy loss per unit volume per cycle. Losses are present through this mechanism whether the sample is placed in an externally applied field or carries transport current. The value of J_c is almost entirely determined by the perfection or imperfection of the sample. A high J_c indicates a sample with many defects which act as pinning centers for penetrating magnetic flux lines.

The distribution of the magnetic field and also the critical current in type-II superconductors has been described in a model by Bean[1] and London[2]; they consider the following conditions.

1. No superconducting current flows in a region where $H_a = 0$.

2. When the magnetic flux reaches the centre of the sample, the critical current density is independent of the magnetic field, so that the current flows throughout the entire volume of the sample.

3. If the current exceeds the critical current of the filaments in the material, the critical current density of the bulk sample $J_c = 0$ (i.e. the sample is normal).

Considering a cylinder of type II material of diameter 2R subjected to a changing magnetic field H_a, applied parallel to its axis. As H_a increases to a peak value H_m field penetrates to a certain depth ,

Fig V 1(a), where $\Delta = \frac{10H_a}{4\pi J_c}$ (Curl $H = \frac{4\pi J}{10}$) and within this superficial layer induced current flows with the critical current density J_c. In decreasing the field to a lower value, $-H_m$, the surface layer experiences an opposite e.m.f. and some flux may be trapped Figure V.1 (b,c) when the field is fully reversed to $-H_m$ the critical current has fully reversed in the same way Figure V.1 (d), when the field is increased again to a value H_m, the process is repeated and a hysteresis loop is obtained Figure V.2, where the energy loss per cycle is proportional to the area of the hysteresis loop ($P = \frac{1}{4\pi} \oint HdB$). In Figure V 2, OA corresponds to the flux penetration in Figure V (a), AC represents the decrease in the average penetration flux below its maximum value B_m, and CD corresponds to the reduced magnetic field $-H_m$. Increasing the field to $+H_m$ again produces flux change corresponding to OA, thus closing the hysteresis loop.

If the applied magnetic field is increased to a higher value H_p so that $\Delta = R$ the radius of the sample, Figure V 3(a), critical current flows throughout the whole volume of the sample, so J_c is a constant. Bean[1] has considered the hysteresis loop to calculate the a.c. power loss. In his model $B = H_a H_m / H_p \pm (H_a^2 - H_m^2)/2H_p \pm (H_m^3 + H_a H_m^2 - H_a^2 H_m + \frac{H_a^2}{3})/4H_p^2$ (V.1) where B is the volume average of the local field, while H_a is the applied magnetic field. H_p is the field that must be applied to the sample in excess of the bulk critical field in order that critical currents may be induced to flow through the entire sample, hence $H_p = \frac{4\pi J_c R}{10}$. The positive signs apply for the half cycle from $-H_m$ to H_m, and negative signs from H_m to $-H_m$. Therefore the energy loss per unit volume per cycle may be calculated from the area of the hysteresis loop

$$W_v = \frac{1}{4\pi} \oint HdB, \qquad (V.2)$$

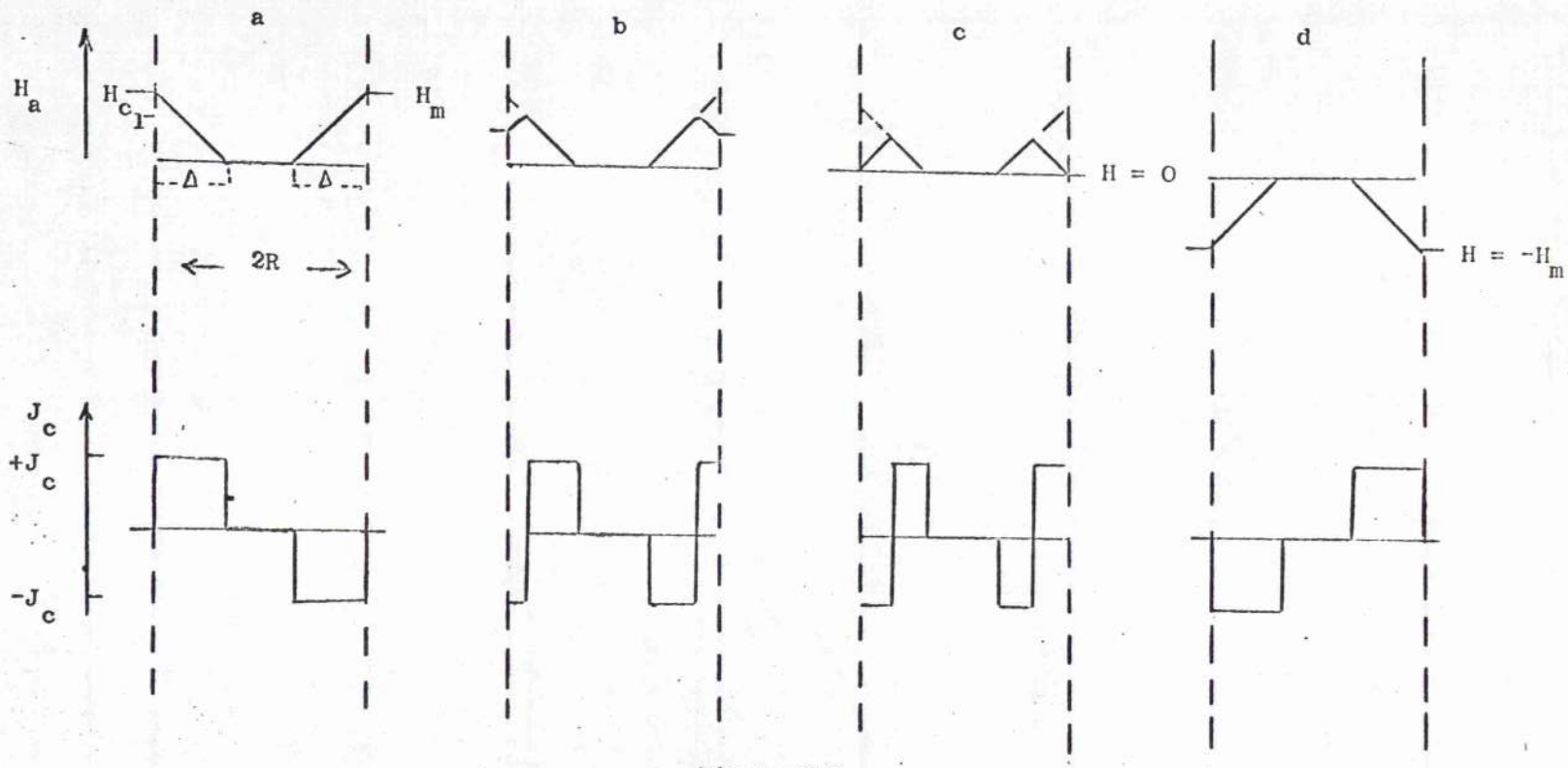

Figure V.1

Field penetration and screening currents inside the sample.

a. initial field penetration and also the critical screening currents,
b. field is reduced from maximum value H_m to a lower value,
c. field reduced to zero,
d. field is depressed to $-H_m$.

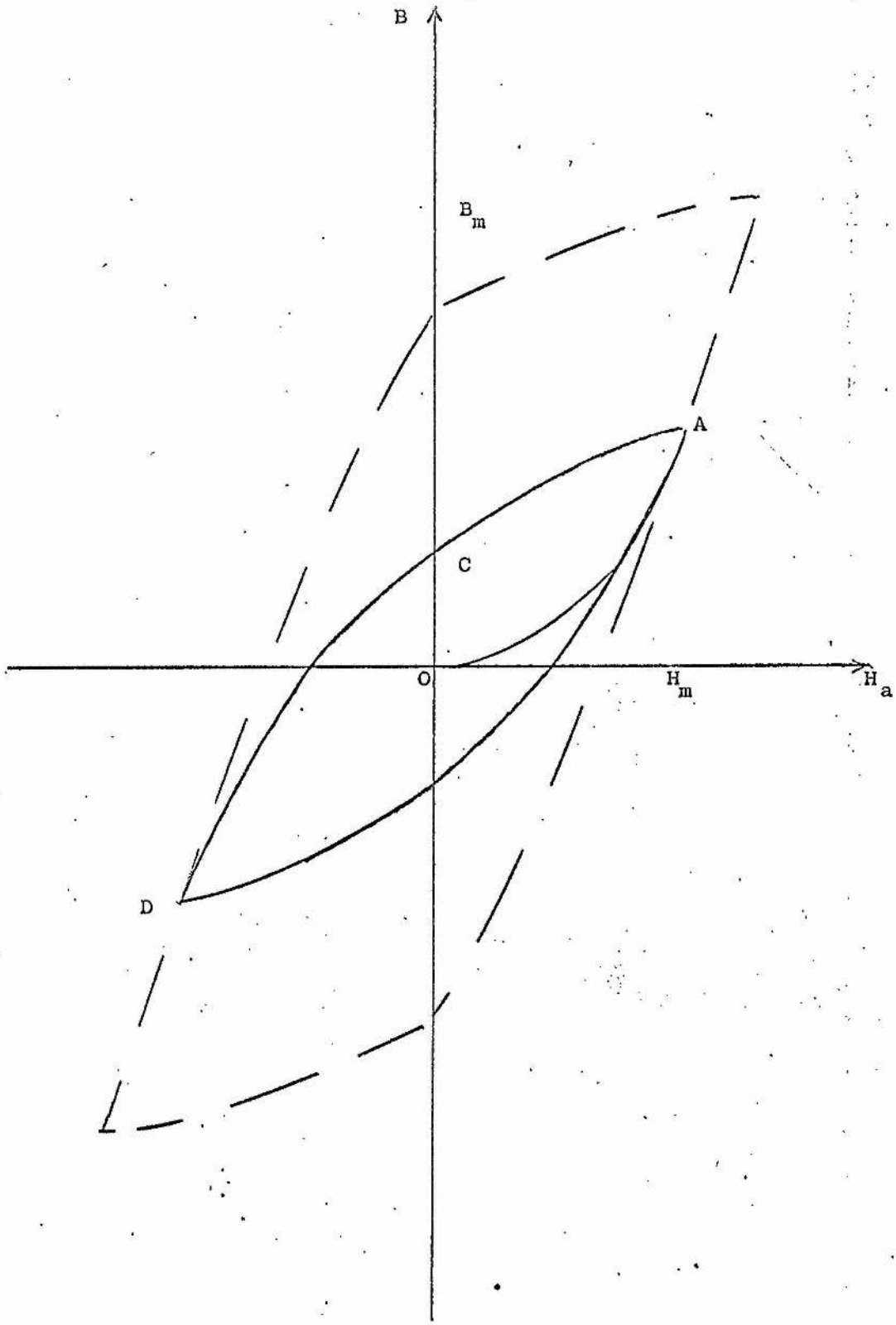

Figure V.2

Hysteresis loop (Bean's Model). The small curve for $\Delta < R$, and the broken curve for the case where $\Delta > R$.

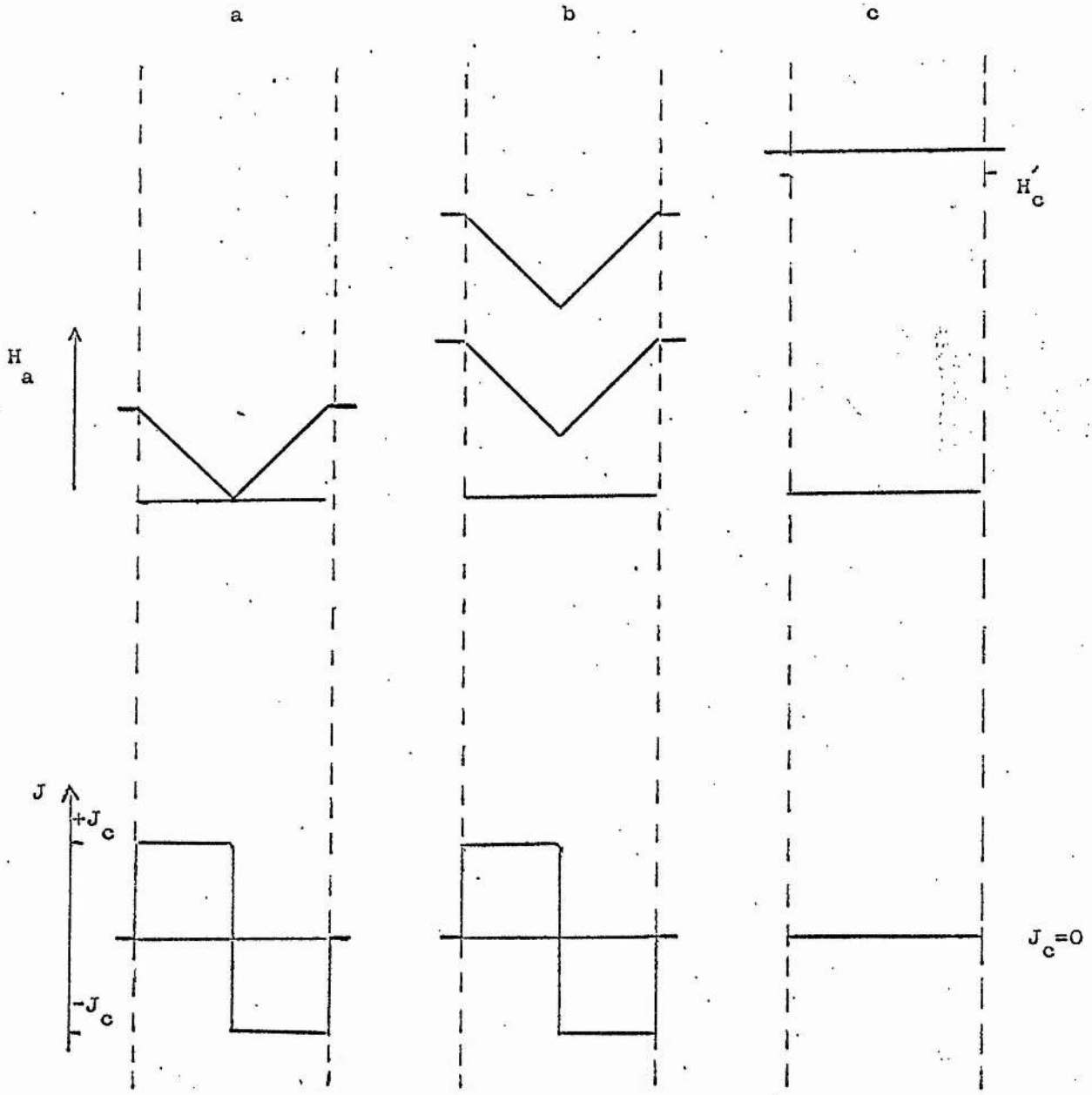

Figure V.3

Field penetration and current flows through the entire volume of the sample, where $H_{c_1} \ll H_m < H_{c_2}$, and $H_m > H_{c_2}$.

a. strong applied magnetic field where $\Delta(H) \gg R$
b. $\Delta(H) > R$
c. the field greater than H_c' the critical field of the filaments, therefore no superconducting current flows.

which gives for the cylindrical sample

$$W_v = H_m^3/3\pi H_p - 5H_m^4/16\pi H_p^2 \qquad (V.3)$$

For the case where $H_m \ll H_p$, the field does not reach the centre of the sample, so the loss in this case is a surface loss and is given by

$$W_s = \frac{5H_m^3}{12\pi J_c} \quad \text{ergs/cm}^2\text{/cycle} \qquad (V.4)$$

Therefore the power loss for an ac applied field of peak amplitude H_m is

$$P = \frac{5H_m^3 f}{12\pi^2 J_c} \times 10^{-7} \quad \text{W/cm}^2 \qquad (V.5)$$

where f is the frequency.

When the critical current is small (sample nearly perfect) and $J_c \propto \frac{1}{H_m}$ the power loss is $\propto H_m^4$.

Ullmaier[41] has extended the usefulness of this equation by considering the loss which occurs with a small modulating field h_m in the presence of steady biasing field H_{ext}. Ullmaier calculated the shape of the hysteresis loop for a type II superconductor consisting of a bulk region, in which the pinning forces dominate the magnetic behaviour, surrounded by a thin surface layer, which is capable of carrying surface current up to critical. The surface currents shield the bulk of the superconductor from the modulating field until this field reaches ΔH, whereupon a further increase of H_m causes an increase in the flux threading the bulk material.

Ullmaier shows that for small ΔH and for nearly constant J_c in the range $(H_{ext}-h_m)$ to $(H_{ext} + h_m)$ the power loss was identical to equation (V 5), with $H_m = h_m$. It is noted here that the critical current is proportional to $\frac{H_m^3}{P_{(ext)}}$, a relation which is used to measure the value of J_c at $H_{ext} > H_{c_1}$ (Section VI.4).

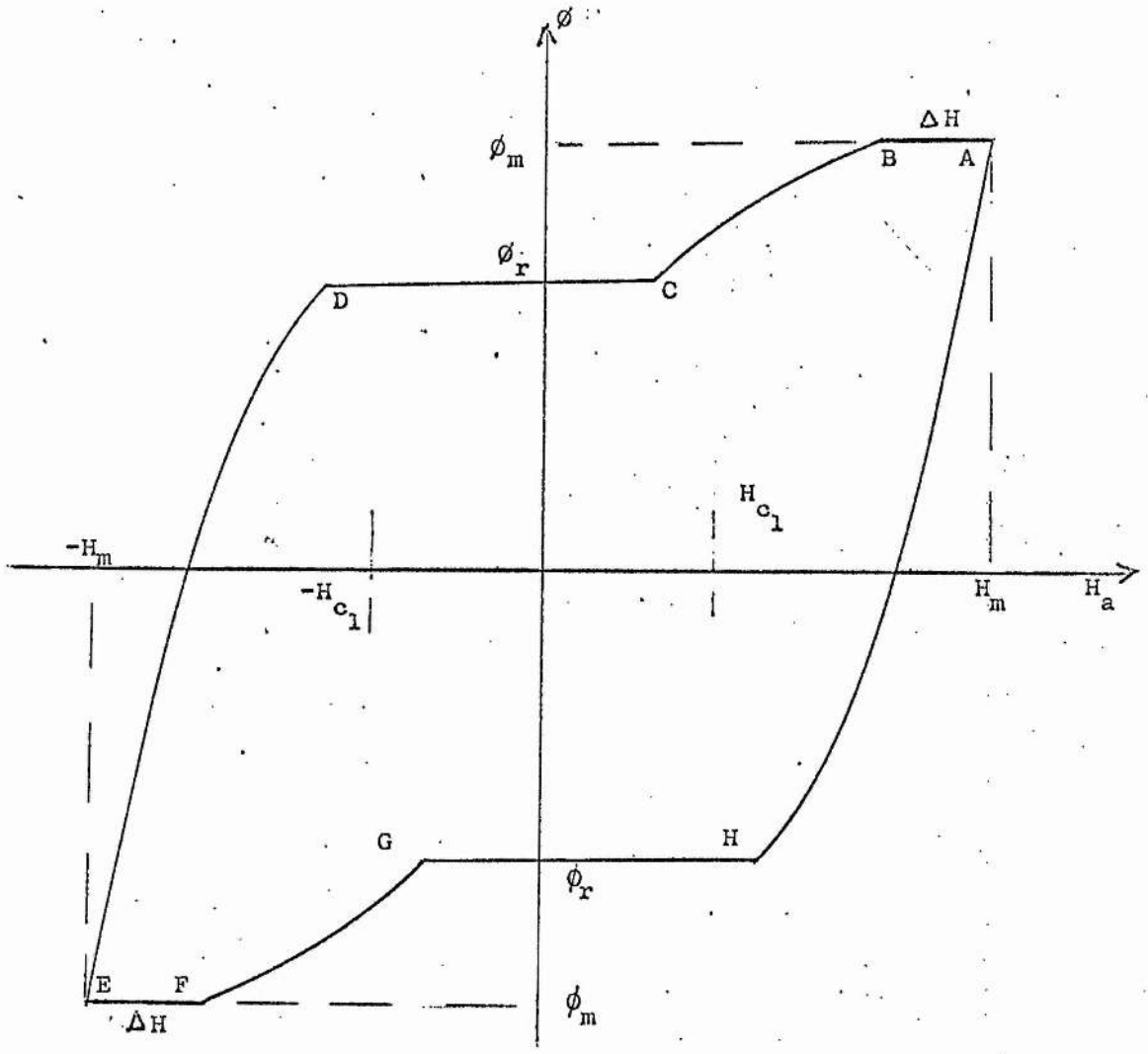

Figure V.4

Form of hysteresis loop based on the shielding currents

The hysteresis loss model described above by Bean (Figures V 1, V 2 and equation (V 5)) is simplified mainly in the feature that it does not include the effects of surface sheath currents present in superconductors in changing fields, H_a, in the range $H_m > H_{c_1}$.

A sample in the presence of an ac magnetic field of peak amplitude H_m (no dc biasing field present) experiences the effect of these diamagnetic currents which screen the interior of the superconductor, at the extreme of the waveform. At the extreme, $\pm H_m$, surface currents screen the bulk of the superconductor and cause flux to be trapped as H_a decreases by ΔH. This is shown in Figure V.4, by portions AB, EF of the ϕ, H_a loop. The effective field in the interior of the sample is altered by ΔH so that trapping for $-H_{c_1} < H_a < H_{c_1}$ is offset, and is indicated by the regions CD and GH in Figure V.4.

Detailed consideration of this type have been made by Dunn and Hlawiczka[42] and lead to an expression

$$P = \frac{5 \times 10^{-7} f}{12 \pi^2 J_c} (H_m')^2 (1.5 H_{c_1} + \frac{3}{2} \Delta H + H_m') \text{ W/cm}^2 \qquad (V.6)$$

where $H_m' = (H_m - \frac{\Delta H}{2} - H_{c_1})$ for the power loss in this range of applied magnetic fields. The effectiveness of this equation in describing ac power losses in superconductor have been considered in this work. In Section VI.3 the power has been calculated from measurements of J_c, ΔH, and H_{c_1} and compared with losses measured experimentally. In any case the loss per cycle is independent of waveform depending solely on the peak applied magnetic field.

In any real sample of type II superconductor the above models are complicated by defects present in the sample. In applied ac magnetic fields with peak fields $H_m < H_{c_1}$ there may be small energy losses which

are due to surface defects[3]. These defects can be impurities in the material, or voids of microscopic dimensions which are close to the surface. These reduce H_{c_1} and cause local premature flux penetration. Surface roughness (perhaps not discernible by eye in a polished surface) reduces H_{c_1} locally, causing early flux penetration. Small losses can arise in this way whereas none would be expected for field values below H_{c_1}.

In type II superconductors, Buchhold[3] considers two possible loss mechanisms for $H_m < H_{c_1}$. The first is due to a magnetic hysteresis loss, which increases with trapped flux and the area enclosed by the hysteresis loop; this loss should be proportional to H_m^2 and to the frequency $f(P \propto f H_m^2)$. The second is due to eddy current loss which is caused by local normal regions in the superconductor. The existence of these regions in the presence of the alternating magnetic field leads to eddy current loss proportional to f^2B^2, where B is the magnetic induction created within a normal layer. Buchhold suggested that the eddy current loss is very much smaller than the hysteresis loss and negligible in the frequency region 25-1000 Hz.

To demonstrate[39] the type of loss encountered when ac magnetic fields are applied to a superconductor, consider a type II superconducting sample which shows irreversibility in its magnetization characteristics. Figure V.5 shows the magnetization curve of a cylindrical sample of type II superconductor, the sample is parallel to an applied magnetic field. It shows three regions of different types of losses. In region I in which $H_m < H_{c_1}$, the sample is diamagnetic, changing the field induces critical shielding currents (either positive or negative) at the surface of the sample which prevent flux from entering the sample. In this region no loss is expected, but if there is any loss it depends on the surface properties of the sample. In region II $H_{c_1} < H_m < H_p$ (H_p when the field

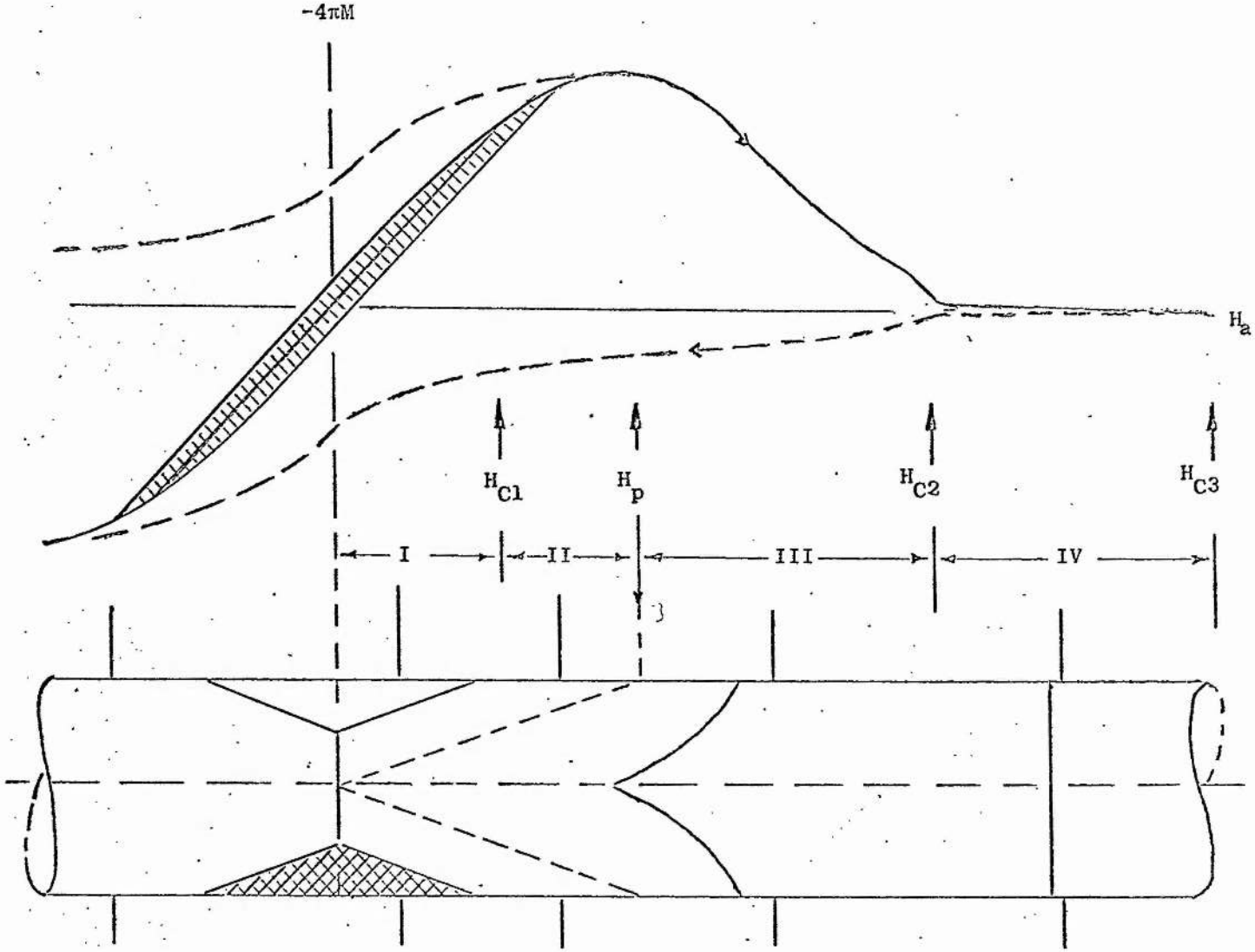

Figure V 5

AC losses regions (Ref. 39)

penetrates the bulk of the sample) flux penetrates the surface as individual quantum flux lines which become pinned to defects and imperfections in the material. In an alternating field flux lines are moved against the pinning forces giving rise to a phase lag between the flux and applied field indicating loss. The effect of pinning is shown in the value of the critical current density of the material J_c in this region.

In region III where $H_p < H_m < H_{c_2}$ flux penetrates the whole volume of the sample and losses occur throughout the volume of the sample. In this region Beall and Meyerhoff[4] reported that ac loss results agreed better when compared on the basis of surface area rather than volume, indicating perhaps that losses still occur mostly at the surface of the sample. In this region a rise of temperature of the whole sample will drastically affect losses through a consequent change in H_{c_2} and J_c.

We should note that losses in superconductors are quite unlike ohmic losses. They depend on the magnitude and direction of the magnetic field. For example in Nb_3Sn strips 7μm x 2.5 mm, if the magnetic field is perpendicular to the current and parallel to the surface of the strip the loss = 0.06 w/m, but for the same strip if H is inclined 10^o to the surface the loss = 3.6 wm^{-1}.[45].

II. Survey of AC Losses at Low Frequencies

In the following section ac losses reported in the literature will be discussed

1. AC losses below H_{c_1}
2. AC losses above H_{c_1}
3. Loss dependance on temperature
4. Effect of edges and thickness on loss
5. AC losses in coils

1. AC Losses Below H_{c_1}

According to Buchhold's model[3], surface roughness, and the presence of voids and imperfections at the sample surface influence field penetration by distorting field lines so that it is possible for H_{c_1} to be exceeded locally although $H_m < H_{c_1}$ for the bulk.

For this reason losses would occur at $H_m < H_{c_1}$ whereas for a perfectly smooth surface no loss would be expected until $H_m > H_{c_1}$. By polishing the surface of a superconductor it is expected that the value of H_m at which energy losses first begin would be increased.

Buchhold[5] et al. (1962) investigated ac losses of cylindrical rods of Nb and Pb at low magnetic fields and low frequencies. Losses were measured by means of measuring the temperature rise of a sample knowing its specific heat. They related the losses to be associated with slight field penetration and flux-trapping which depends on the surface properties and arises from the alternating trapping and releasing of small amounts of flux during each cycle of the external field.

Wisseman et al.[6] (1964) measured ac losses in Nb-25% Zr wires as a function of frequency. The power loss was found to be linear with frequency, which is in agreement with Buchhold[3] and Rocher[7] et al., and indicates that losses are hysteretic in nature.

Rocher[7] et al. (1967) reported that losses depend, apart from field and frequency, on a number of factors such as resistivity ratio, cooling in the absence of magnetic field, and on the surface finish. Surface roughness and trapped flux were found to be the main factors responsible for losses. These conclusions are consistent with results reported by Easson[8] et al. (1967) that losses in Nb foils increased with roughness of the surface. Brankin[9] et al. (1970) suggested that losses in Nb arise from penetration of flux lines at surface roughness and at impurities. Male[10] (1970) has reported recently 50 Hz loss measurements in foils and

tubes, finding that loss was caused by trapped flux in the surface of the sample.

These results show that the nature and properties of the surface play a fundamental role in determining ac losses for H_m below H_{c_1}.

2. AC Losses above H_{c_1}

The transition at the first critical field H_{c_1} is accompanied by a large change in the power loss. This change depends on the surface state of the sample, if the surface is smooth the change in loss is sharp, but if the transition at H_{c_1} is gradual due to impurities and surface roughness, the change in ac loss also takes place gradually.

At magnetic fields $H_m > H_{c_1}$, the field penetrates as flux lines carrying quantum of flux and because of dislocations and impurities in the material these lines are trapped forming fluxoids. Movement of flux lines causes circulating currents around the trapping centres, giving rise to power dissipation in the sample. This has been predicted by Bean[1] (1962, 1964) and London[2] (1963) and is known as "the critical state" model. According to this model, the loss per cycle is proportional to H_m^3 when J_c is independant of H_a. To check the Bean-London model, that losses are hysteresis losses, Kamper[11] (1962) measured ac losses of rings made of a eutectic alloy of lead and bismuth, and Figgins and Shepherd[12] (1964), made similar measurements. Both results confirmed the Bean-London model for both showed a linear dependence of power loss on frequency. Hart and Swartz[13] (1964) compared the losses of V_3 Ga powder and Nb_3-Sn rings and found agreement with the model at both 60 and 600 Hz within a factor of two over a wide range of ac magnetic fields. From these and similar measurements[14,4] the validity of the Bean-London model appears to be good.

3. Loss Dependance on Temperature

The value of H_{c_1} depends strongly on temperature. Finnemore[15] et al. (1966) studied the superconducting properties of pure Nb, showing that the variation of H_{c_1} with temperature T follows the form expected from two fluid model.

$$H_{c_1}(T) = H_{c_1}(o)\left[1 - \left(\frac{T}{T_c}\right)^2\right] \qquad (V.7)$$

In the case of niobium T_c for pure material is 9.2 K.

Easson[8] et al. (1967) measured H_{c_1} as a function of $(\frac{T}{T_c})$ to obtain H_{c_1} = 1.4 K gauss at 4.2 K. Extrapolation to OK gave $H_{c_1}(O)$ = 1.74 K gauss in good agreement with results of Finnemore[15]. Wisseman[6] et al. (1964) measured ac losses in Nb-Zr wires as function of temperature, and found that losses decreased approximately as $T^{2.5}$ in the temperature range 2.0 to 4.2 K. No other ac loss measurement has been made so far below the λ-point of liquid helium, making use of superfluid helium as a heat exchanging medium. Rogers[16] et al. (1964) investigated 50 Hz losses in Nb foils as a function of increasing temperature from 4.2 K to 6.5 K, and found for 25 μm foils, and current density 375 A cm^{-1} at 4.2 K no detectable loss, and could maintain the same current density at 6.0 K with loss no more than 10 $\mu W/cm^2$. Buchhold[17] et al. (1969) made measurements of ac losses in cylindrical Nb samples with machined and mechanically polished surface as a function of increasing temperature, finding that the loss was several hundred times lower if the sample was cooled quickly from room temperature to liquid helium temperature than if the sample was cooled at a slow rate, e.g. cooling in liquid N_2 overnight. This phenomenon is due apparently to metallurgical changes in the cold-worked Nb surface under slow cooling. They observed also the residual deformation of the surface of a highly polished sample caused by slow cooling under a microscope after warming

the sample to room temperature. Grigsby[18] et al. (1970) on the other hand could find no change of ac loss in 120 μm Nb foils when they were cooled rapidly or slowly. As the surface of these foils was not highly polished the influence of surface roughness probably masked any effect on losses due to cooling. These results confirm the importance of the surface finish and the history of the sample on ac losses.

4. Effects of Edges and Thickness on Losses

1. Edges Effect

When a superconducting sample is subjected to a magnetic field, where the field is the same value along the sample, the ends of the sample may be a source of dissipation. Because screening current concentrates in the surface at the ends, the local critical field is lowered so that edges will show larger loss than the centre of the sample. Heat will flow from edges into the rest of the material and into surrounding medium at a rate which depends on the temperature increase of the edges. Therefore in ac losses measurements, the edges of the sample should be prepared in such a way that would not produce loss before the rest of the sample.

Easson[19] et al. (1967) measured ac losses of Nb rings with different lengths, they observed that losses are higher in short samples. Rogers[16] et al. (1969) found that losses of 25 μm foils of Nb decreased by folding the edges, and this has also been reported by Grigsby[18], using Nb foils with various thickness (25 μm $\rightarrow$ 175 μm).

2. Thickness Effect

It has been suggested and demonstrated by some workers that ac losses are surface losses and that the currents leading to loss are present in the surface.

Tanako[20] (1967) made measurements of ac losses of Nb, Nb-Ti and Nb-Zr wires in various diameters (ranging from 0.13 mm to 0.5 mm, and 10 m long) and found that losses decrease with the wire diameter. Easson[21] et al. (1966) did not observe any change in ac losses of small rings of Nb with thickness ranging from 0.06 to 10 cm diameter. The variation in losses from sample to sample is difficult to observe, because the reduced loss in decreasing the thickness is compensated, because the edges become important in increasing losses with decreasing thickness. In recent measurements of ac losses of Nb strips of different thickness (25 μ m to 250 μ m) Linford[22] et al. (1971) found that losses decrease with decreasing thickness of the strip and also the thinnest sample had the highest critical current density. Grigsby[18] et al. observed that losses decrease if Nb strip is hardened.

We may conclude for ac applications that thin Nb strips with a good surface finish which can be easily handled are the most promising type for superconducting cables and machinery.

5. AC Losses in Coils

Losses in superconducting coils are measured usually by the boil-off helium method. This is done by passing an ac transport current[20,23] through the coil, or subjecting the coil to an ac magnetic[24] field, or both[25]. London[2] (1963) predicted a model for ac losses in coils, considering a long coil closely wound from superconducting flat strip, where the thickness of the winding is much smaller than the radius of the coil, assuming that the temperature in the coil does not change. The loss per cycle per unit surface of the whole coil is given by

$$P = \frac{4}{3} \left(\frac{H_m^2}{8\pi} \right) t \quad W/cm^2/cycle \qquad (V.8)$$

where t is the thickness of the strip. Jones[25] et al (1963) reported measurements of ac losses of Nb-25% Zr coils. They interpreted their results as eddy current losses, finding an expression for the power loss $P \alpha (H_m^2 f^{\frac{1}{2}})^x$ where $x \simeq 3$. The exponent x is due to the temperature rise in the coil. London suggested that their results could be interpreted on the basis of a hysteresis model, where the power loss is given by $P \alpha H_m^4 f$.

Zar[26] (1964) measured ac losses in Nb-25% Zr wire in the form of short-circuited coil, finding the loss per cycle proportional to I_m^2 which is consistent with London's model. Rhodes[27] et al. made measurements of 50 Hz losses in Nb, pb, and Nb-Zr coils over a wide range of current densities up to the critical values of the coils. They found that losses occur at currents less than the critical value and increase rapidly as the critical current is approached. Their results show that the losses are surface losses. Grenier[28] et al.(1965) investigated ac losses in various coils of Nb-25% Zr wire at frequencies between 45 to 400 Hz, with results in good agreement with London's model. Petch[23] et al. (1967) suggested from their results on different coils of Nb Zr that ac losses occur at the surfaces of the layers in the windings of the coils.

We may conclude therefore that ac losses in superconducting coils below the critical current of the coil can be explained as surface losses of a hysteretic nature in agreement with London's model. When the temperature of the coil rises due to approaching the critical current, the contribution of eddy currents caused by normal regions must be taken in account, so that the total loss is the sum of hysteresis and eddy currents losses.

III. Methods of AC losses Measurements

Different techniques have been used for ac losses measurements.

1. Boil-off Calorimetry
2. Adiabatic Calorimetry
3. Current-voltage Measurements
4. Hysteresis loop Measurements
5. Q-Measurements on L-C Circuits
6. Wattmeter Techniques. (Used in this study)

1. Helium Boil-off Calorimetry

This technique is suitable for measuring ac losses of superconducting long wires and coils. The calorimeter is usually made of nylon, which is immersed in the helium dewer. It has small holes in the bottom for passing liquid helium into its interior, the top is connected to a tube leading to a gas flowmeter. The heat produced in the sample, which is placed inside the calorimeter, is measured from the amount of helium gas evolved in a given time. The sensitivity of the measurement depends on the sensitivity of the gasmeter. The minimum power dissipation which has been achieved so far by this method is about 0.05 μ w.

Various results have been obtained by this method[25,27,30] and good agreement has been achieved with other methods[30,14,4] of measuring losses.

The advantages of this technique are that it is a simple, straightforward measurement, and it measures the total loss whatever its nature. On the other hand it has disadvantages, it is not sensitive enough, does not differentiate between hysteresis and eddy current losses, heat leaks into the calorimetry are unavoidable, and it is not suitable for short samples.

2. Adiabatic Calorimetry

A similar technique has been used for measuring the thermal conductivity[31]

and specific heat[32] of superconducting materials, and also non-superconducting[33] materials in the low temperature range. The principle of this technique determines that the sample is placed inside a chamber which is immersed in liquid helium, the sample in the calorimeter is subjected to an external ac magnetic field and its temperature rise measured by a resistance thermometer. The power loss can be calculated from the temperature rise, the known heat capacity of the sample and the time for which the field was applied.

Buchhold[5] et al. (1962) the first workers to measure ac losses of Nb, Pb and Nb-Zr cylindrical samples subjected to alternating magnetic fields. The sensitivity of their measurements was about 5×10^{-10} W/cm^2/cycle. Wisseman[6] et al. (1964) also reported measurements of ac transport current losses of Nb-Zr wires, by measuring the thermal conductivity of the samples, using the same technique, the minimum power loss observed was as low as 10^{-13} W/cm^2/cycle with a minimum detectable change of temperature of 0.15 m.deg. K. Other workers[7,16] measured ac losses of Nb using the same technique and similar principle of the measurement. The high sensitivity of this technique makes it preferable for power dissipation measurements below H_{c_1}. It is not a suitable technique for large samples, because thermal isolation is difficult, and also it is not good for long samples, because the time constant for thermal equilibrium is too long.

3. Current-voltage Measurements

AC losses have been measured by this method by a number of workers[30,34,3] The sample in this case carries transport current, in some cases in presence of magnetic field. Losses are obtained by measuring the resistance across the sample, where the observed voltage is proportional to the losses. This technique is not suitable for ac measurements at low fields, the measured losses are near the upper critical field H_{c_2}. Sensitivities

are limited to 10^{-5} W/cm^2/cycle.

4. Hysteresis Loop Measurements[11,12,21]

By means of a pick up coil wound on to the sample an induced voltage can be obtained which is proportional to the rate of change of flux crossing the surface of the sample. The total flux penetrating the sample is obtained by integrating this voltage. The sensitivity of this method is about 5×10^{-4} W/cm^2/cycle.

5. Q-Measurements on L-C Circuits[36]

At very high frequencies (h.f. and v.h.f. ranges) the Q of a resonant circuit containing a coil of superconducting wire is measured. This method can be used for many sample configurations. The measured Q of the circuit leads to a measure of the average rate of loss in the circuit. To achieve high Q's it is found that material free from strain and impurity must be used, and that the highest Q's are obtained for highly polished materials ($Q = 10^{10}$ for high surface finish in Nb). Microwave cavities plated with a superconductor can be used at higher frequencies in these measurements.

The interest in the latter arises from their possible use in linear accelerators.

6. Wattmeter Technique (Technique employed here)

This technique was adopted by Buchhold for ac losses measurements. In this technique the superconducting sample is subjected to an external ac field, and a pick up coil is wound directly on the surface of the sample to detect the time rate of change of flux $(\frac{d\phi}{dt})$ penetrating the sample. The average power loss per unit surface area is derived from the following expression,

$$P = \frac{1}{NST} \int_0^T Hedt \qquad (V.9)$$

where T is the period of the modulating field, S is the sample area, e is the voltage signal from the pickup coil of effective number of turns N. This technique has been used recently by a number of workers[24,38,21,17,22], particularly because of its accuracy and simplicity, and for this reason this was chosen for the current work. The sensitivity in the range of 10^{-8} W/cm^2/cycle has been quoted.

IV Theory of Watimeter Technique for Ac Losses Measurements.

When an alternating magnetic field $H_m \geqslant H_{c_1}$ is applied to a superconducting sample, the instantaneous rate of flow of energy into the sample is given by Poynting's vector

$$\frac{dW}{dt} = \frac{1}{4\pi} (EXH) \text{ c.g.s. electromagnetic units} \qquad (V.10)$$

where W is the instantaneous energy per unit surface area of the sample, E is the electric field caused by the change in magnetic flux at the surface of the sample, the relation being

$$E = -\frac{1}{S}\frac{d\phi}{dt} \qquad (V.11)$$

$S = 2\pi r$ where r is the radius of the cylindrical sample. As E and H are mutually perpendicular, then

$$\frac{dW}{dt} = \frac{1}{8\pi^2 r} H(t) \frac{d\phi}{dt}$$

The output voltage of the pickup coil e(t) is given by

$$e(t) = -N \frac{d\phi}{dt} 10^{-8} \text{ volts} \qquad (V.12)$$

e(t) is the penetration voltage and N is number of turns of the penetration coil. Hence

$$\frac{dW}{dt} = \frac{10^8}{8\pi^2 rN} H(t).e(t) \qquad (V.13)$$

and the total energy dissipated in one complete cycle per unit surface area of the cylindrical sample is given by

$$W = \frac{10^8}{8\pi^2 rN} \int_0^T H(t),e(t)dt \quad \text{erg/cm}^2$$

The power loss at frequency f is P = Wxf

$$P = \frac{10f}{8\pi^2 rN} \int_0^T H(t).e(t)\ dt \quad W/cm^2 \qquad (V.14)$$

In experimental measurements the value of H(t) is obtained from the voltage $V_H(t)$ appearing across a standard resistance placed in the coil circuit which produces the external field. Hence $H(t) = K_H V_H(t)$ and

$$P = \frac{10fK_H}{8\pi^2 rN} \int_0^T V_H(t).e(t)\ dt \qquad (V.15)$$

Again experimentally the value of $V_H(t)\ e(t)$ is obtained by using an electronic multiplier, the output voltage of which can be expressed as $V_p = K_c V_H(t)\ e(t)$ when the phase of $V_H(t)$ and e(t) is correctly adjusted, where K_c is the multiplier constant so that

$$P = \frac{10fK_H}{8\pi^2 rNK_c} \int_0^T V_p\ dt \qquad (V.16)$$

The integral of V_p can be obtained from a trace of the multiplier voltage taken over one full cycle of the external field.

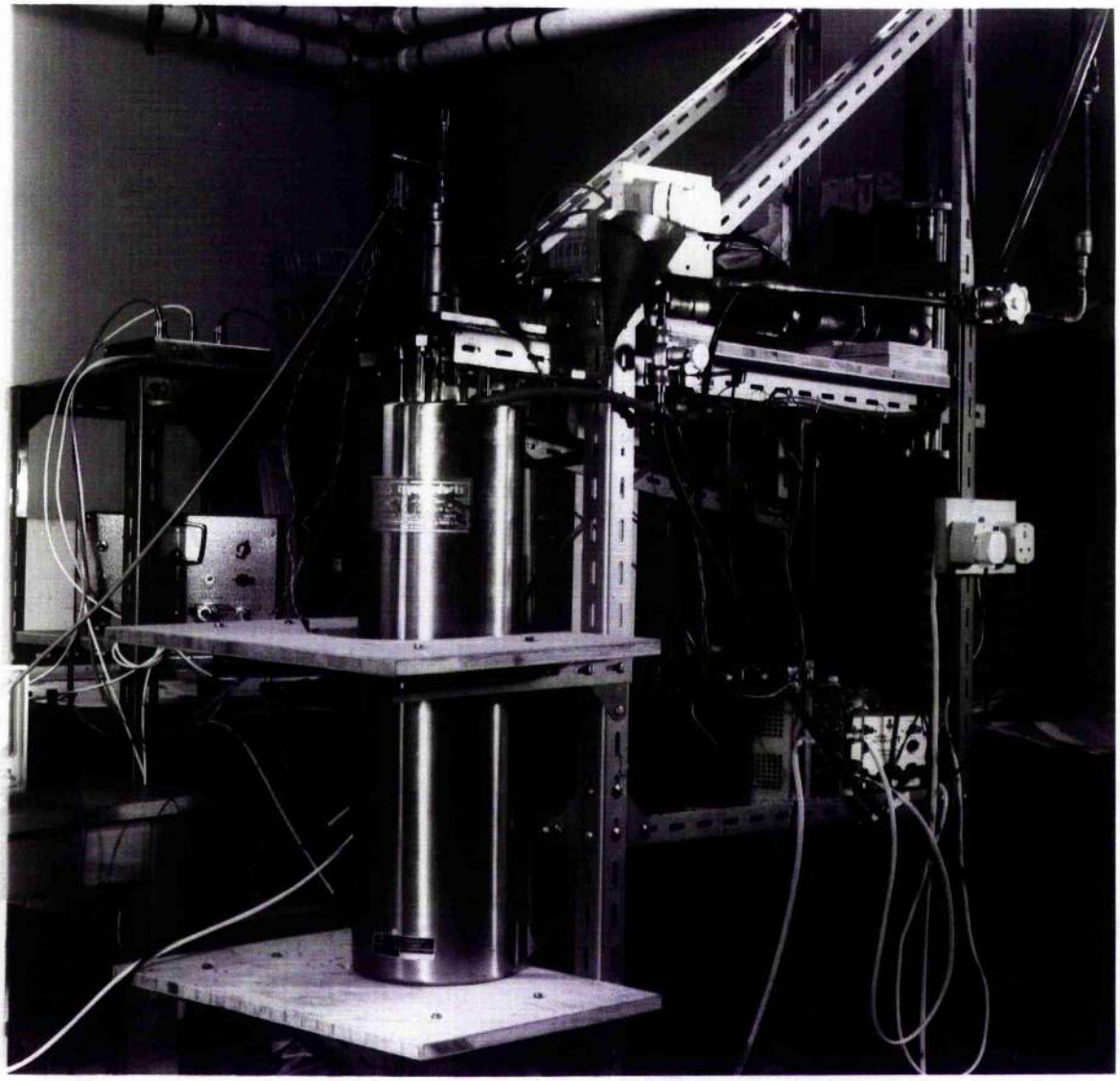

CRYOGENIC PART OF THE APPARATUS

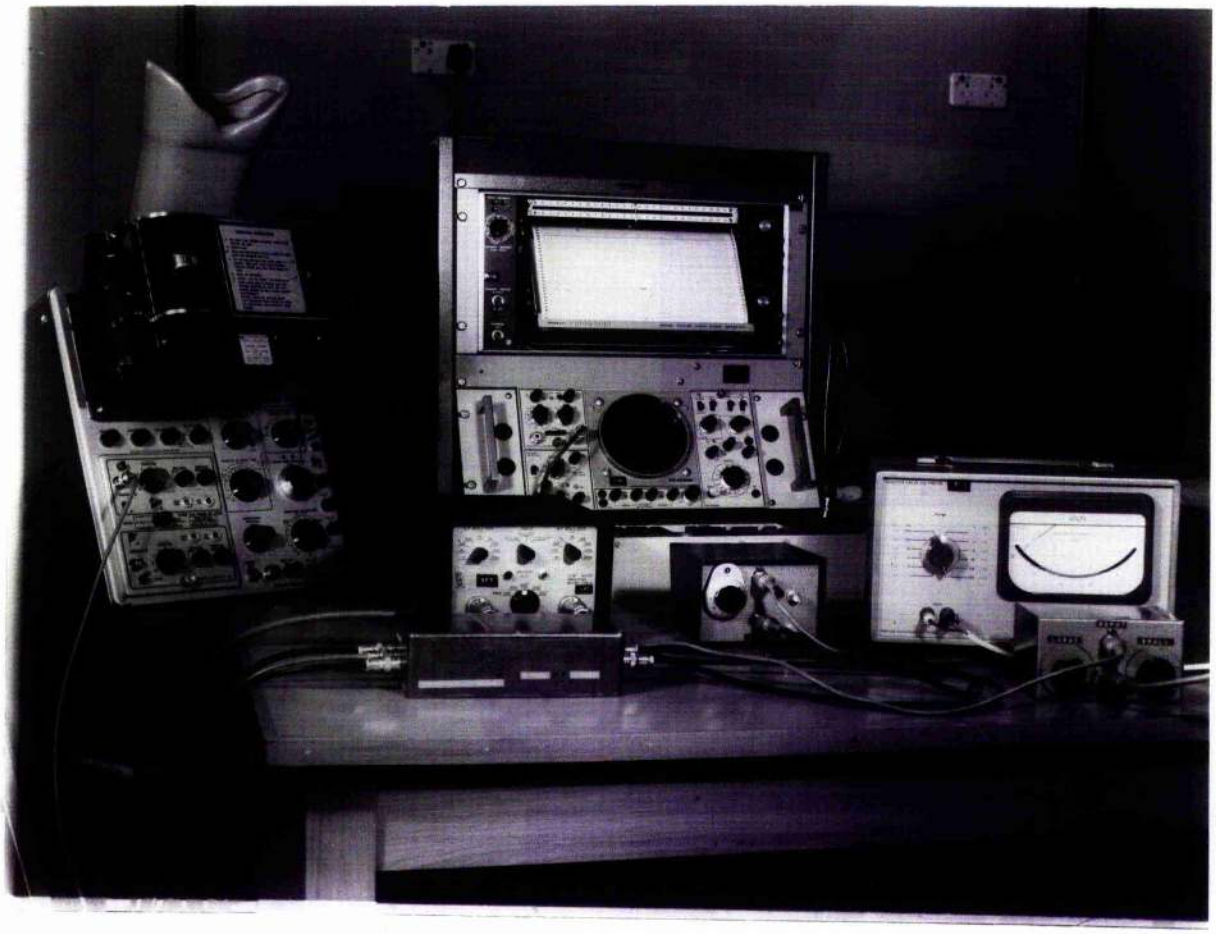

ELECTRONIC PART OF THE APPARATUS

CHAPTER VI

The Experimental Technique

1. AC Losses Measurements

1.1 In this technique the cryostat is contained in a tailed glass dewar which contains the liquid helium. The tail of this dewar vessel fits into a copper solenoidal coil cooled with liquid nitrogen, which produces an ac magnetic field across the Nb sample. Liquid nitrogen for cooling the coil and the helium dewar is contained in a large metal dewar (length 70 cm, 16 cm I.D.). Liquid nitrogen is usually transfered to the dewar by using a pump operating from a small nitrogen storage vessel, the N_2 level in the dewar being controlled automatically. The helium dewar is glass, 60 cm long, with outside diameter of 6.9 cm, the tail being 14 cm long and 4.4 cm outside diameter. The level of the liquid helium is determined by using Allen-Bradley resistors.

The alternating magnetic field is supplied by a copper solenoid (12 cm long, 5 cm inside diameter) (Figure VI.1) wound on a thin stainless steel former which has a 2 mm slot along its length. The flanges of the solenoid are tufnol. Three stainless steel tubes screwed to the top flange secure the solenoid to the top of the cryostat.

A precision search coil was used to calibrate the magnetic field of the solenoid, from which a peak field of 2040 gauss is obtained at 9.5 amp r.m.s. The uniformity of the ac field was measured over a distance of 2 cm in the centre of the coil, there was no detectable change in field within the limit of accuracy of the measurements, 0.3%. The solenoid is connected to the mains supply (50 C/S) through a variac and isolating transformer, Figure V1.2, the inductance of the solenoid is tuned out using a bank of capacitors, which gives a resonant circuit. This resonant circuit increases the maximum field obtainable and ensures a good sinusoidal waveform. The current is measured across 0.5 Ω (0-2%) standard resistance

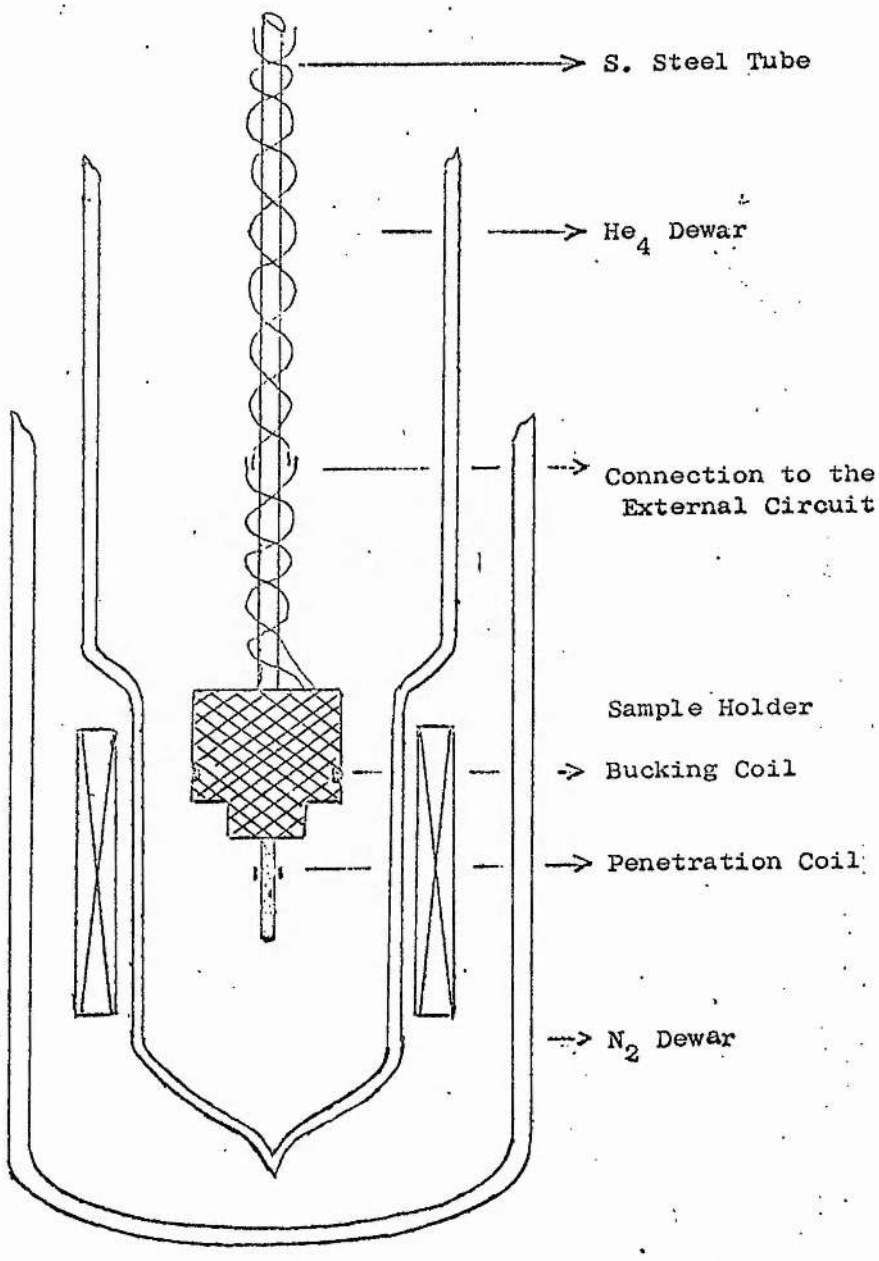

Figure VI.1

The experimental apparatus, showing solenoid (in liquid nitrogen); sample (in liquid helium); pick up coils and sample holder.

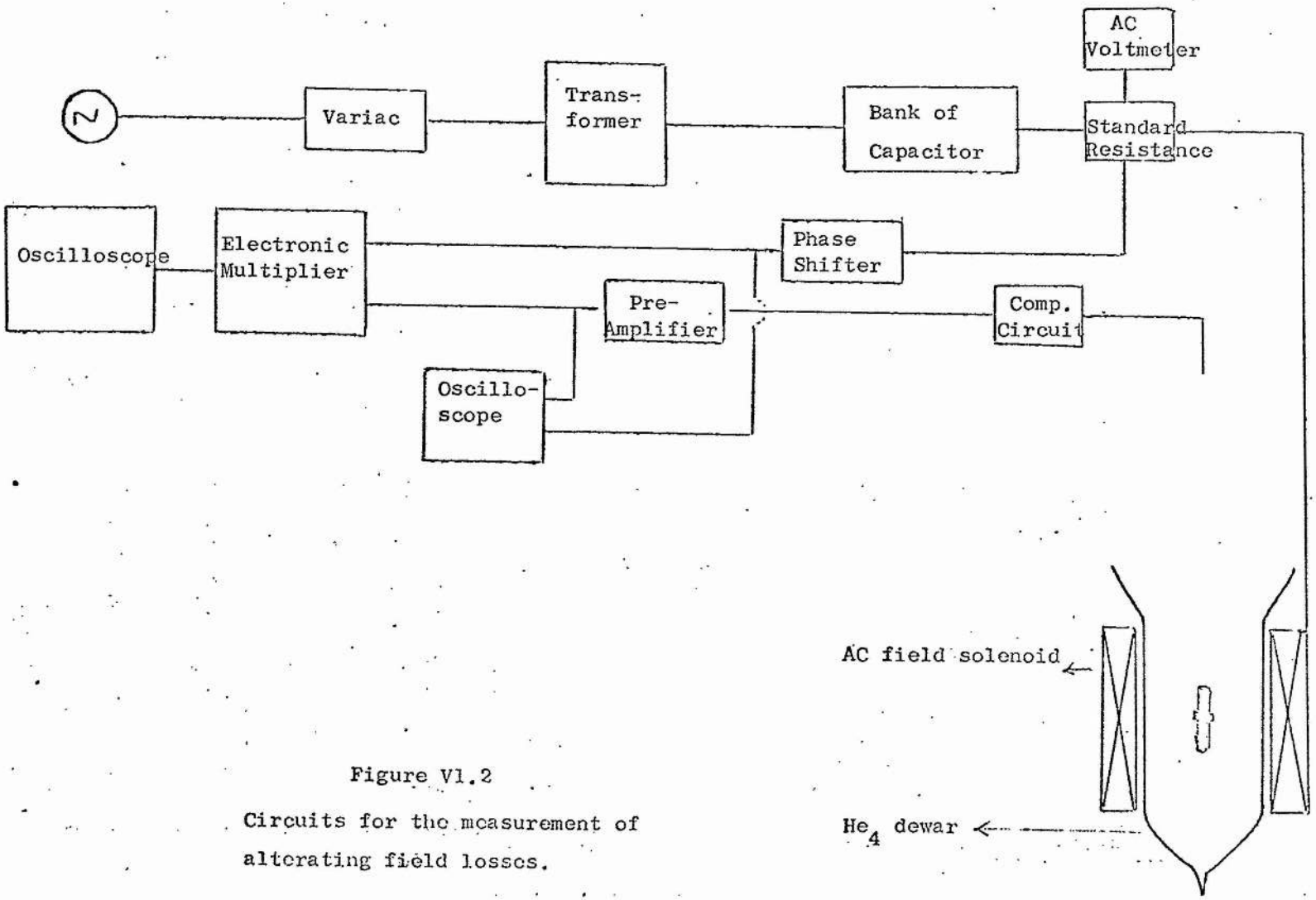

Figure VI.2

Circuits for the measurement of alterating field losses.

using a sensitive valve voltmeter ($\pm$ 1% full scale).

1.2 The sample holder

The holder is a perspex rod, 3 cm in diameter and 5 cm long. In the central lower part of the holder is a small hole of 0.5 cm diameter for holding the sample by supporting it on nylon screws Figure V1.3. The upper part of the holder is connected to a stainless steel support tube which is also connected to the top of the cryostat.

1.3 Pick up coils

The penetration coil is 200 turns of 48 s.w.g. insulated copper wire wound directly on the central part of the sample. Another pick up coil with about 10 turns of the same wire is wound (on the sample holder) in the opposite sense to the penetration coil; this is the bucking coil. The wires of the penetration and bucking coils are twisted together and taken up and connected to the external cricuit. The phase difference between the voltage induced by the external field in the penetration and bucking coils is 180^{o}. The e.m.f. generated in the penetration coil has two parts. One is sinusoidal and proportional to the rate of change of the driving field. The other part of the e.m.f. is proportional to the rate of change of flux penetrating into the material of the sample. The e.m.f. generated by the bucking coil is just proportional to the rate of change of the driving field. In order to obtain the voltage which is proportionnal to the flux linkage to the sample, the outputs of the coils are connected to a compensation circuit Figure V1.4.

The purpose of the compensation circuit is to isolate the penetration voltage e(t), which is proportional to the flux penetration into the sample. This is done by adjusting the compensation circuit in the presence of the superconducting sample, before flux penetration starts, at a magnetic field less than H_{c_1}. The output from the compensation circuit is displayed on an oscilloscope and adjusted as closely as possible to zero. When the magnetic field $\pm H_m$ penetrates the surface of the sample the penetration

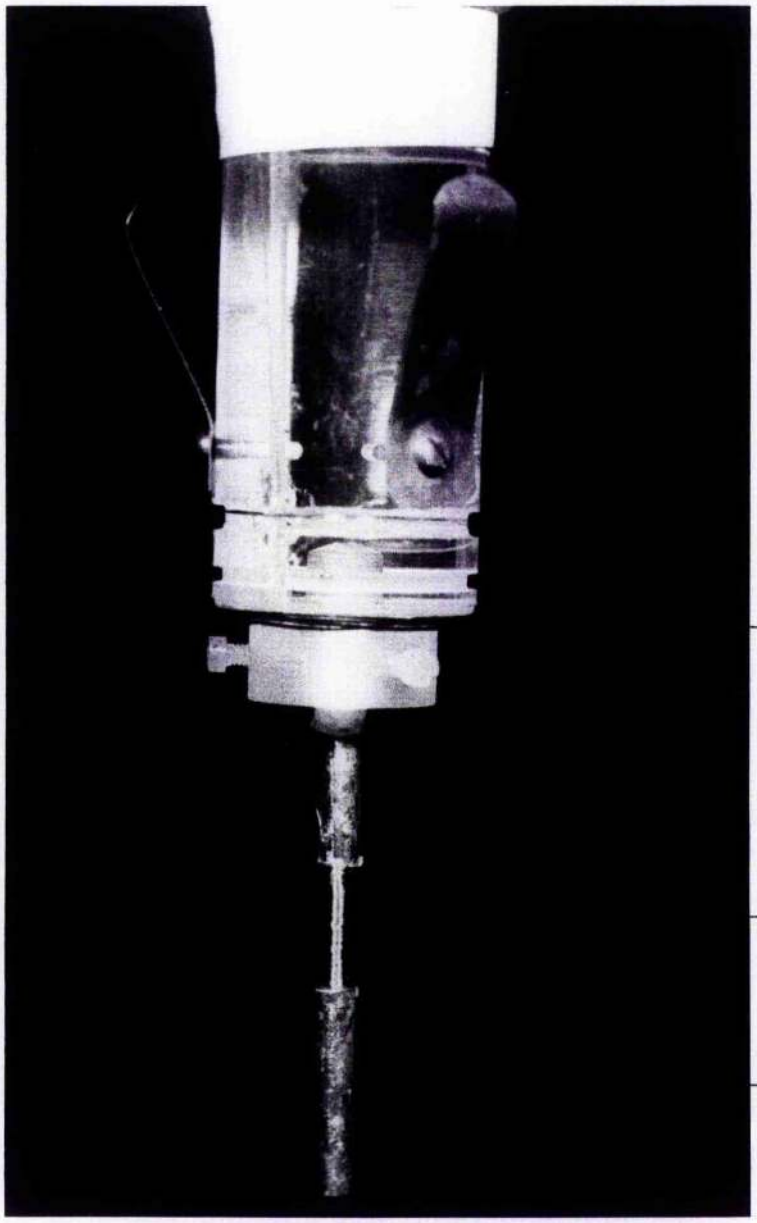

SAMPLE HOLDER

Figure V1.3

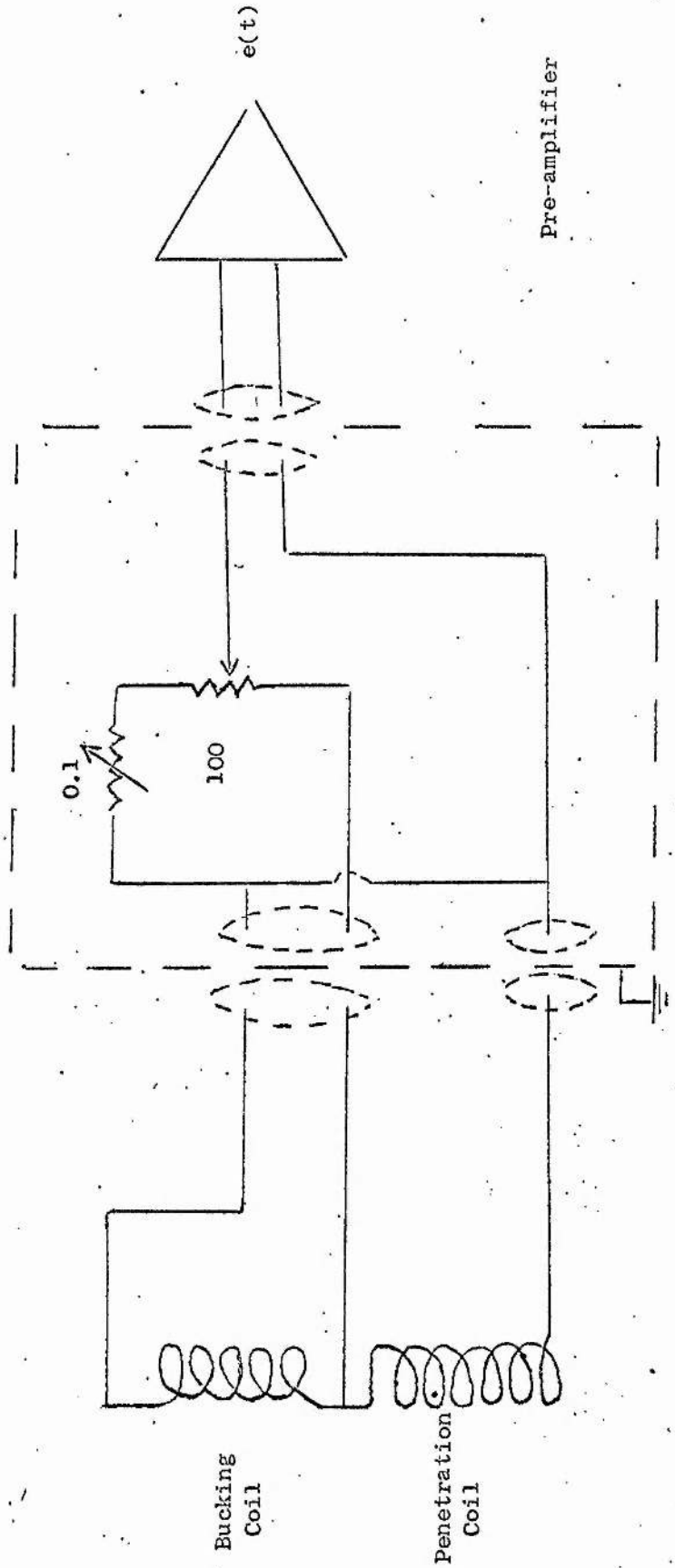

Figure VI.4

Compensation Circuit

voltage waveform is displayed alone showing sharp kinks as Figure V1.5 a,b, and the amplitude of e(t) can be observed with increasing magnetic field. The penetration voltage e(t) is given by $e(t) = -N\frac{d\phi}{dt} \times 10^{-8}$ volt where N is number of turns of the penetration coil. e(t) is about 1 μV when the flux starts to penetrate the surface of the sample. (At turning points of $\pm H_m$, the critical surface current is maximum $e(t) \alpha \frac{d\phi}{dt} = 0$, See Figure V1.5 a,b).

The output of the compensation circuit e(t) is amplified up to 10^4 times using a differential pre-amplifier (PAR Low Noise Amplifier CR4-A) and the output of the amplifier is fed to the X input of an electronic multiplier. The voltage developed across the 0.5 Ω standard resistance in series with driving solenoid, which is proportional to the applied magnetic field H_m sin wt, is connected to a phase shifter and the output is connected to the Y input of the electronic multiplier. The error in the phase shifter setting is less than 3^o.

The output e(t) of the differential pre-amplifier and output of the phase shifter are also connected to an oscilloscope in order to observe and correct the phase shift between them before taking the multiplier readings.

1.4 The Electronic Multiplier

In order to obtain the power loss experimentally, the signal which is proportional to the applied magnetic field is multiplied by the penetration voltage e(t), equation V. 16 . This is done using an electronic multiplier, Figure V1.6, which is designed to give an output voltage linear with the two input voltages (X, Y). The circuit has $\pm$ 5 volts inputs and operates from a $\pm$ 15 volt supply. The multiplier differential output is connected to an operational amplifier which is used for level shifting and has the advantage of being relatively temperature insensitive.

To obtain the best accuracy in the output of the multiplier, several

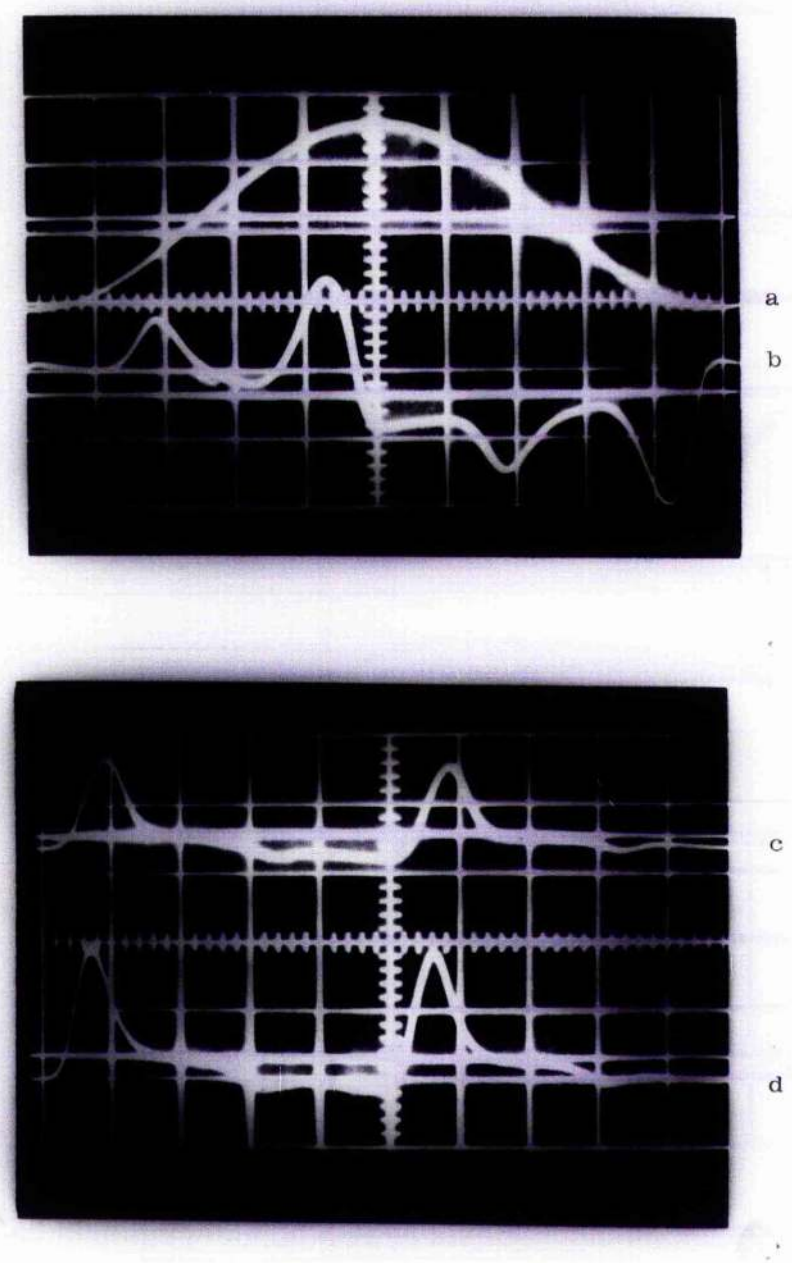

(a) Waveform for sinusoidal applied magnetic field H_m = 516 gauss

(b) Penetration voltage of electropolished and mechanically polished polycrystaline Nb.

(c) Instantaneous power waveform for peak applied field of 516 gauss.

(d) Instantaneous power waveform for peak applied field of 473 gauss

Figure V1.5 (a)

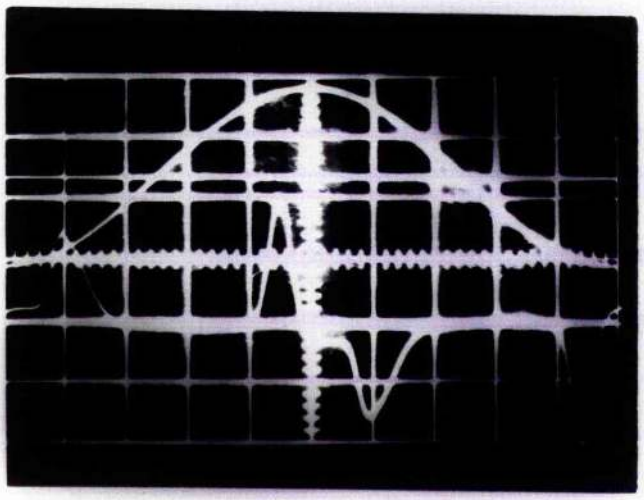

a

b

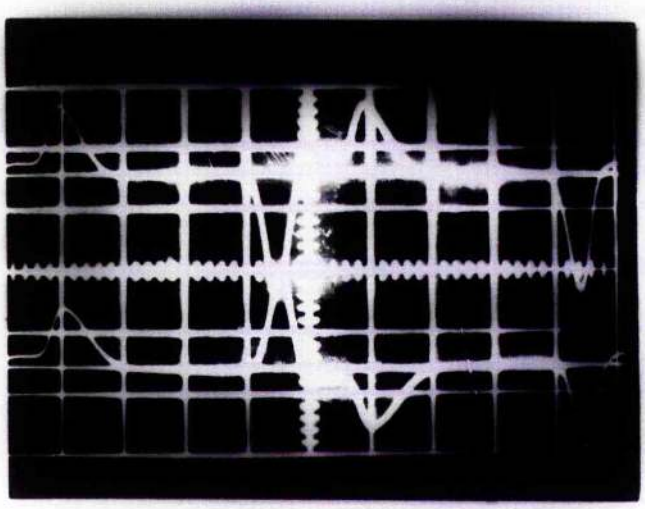

c

a) Sinusoidal a.c. field of H_m = 1376 gauss.

b) Penetration voltage waveform of electropolished single crystal Nb for the peak field of 1376 gauss.

c) Instantaneous power waveform for the same field.

Horizontal scale 2 msec per large division.

Figure V1.5 (b)

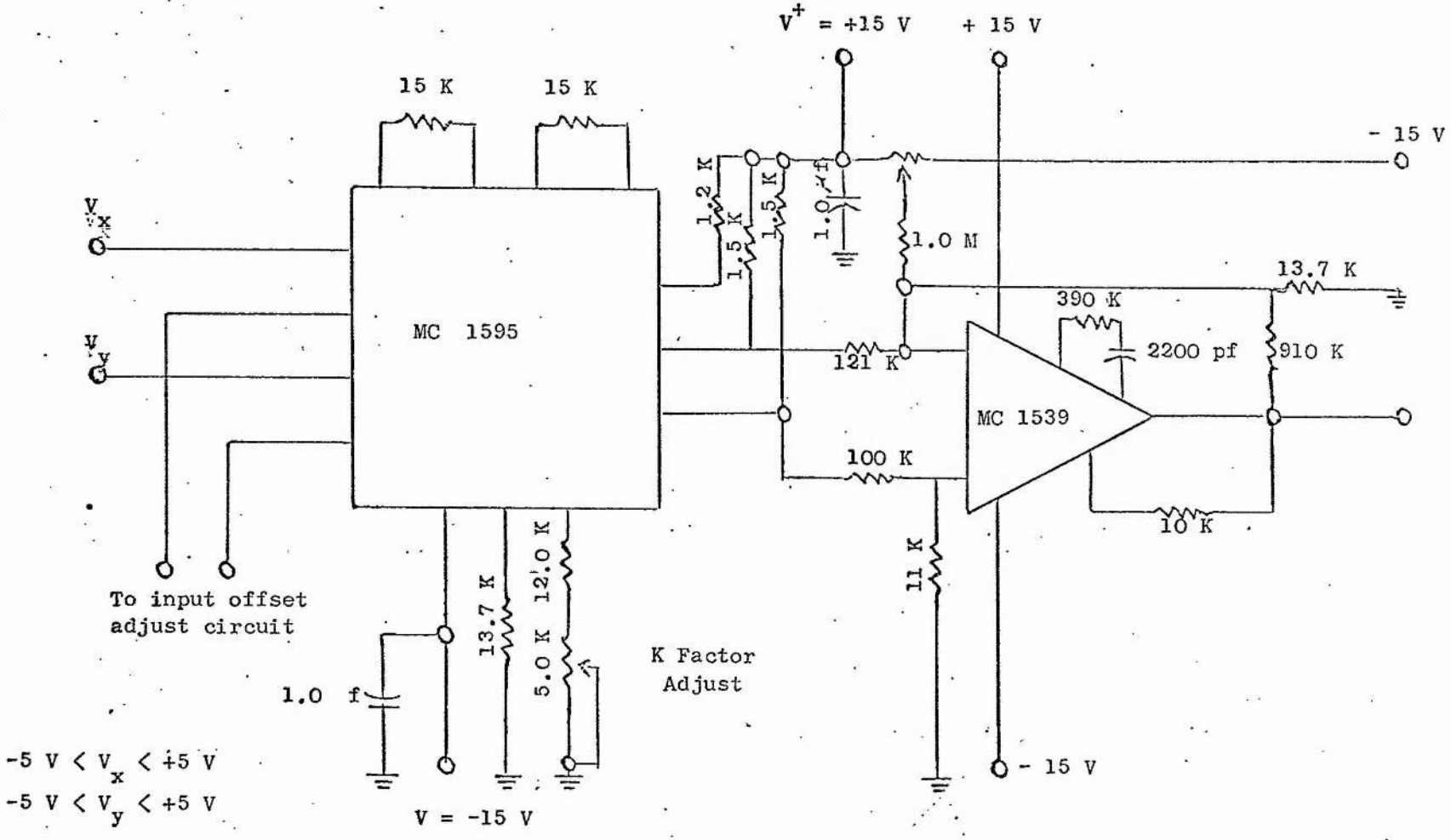

Figure V1.6

Electronic Multiplier

adjustments should be made. The X and Y zero offsets are adjusted, the output offset is adjusted to zero and the scale factor K_c is adjusted. The factor K_c is carefully measured with calibrated ac inputs before experimental runs. The output of the multiplier is given by

$$V_p = K_c V_x V_y \qquad (K_c \simeq \frac{1}{10})$$

The output product depends on the input to output phase shift. The output voltage is fed to an oscilloscope, where the signal is photographed from which record the power losses are calculated. The time average over one cycle is calculated from total area under the waveform projected i sto the zero axis.

2. The Experimental Results

Power losses at 50 Hz are measured in cylindrical rods of Niobium as a function of peak applied magnetic field H_m below and above the first critical magnetic field H_{c_1}, on samples of different surface treatments.

2.1 AC losses in single crystal Nb below H_{c_1}

Figure V1.7 shows three curves of ac losses versus an applied magnetic field H_m in single crystal Nb with different surface treatments. The minimum power which could be observrd by our experimental measurements is about 4×10^{-9} w/cm^2/cycle. The limit to the sensitivity is set by 50 Hz noise introduced into the system as stray pickup. The curves of Figure VI.7 have been corrected for the noise in the system. The three curves for the samples A, B and C show a rapid rise in loss at applied fields around H_{c_1} followed by a region in which ac losses do not rise so rapidly.

In curve A, the losses for Sample A are shown. No loss is measurable below 1200 gauss indicating that there is no penetration of magnetic field into the sample below this value. A distinctive change in the

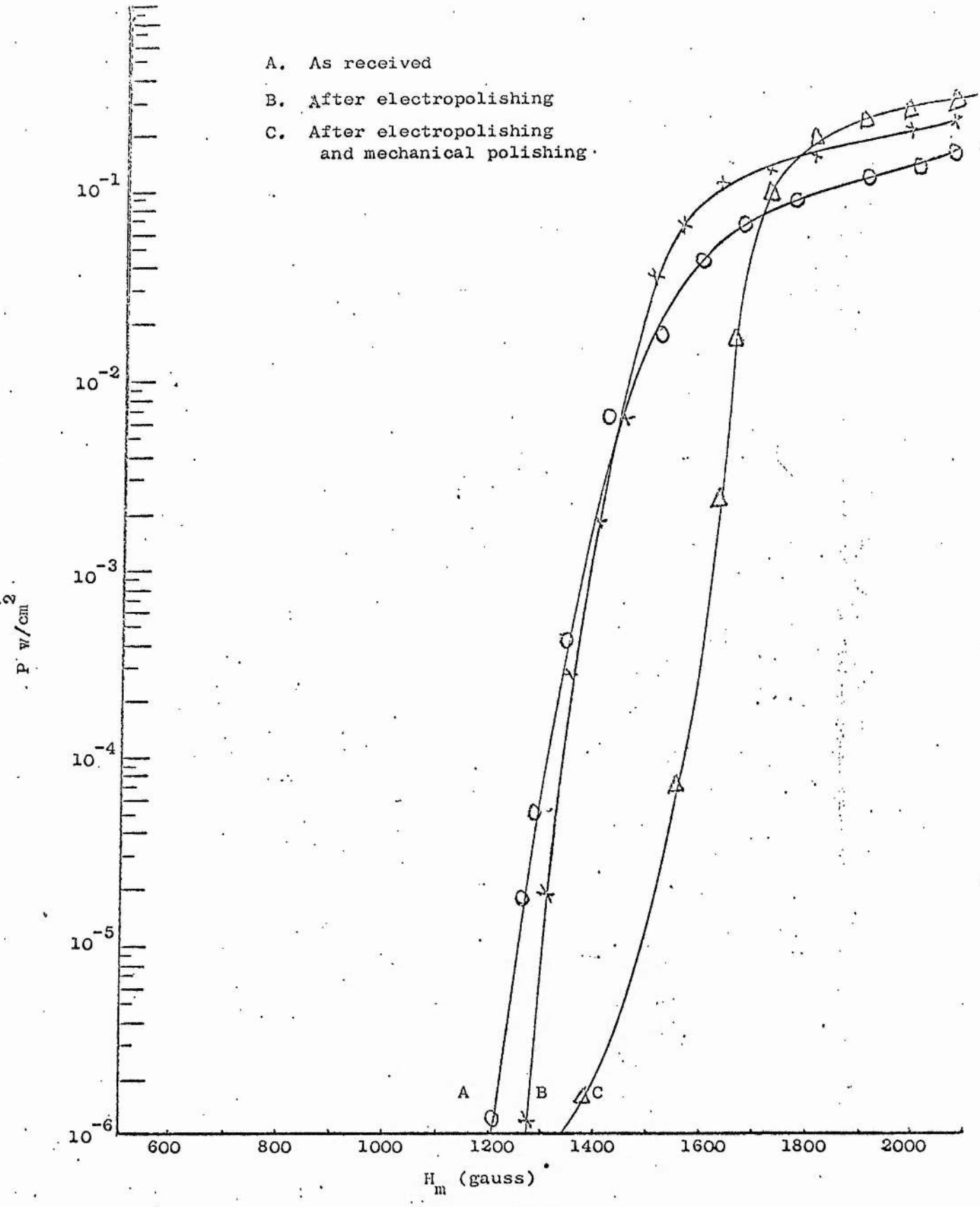

Figure V1.7

The surface loss measured at 50 Hz as function of peak applied field Hm for single crystal Nb with three different surface conditions.

penetration coil waveform shows that penetration of field begins at about 1200 gauss, loss rises rapidly from 10^{-6} w/cm^2 at H_m = 1200 gauss to 10^{-2} w/cm^2 at H_m = 1400 gauss. The losses for sample B (Sample A after electropolishing) are shown in Curve B. Again losses are just measured at field penetration of 1270 gauss (H_{c_1} = 1355 gauss), there is more rapid rise in loss than in sample A so that for $H_m > H_{c_1}$ the loss in sample B is greater than in sample A.

The losses for sample C (sample B after mechanical polishing) are shown in Curve C. Here H_{c_1} is measured to be 1550 gauss, but penetration of field and hence power loss in the sample are detected down to 1350 gauss. Increase in loss is gradual until H_{c_1} is reached whereupon loss rises very rapidly until $H_m >$ 1700 gauss, then loss increases very gradually at a value greater than either sample A or B.

From Figure VI.7, Curves A, B and C for three samples which have different surface conditions of the same single crystal Nb, the value of H_{c_1} and the degree of surface roughness are highly important in determining the ac power loss. The point of the onset of power loss and the sharpness of its rise with H_m is determined by the value of H_{c_1}. In these three samples ac power loss is postponed to the highest value of H_m in sample C due to its high value of H_{c_1}.

Our results show that for a smooth surface of single crystal Nb the losses are less than any losses have been studied so far for pure Nb sample up to magnetic fields of 1550 gauss.

2.2 AC Losses in polycrystalline Nb below H_{c_1}

Power losses have been measured in cylindrical rods of polycrystalline Nb as a function of an applied magnetic field H_m at three different surface states. We tried to measure ac losses of polycrystalline Nb as received but there was no detectable flux penetration up to H_m = 2000 gauss therefore there was no measurable loss. This confirms that $H_{c_1} >$ 2.0 K gauss

as measured from the samples magnetization measurements (Section III, Figure III.2).

After annealing the sample (as described in Chapter II) H_{c_1} decreased considerably to a low value. AC loss measurements were taken with three different surface treatments with annealed sample and the results show clear evidence that annealed polycrystalline sample exhibits loss at very low fields.

Figure VI.8, Curve D shows ac losses in the annealed sample (Sample D), where flux penetrates at magnetic field H_m as low as 180 gauss, at which field losses are observed. Losses occur at such low fields because of impurities and roughness in the surface which cause flux penetration at magnetic fields well below H_{c_1}. H_{c_1} is about 656 gauss, which was obtained from the magnetization measurements (Chapter III, Figure III.6). Losses increase gradually up to about 1000 gauss, then increase very slowly with increasing magnetic field. There is no noticeable sudden jump in losses at H_{c_1} as was observed with the single crystal Nb sample. Curve E shows losses for the same sample after electropolishing (Sample E). After this treatment the surface became rougher than the surface of Sample D (See Chapter II, Figures 4, 5), because the surface is deeply etched showing the crystalite faces in the surface, H_{c_1} decreased to about 455 gauss (see Chapter III, Figure III.7a). Losses are observed at magnetic fields of about 200 gauss with a loss of 2.0×10^{-7} w/cm^2 (not shown in Curve E). Losses in Sample E are higher than losses in Sample D at the same magnetic field. The increase in loss around H_{c_1} in sample E is sharper than that in sample D, this is due to the surface of the sample E being rougher so that flux can penetrate the surface easily, but in sample D the surface is relatively smooth and screening currents can build up giving gradual increase in loss. This also can be seen by comparing the d.c. magnetization curves of the two samples (see Chapter III, Figures 6, 7a). At magnetic field of about

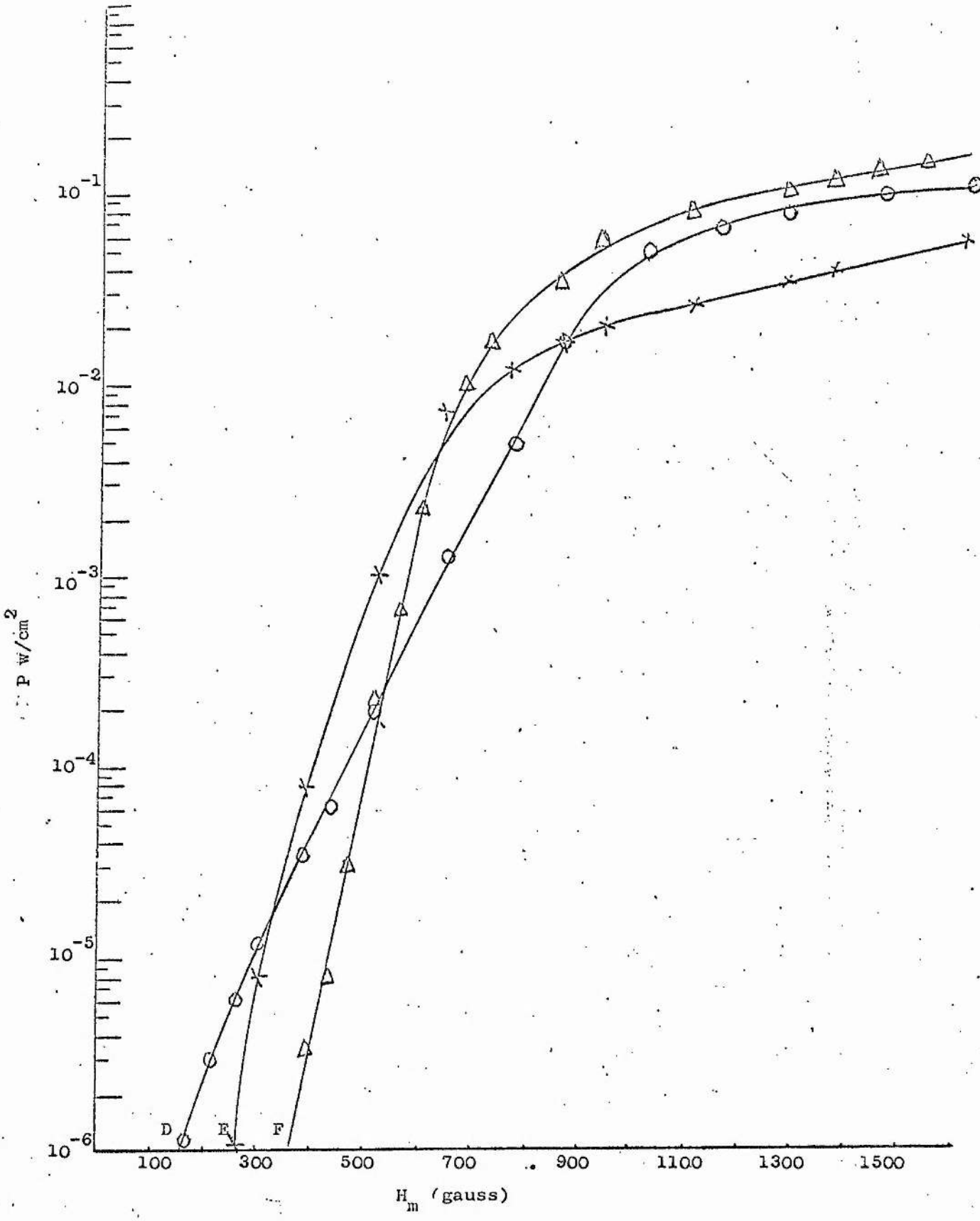

Figure V1.8

The surface loss measured at 50 Hz as function of peak applied field Hm for polycrystalline Nb with three different surface conditions.

650 gauss losses in sample E increase very smoothly with the applied magnetic field. Curve F shows losses of the sample after it has been mechanically polished (Sample F). Loss is first observed at H_m = 380 gauss, after it rises fairly rapidly to about 750 gauss. The delay in the occurance of loss to 380 gauss in this sample, as opposed to 180 gauss in sample D and 2000 gauss in sample E, is attributed to the smoothness of the surface.

Our results show that losses below H_{c_1} in both single crystal and polycrystalline Nb decrease with smooth surfaces. These confirm the loss mechanism that surface roughness and impurities are the main factors in governing ac losses. Our results are in agreement with other worker's results that to achieve a minimum loss it is of primarly importance to use materials with smooth surfaces.

3. AC losses above H_{c_1}

When the applied magnetic field H_m is in the range $H_{c_1} > H_m > H_{c_2}$, where $H_m > H_p$, magnetic flux penetrates the sample to a depth given by Equation V.6.

In the samples investigated, this depth is shown in Figures V1.7 and V1.8 for applied fields H_m up to 2000 and 1600 gauss, respectively. It can be seen that in no case does flux penetrate to the centres of the samples. AC losses are therefore still surface losses, and consequently surface conditions play a vital role in determining losses in this region.

3.1 AC losses in single crystal Nb above H_{c_1}

Figure V1.7 shows ac losses of samples A, B, C, for fields <2000 gauss indicating that the largest loss occurs in sample C, for powers $P_C > P_B > P_A$, which has the smoothest surface. It is noted again that

the inception of losses is delayed to the highest value of H_m in sample C due to its high value of H_{c_1}. Losses in this smooth sample grow rapidly, on the other hand, to overtake those in the rougher samples at fields some-what higher than H_{c_1}. The form of the losses above H_{c_1} of three samples in Figure VI.7 should be explainable by the critical state model in terms of H_{c_1}, ΔH and J_c. According to the model by Dunn et al presented in section V.1, the losses are described by equation V.6 which is based upon the area of the hysteresis loop described in terms of H_{c_1}, ΔH and J_c. The losses for samples can be calculated from this model (Equation V.6) using the values of H_{c_1} already presented (Section III), and J_c and ΔH to be presented later in section VI.4 and VI.5. Measurements of H_{c_1}, J_c, ΔH were made for each sample before its surface was altered by polishing to produce a new sample with new surface state. Calculated values of ac loss according to this model are shown in Figure VI.9.

In Figure VI.9 it is seen that in the region $H_{c_1} > H_m > H_{c_2}$ the calculated loss is largest in sample A, $P_A > P_B > P_C$ in contradiction with the measured values. The order of magnitude of the calculated values of loss is nevertheless the same as the measured loss.

3.2 AC losses in polycrystalline Nb above H_{c_1}

Figure VI.8 shows the measured ac losses in polycrystalline samples of Nb, Samples D, E and F in the range $H_{c_2} >> H_m > H_{c_1}$. In this region the highest loss is due to sample F, again the sample with the smoothest surface, such that $P_F > P_D > P_E$. The calculated losses according to the critical state model can be seen in

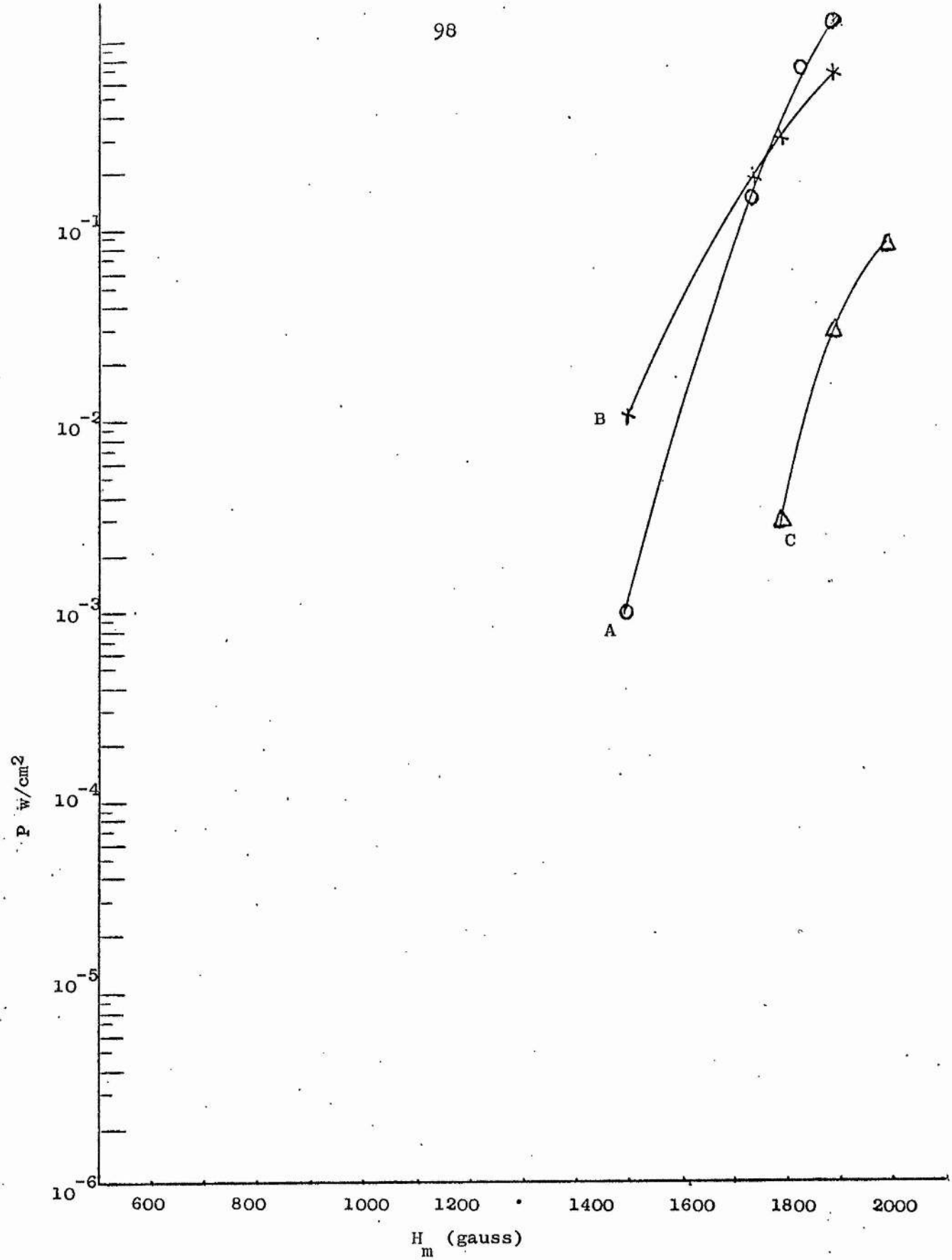

Figure V1.9

AC Power loss predicted by equation (V.6) plotted against H_m, for single crystal Nb, with three different surface treatments.

Figure VI.10, where $P_E > P_D > P_F$.

The results using the wattmeter technique were confirmed by displaying the hysteresis loop of Samples D, E, F directly on an oscilloscope using the oscilloscope to display Ø against H_a. These results were taken at H_m = 537 and 1462 gauss and the hysteresis loops are shown in Figure VI.11 and VI.12 for Samples E and F. The area of the loop representing the loss in Sample E (rough surface) is seen to be less than that for Sample F (smooth surface) in confirmation of experiments using the wattmeter technique.

3.3 Discussion of discrepancy between measured and calculated loss.

In discussing the discrepancy between experimental results and those calculated by the critical state model according to Dunn et al.,[42] it is important to scrutinize the significance of parameters J_c, H_m, H_{c_1} and H used to calculate the power loss p, by use of Equation V.6. Of these parameters only H_m, H_{c_1} and H are measured by a direct method. The measured value of J_c is inferred, however, from ac loss measurements in the presence of adc biasing field H_a, see Section VI.4. The fact that J_c is measured in these experiments as a dynamic quantity related particularly to the surface conditions (Section II) implies that it is not entirely of the nature of the critical transport current. The measured value of J_c depends on the surface state (Figures VI.16, 17), and is higher for smooth surface than for a rough one. It is important therefore to consider the use of J_c in Equation V.6, since in the critical state model the parameter J_c represents the critical transport current density, a quantity which is taken as a constant over the section of the material and which should be nearly independent of surface condition.

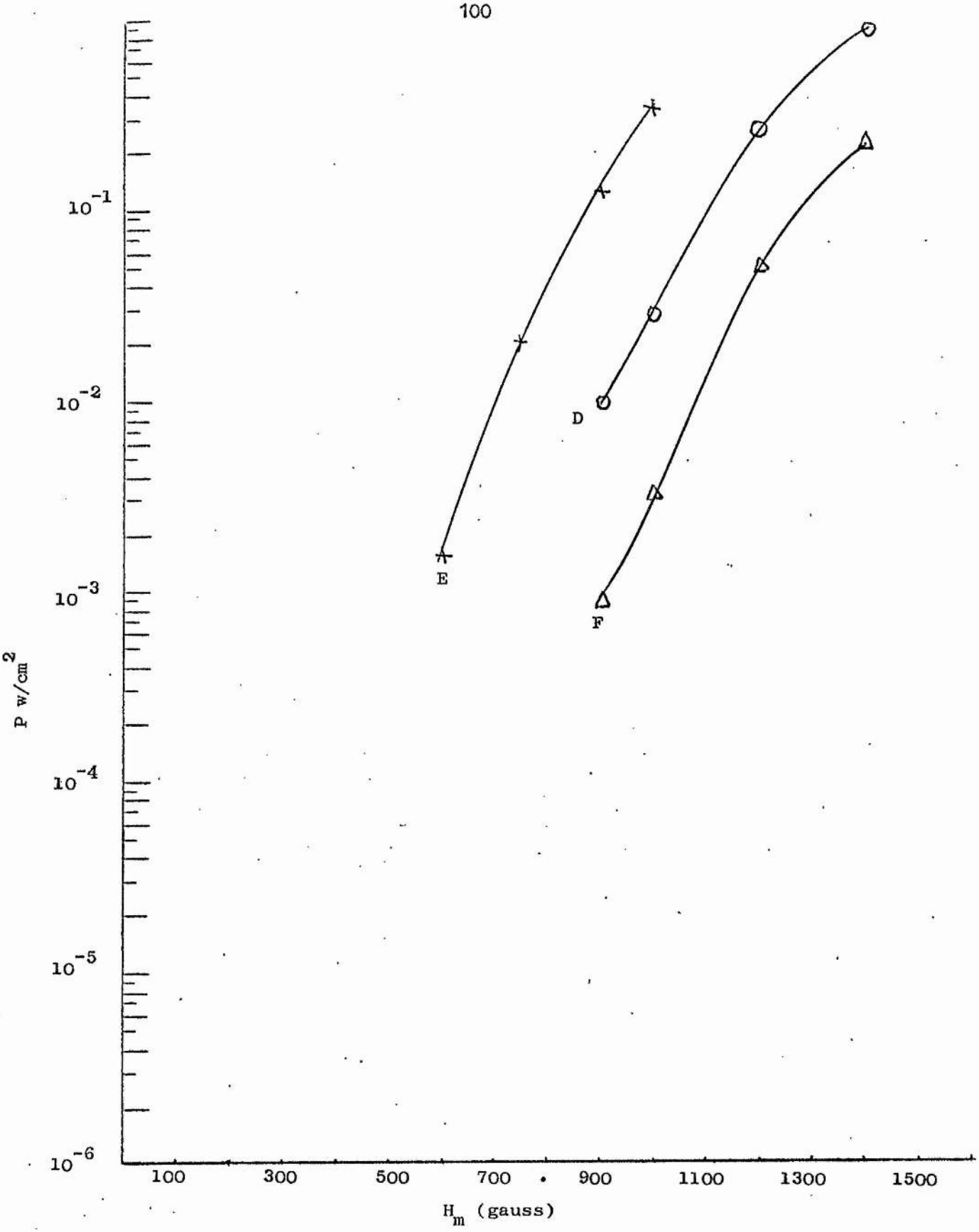

Figure V1.10

AC power loss predicted by equation (V.6) plotted against H_m, for polycrystalline Nb with three different surface conditions.

As measured here (Section V1.4), J_c is the surface critical current which takes into account the chemical and mechanical state of the surface. It is noted in Section V1.4 that J_c is larger in samples with smooth surfaces than in rough samples. This leads to a smaller calculated value of loss from Equation V.6 for smooth samples as depicted in Figures V1.9 and V1.10. On the other hand, it is expected that the critical transport current should not be greatly different in any of the single crystal samples (A, B, C), or in the polycrystalline samples (D, E, F). With a constant J_c the critical state model would lead to relative losses based upon the values of H_m, H_{c_1} and H. Scrutinising Equation V.6 leads to calculated losses with the same inequalities as have been measured $P_C > P_B > P_A$ and $P_F > P_D > P_E$.

It is noted finally that in very thin samples used by others[22] where the transport critical current and the surface critical current must be identical, (flux penetrates to the centre of the sample), the measured losses and those calculated using the critical state model agree very well.

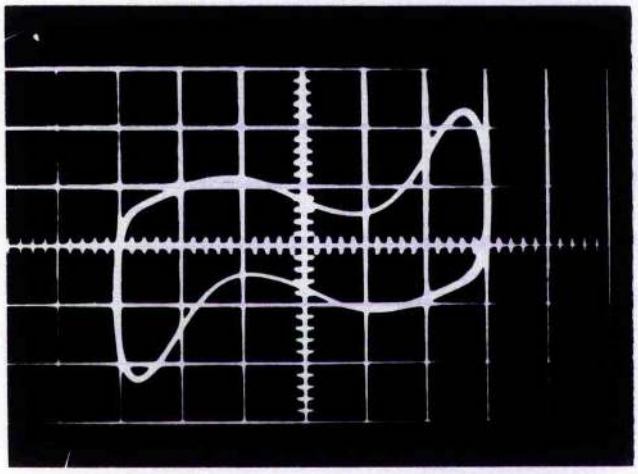

a

Ø

Penetration Flux

AC Field H_a

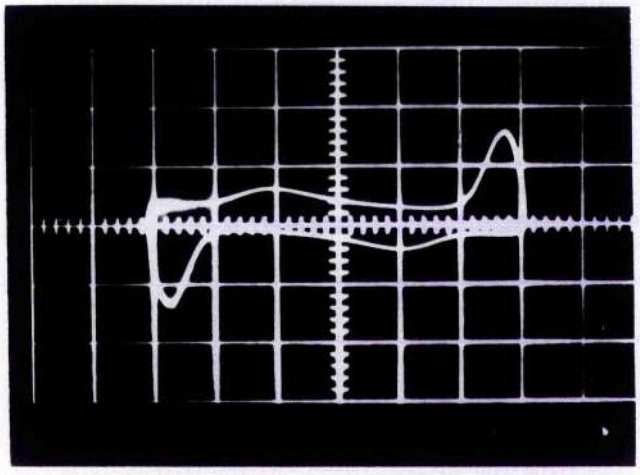

b

Hysteresis loops where the a.c. applied magnetic field is out of phase with integrated penetration voltage.

a) Hysteresis loop for peak applied magnetic field of 537 gauss, for electropolished and mechanical polished polycrystalline Nb (smooth surface).

b) Hysteresis loop for the same field, of electropolished polycrystalline Nb (rough surface).

Figure VI.11

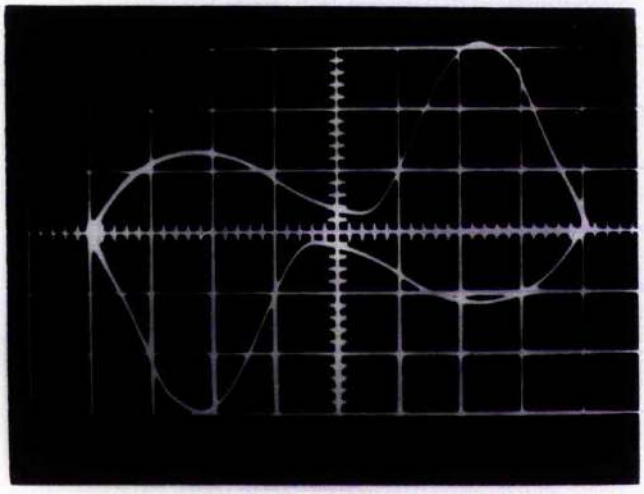

a

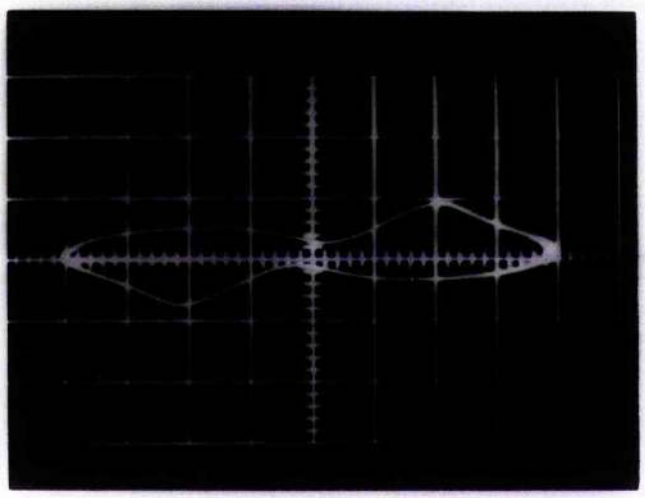

b

Hysteresis loops where the a.c. applied magnetic field is out of phase with integrated penetration voltage.

a) Hysteresis loop for peak applied field of 1462 gauss of polycrystalline Nb (smooth surface).

b) Hysteresis loop for the same field, of polycrystalline Nb (rough surface).

Figure VI.12

4. Critical Current Measurements.

The wattmeter technique used in this work for measuring ac losses leads to a means of measuring the critical current of a sample at varying applied magnetic field. Bean[1] has demonstrated that when a small ac applied magnetic field (h) superimposed on a large dc field, $h \ll H_{ext}$, the critical currents may be induced in the surface at the field H_{ext}. He assumed that the induced current on the surface of the sample which is proportinnal to amplitude of the ac field, is the same through the entire section of the sample. According to this, if the superconducting sample has a pickup coil of N turns wound on its surface, the induced coil voltage which is related to the induced surface currents in the sample. This coil voltage is given by

$$V = - \frac{4h_m^2 fNR}{J_c(H)} \times 10^{-8} \text{ volts}$$

which will not be sinusoidal with time although the small ac field (h) is sinusoidal. This method has been reported by Love[40] in measuring the critical current density of Nb-Zr rods, where he found that the critical current density by this method is higher than the critical current density measured by passing a direct current through the sample. Ullmaier[41], used modulating coils with triangular fields in the presence of a steady bias field H_{ext} where $H_{ex} \gg h$, $H_{ex} \gg H_{c_1}$, for measuring the critical current density of Pb-In, Nb-Zr and Nb-Ta cylindrical samples. He assumed as did Bean[1] that the properties of layers close to the surface of the sample are influenced by the ac field to the same extent through the cross section of the sample, so that

$$J_c (H_{ext} + h_m) \simeq J_c (H_{ext} - h_m) \simeq J_c (H_{ext})$$

Linford[22] et al. have recently measured the critical current density of thin strips of Nb, using the same technique and assumption as Ulmaier[41].

Our method of measuring the critical current density of Nb samples is rather similar to Linford's[22] method and is based on measuring ac

losses caused by an applied ac field in the presence of a dc magnetic field. We divide our experimental arrangements into two parts (two Figures) Figure V1.13 shows the superconducting magnet (the same magnet and power supply as described in the magnetization measurements) producing the H_{ext}. The ac field (h) is produced by a modulating coil wound on the central part of a perspex former of length 20 cm with outside diameter 1.4 cm. The length of the coil is 8 cm made up of 946 turns of 4 layers (S.W.G. 30). It was calibrated and gives 200 gauss/Amp$_{(rms)}$ and in use can give ac fields up to 400 gauss. The coil is energised by 50 Hz sinusoidal current, fed from the mains supply through a variac, matching transformer and 0.5 Ω standard resistance. The coil and its perspex former is inserted inside the superconducting magnet, the perspex has a hole = 0.5 cm diameter along its axis for the sample to be inserted centrally within the coil arrangement.

Figure V1.14 shows the penetration coil (200 turns) wound in one layer directly onto the central part of the sample. It is connected to a bucking coil with opposite winding direction wound on small perspex rod, placed on the top of the sample. As before the outputs of the pickup coils are connected to a compensation circuit, and the output of the compensation circuit is fed to pre-amplifier, then to the electronic multiplier. The voltage across the standard resistance 0.5 Ω in the modulating coil circuit, which is proportional to the ac field of the modulating coil (h), is connected through a phaseshifter to the electronic multiplier. The output voltage of the multiplier (V_p) is proportional to the product of the two output voltages. As before in measuring ac losses the two signals to the multiplier should be in phase. The output of the multiplier displayed on an oscilloscope is photographed, Figure V1.15 and the power loss per cycle is calculated from the total area of the trace projected onto the zero line. The power loss is given by equation (V.16).

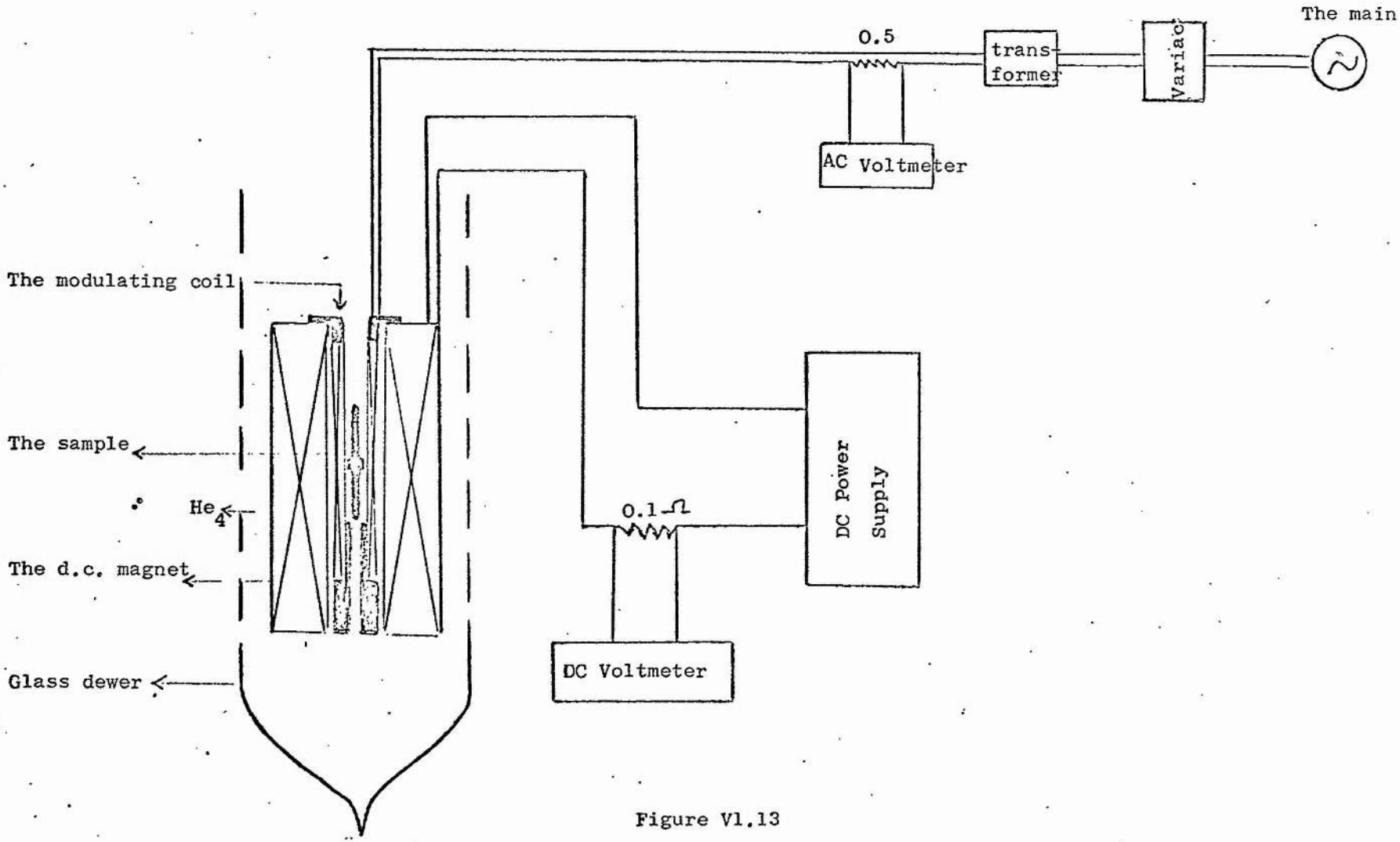

Figure V1.13

Circuit 1. Experimental arrangement for critical current J_c and ΔH measurements.

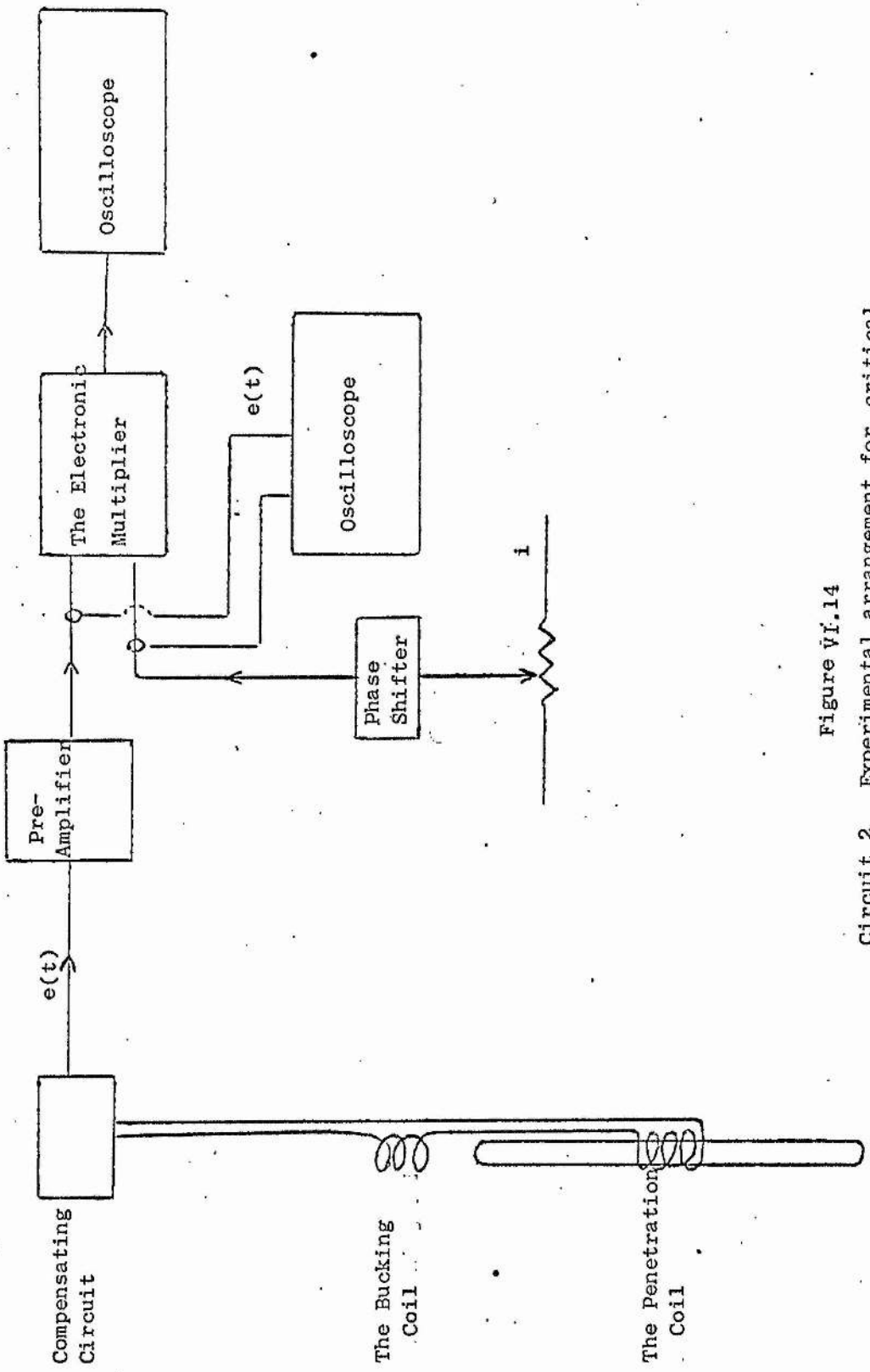

Figure VI.14

Circuit 2. Experimental arrangement for critical current density J_c and ΔH Measurements.

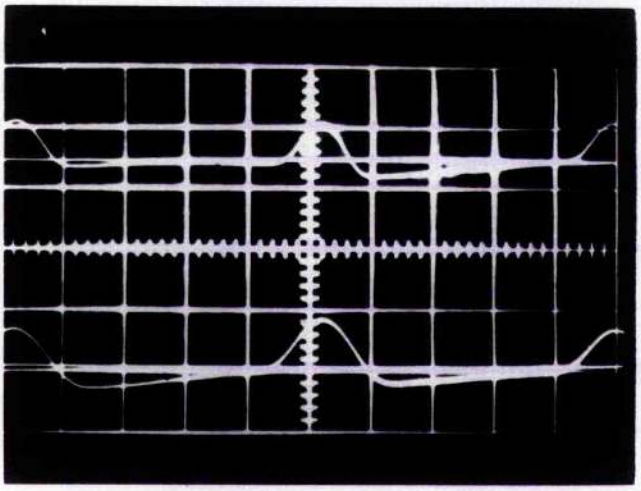

a

b

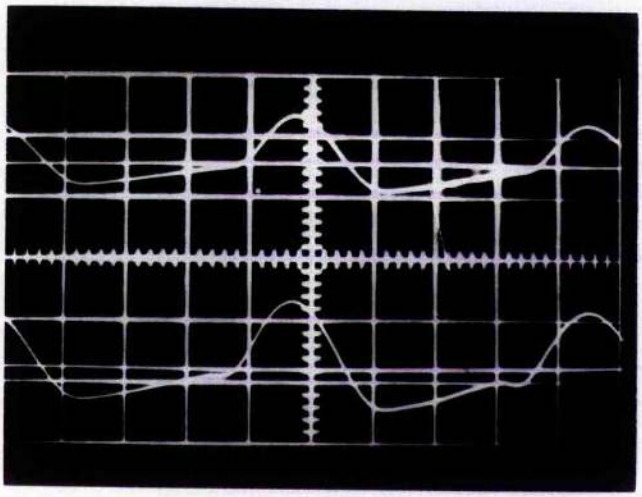

c

d

Instantaneous power waveform for electropolished and polished single crystal Nb.

a) D.C. = 1929 gauss (h_m = 280 gauss)
b) D.C. = 2100 gauss (h_m = 280 gauss)
c) D.C. = 2440 gauss (h_m = 280 gauss)
d) D.C. = 2440 gauss (h_m = 320 gauss)

Figure VI.15

In order to find the critical current density J_c, power loss per cycle (P) was made in the usual manner in terms of the peak modulating field h_m, where $h_m << H_{ext}$ at each value of the steady field H_{ext}, and graph of loss versus h_m^3 plotted in which J_c was determined from the slope of the linear section of the plot and using Bean's equation

$$J_c\ (H_{ext}) = \frac{5h^3_m}{12\pi^2 P} \times 10^{-7} \quad \text{Amp/cm}^2$$

These measurements were carried out for the samples studied before, single crystal and polycrystalline Nb in rod form, each sample being studied for three different surface conditions noted before.

4.1 The results $J_c(H_{ext})$

4.1.1 Single crystal niobium (Samples A,B,C)

Figure V1.16 shows three curves of critical current density of the single crystal Nb sample versus dc applied magnetic field for different surface treatments. These results were obtained by measuring the ac power loss in the samples as described above, the sample being placed in the dc field H_{ext} and being subjected to a small constant ac magnetic field h_m = 280 gauss.

Figure V1.16, Curve A shows the critical current density of the sample as received (Sample A) without any surface treatment, Curve B shows the critical current density for the same sample after electropolishing (Sample B), Curve C represents the critical current density for the same sample after polishing the surface by fine polishing powder to give smooth surface (Sample C).

The value of $J_c(H_{ext})$ should be considered in relation with the magnetization curves (Chapter III, Figures III.3,4,5) for the samples A, B and C. Two tendencies are seen in J_c in Figure V1.16, firstly, the rise in J_c at low fields indicates the value of H_{c_1} in a manner correspondin to that obtained from the magnetization measurements, H_{c_1} increases slightly in electropolished sample (A to B) confirming the finding from the magnetization curve of an increase of 20 gauss when the sample is

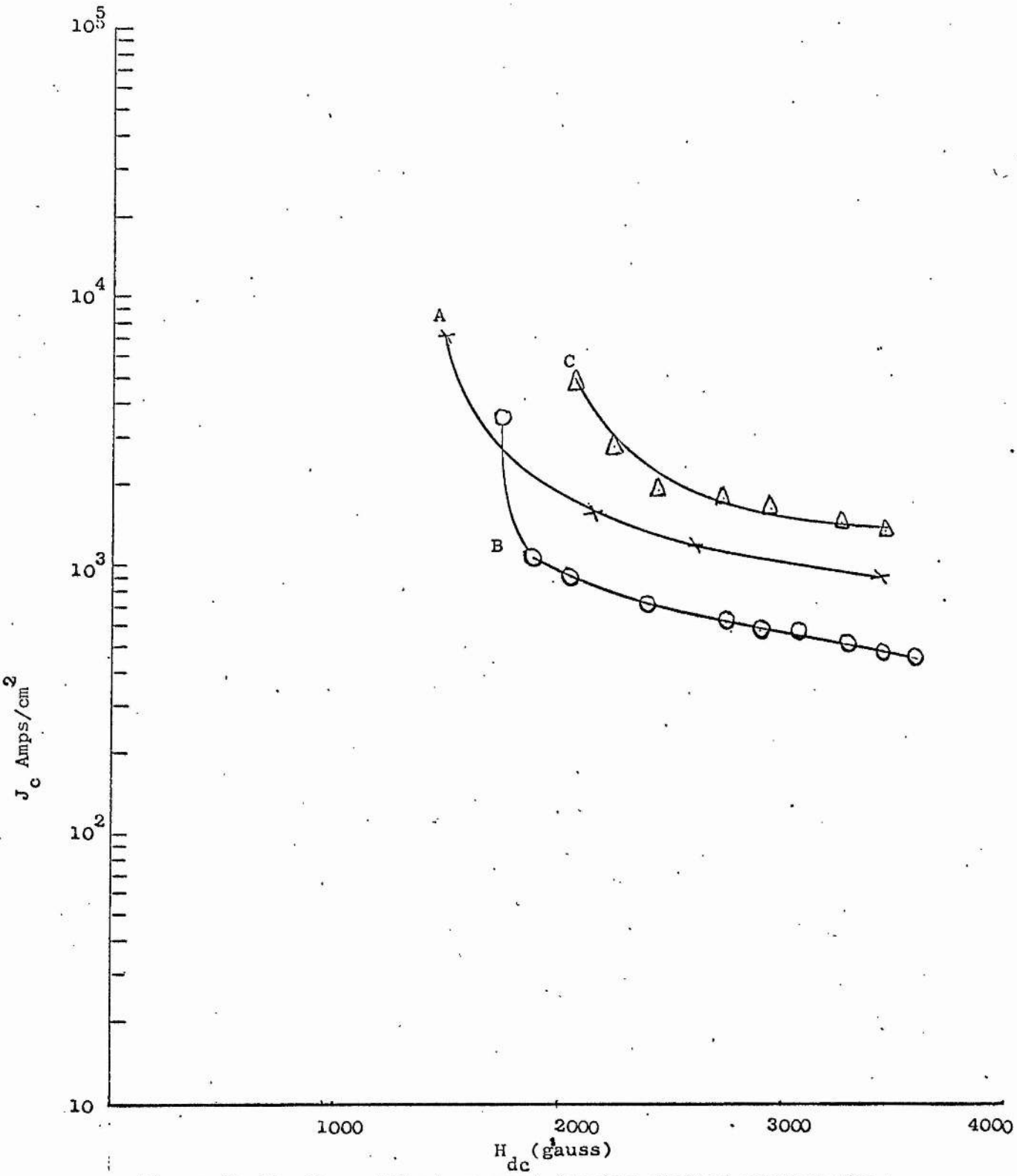

Figure VI.16 The critical current density plotted against the applied magnetic field for single crystal Nb.

mechanically polished (sample B to C) H_{c_1} rises considerably to the value of 1550 gauss found from its magnetization curve. Secondly, for $H_{ext} > H_{c_1}$, $J_c(C) > J_c(A) > J_c(B)$. These inequalities indicate that on electropolishing to obtain sample B the surface has changed responding to the electropolishing solution, enabling flux to penetrate the surface more easily hence lowering the critical current. On mechanical polishing (sample C) the surface is made very smooth so that flux is prevented from penetrating the surface of the sample, leading to a high J_c.

4.1.2 Polycrystalline Niobium (Samples D,E,F)

Figure V1.17 shows the critical current density for polycrystalline Nb versus dc applied magnetic field. Curve D shows J_c for the sample after annealing without any surface treatment. Curve E represents J_c for sample E obtained by electropolishing sample D as explained in Chapter II. Finally, after mechanical polishing to obtain smooth surface (sample F) the criticalcurrent is shown in Figure V1.17, Curve F. Similar comments are applicable here as in the proceeding section. The values of J_c confirm the results from magnetization measurements, that H_{c_1} is altered by the surface treatment. For H_{ext} greater than H_{c_1} the critical current confirms the degree of smoothness of the surface, upon electropolishing the surface becomes rough showing the faces of individual crystalites (Chapter II, Figure II.5) and J_c decreases (sample D to E). On mechanical polishing the surface becomes bright and smooth and J_c again increases (dample E to F). The interesting feature of this process is that above H_{c_1}, J_c is about the same for sample D and F, only significant difference being in the value of H_{c_1} for these two samples (sample D, H_{c_1} = 656 gauss, and sample F, H_{c_1} = 616 gauss). In other words the limitation on J_c is not so much the state of the surface of the sample, but in the crystalline state, or surface impurities state remaining after annealing.

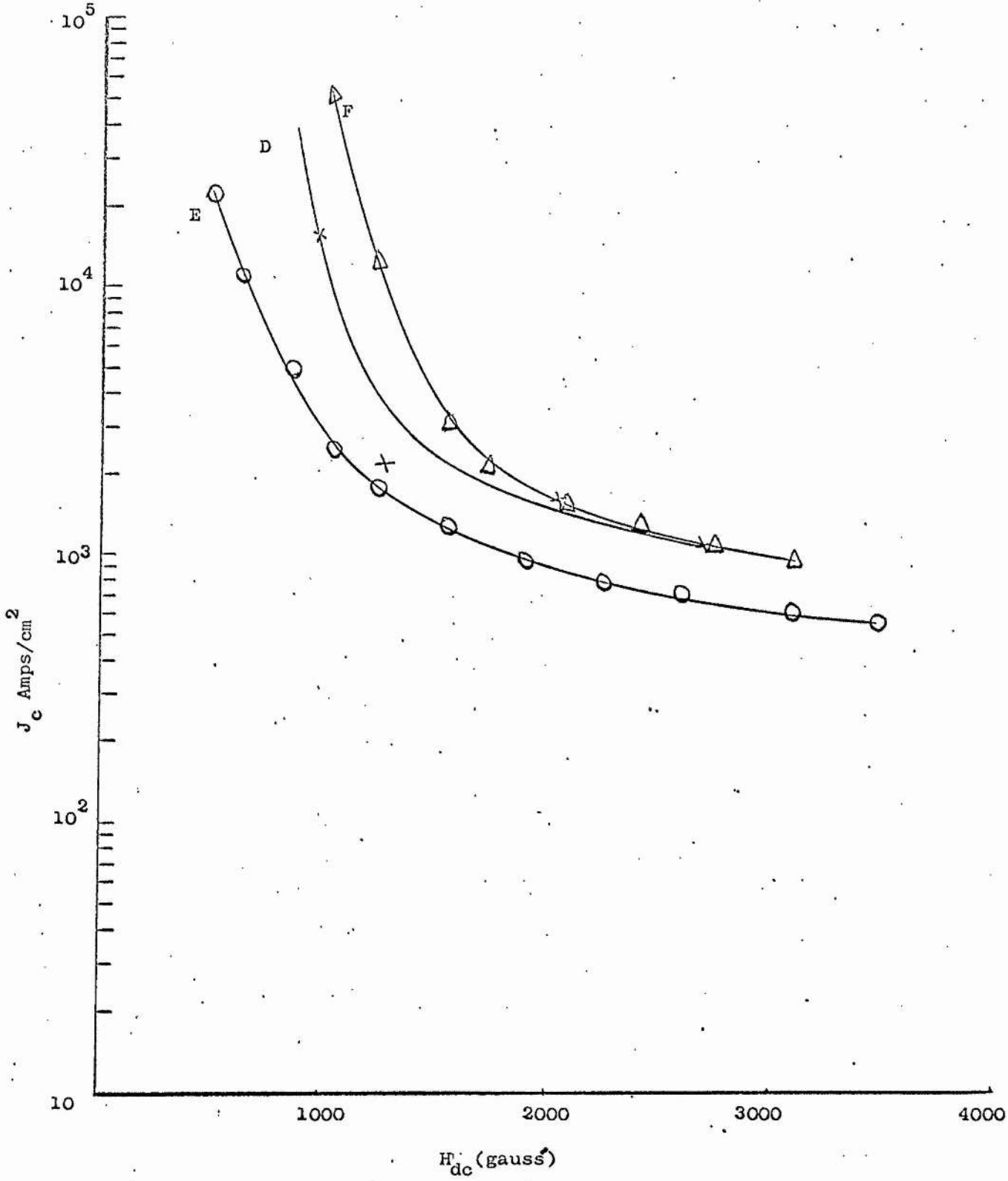

Figure V1.17

The critical current density plotted against the applied magnetic field for polycrystalline Nb.

5. Shielding surface currents ΔH

At an applied magnetic field $H_a > H_{c_1}$ the external magnetic field may change by a certain value ΔH without influencing the bulk flux distribution. The occurance of ΔH has been described in Section V.1.

5.1 ΔH Measurement

The same technique is used to measure ΔH as is used in the measurement of the critical current density. The penetration voltage of the sample, e(t), which is proportional to $\frac{d\phi}{dt}$ is observed on an oscilloscope (Figure V1.18). In the presence of an ac modulating field of peak amplitude h_m flux penetrates the sample whenever the induced surface current exceeds J_c. When decreasing the modulating field h from its peak value h_m, the induced currents drop below J_c so that the flux ϕ within the sample does not change because surface sheath currents screen the bulk of the sample and completely trap flux. For this period of time there is displayed a zero in the penetration voltage as h decreases over the range ΔH, h_m to $h_m - \Delta H$. By measuring the time Δt that a zero is displayed in e(t) the value of the screening field ΔH can be calculated from $\Delta H = h_m (1 - \cos 2 \pi f \Delta t)$. ΔH measured in this way is plotted against the externally applied d.c. field in Figure Vii.19 for the single crystal Nb samples (A,B,C) and in Figure V1.20 for the polycrystalline samples (D,E,F).

5.2 The results

5.2.1 Single crystal niobium

Figure V1.19 shows plot of ΔH versus the external applied magnetic field for a single crystal Nb, with different surface states. Curve A is the shielding surface field for the sample (sample A) as received without surface treatment. Curve B is for the same sample after electropolishing (sample B) where ΔH has decreased below the value for sample A, this is also observed with the critical current density of

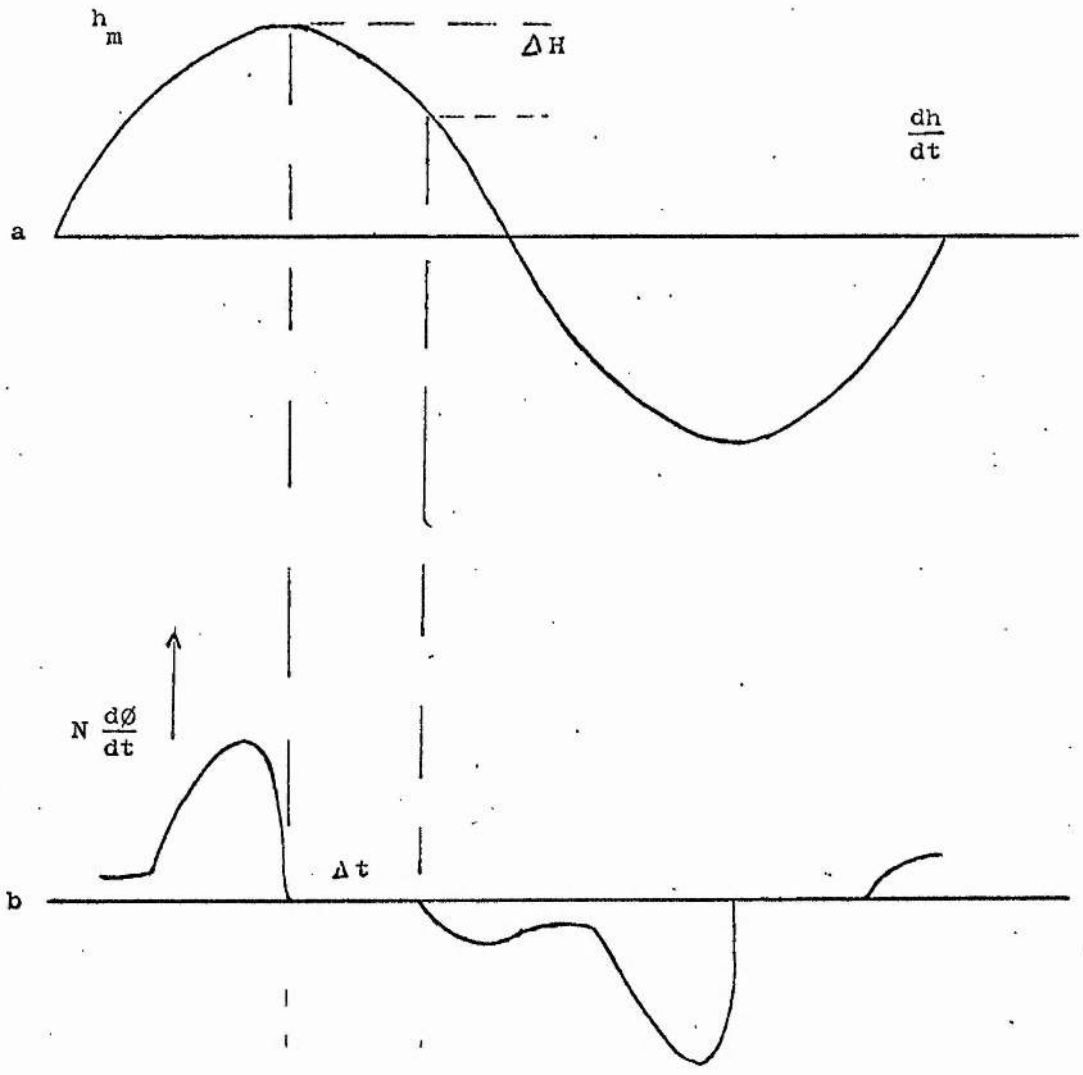

Figure VI.18

(a) The a.c. field of the modulating coil, $h_m \ll H_{ext}$

(b) The penetration coil voltage e(t), which is corresponding to the a.c. field

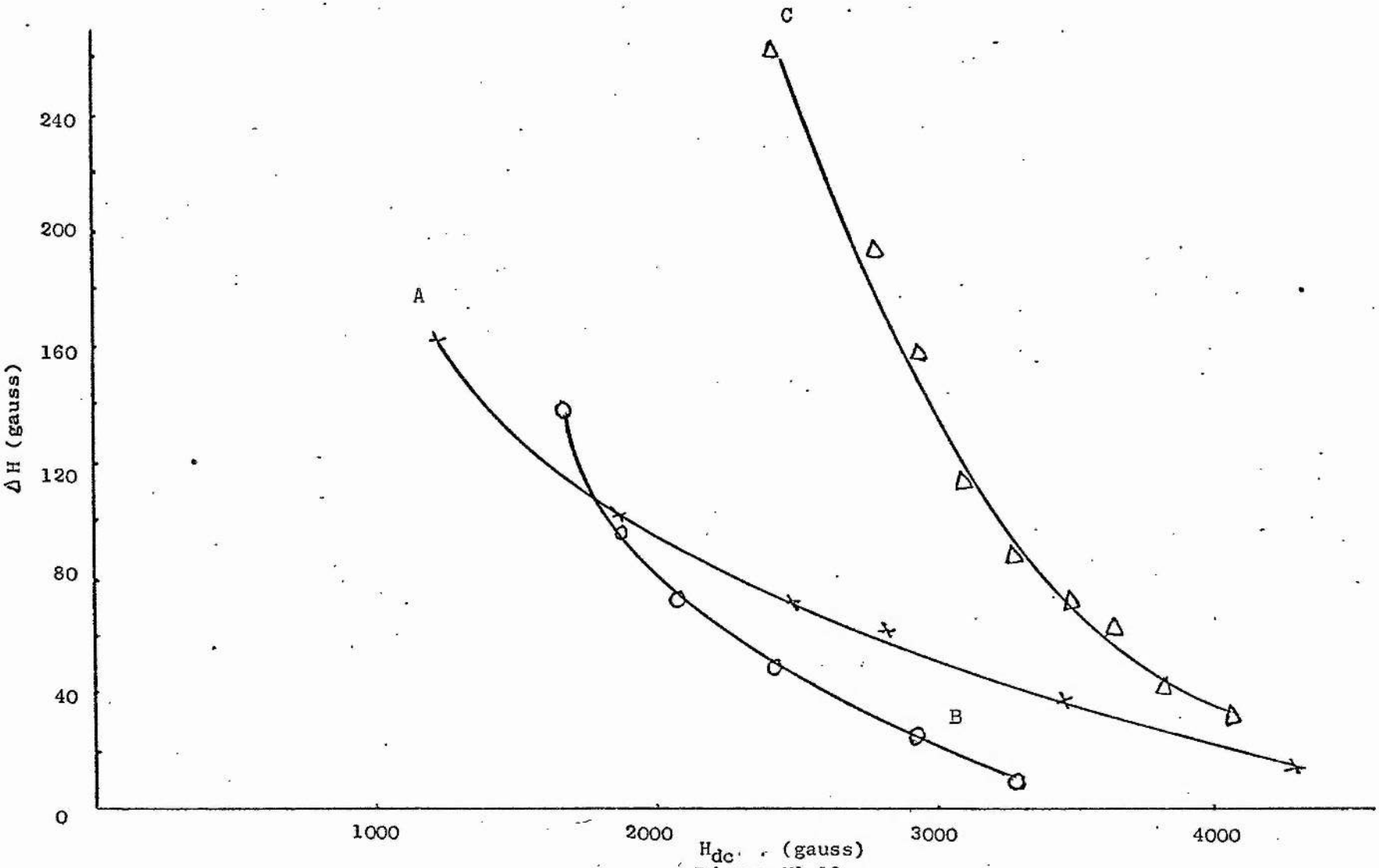

Figure V1.19

The shielding field ΔH plotted against the applied magnetic field, for single crystal niobium.

the same sample. Curve C shows ΔH for sample C where the sample surface has become very smooth so that the shielding surface current increased responding to the surface condition.

5.2.2 Polycrystalline Nb

Figure V1.20 shows ΔH versus the external applied magnetic field for polycrystalline Nb with different surface states. Curve D is for the sample after annealing treatment. Curve E is for the same sample after it has been electropolished where the surface became rough (sample E) because of the exposure of crystalite faces and impurities on the surface; ΔH decreased corresponding to the change in surface. Curve F is for the sample after the surface has been mechanically polished, the surface being very smooth. The shielding surface current is higher than before. We conclude that the surface properties are very important in determining the value of ΔH, where its value increases with the surface smoothness. This has been reported by Ullmaier[43,44].

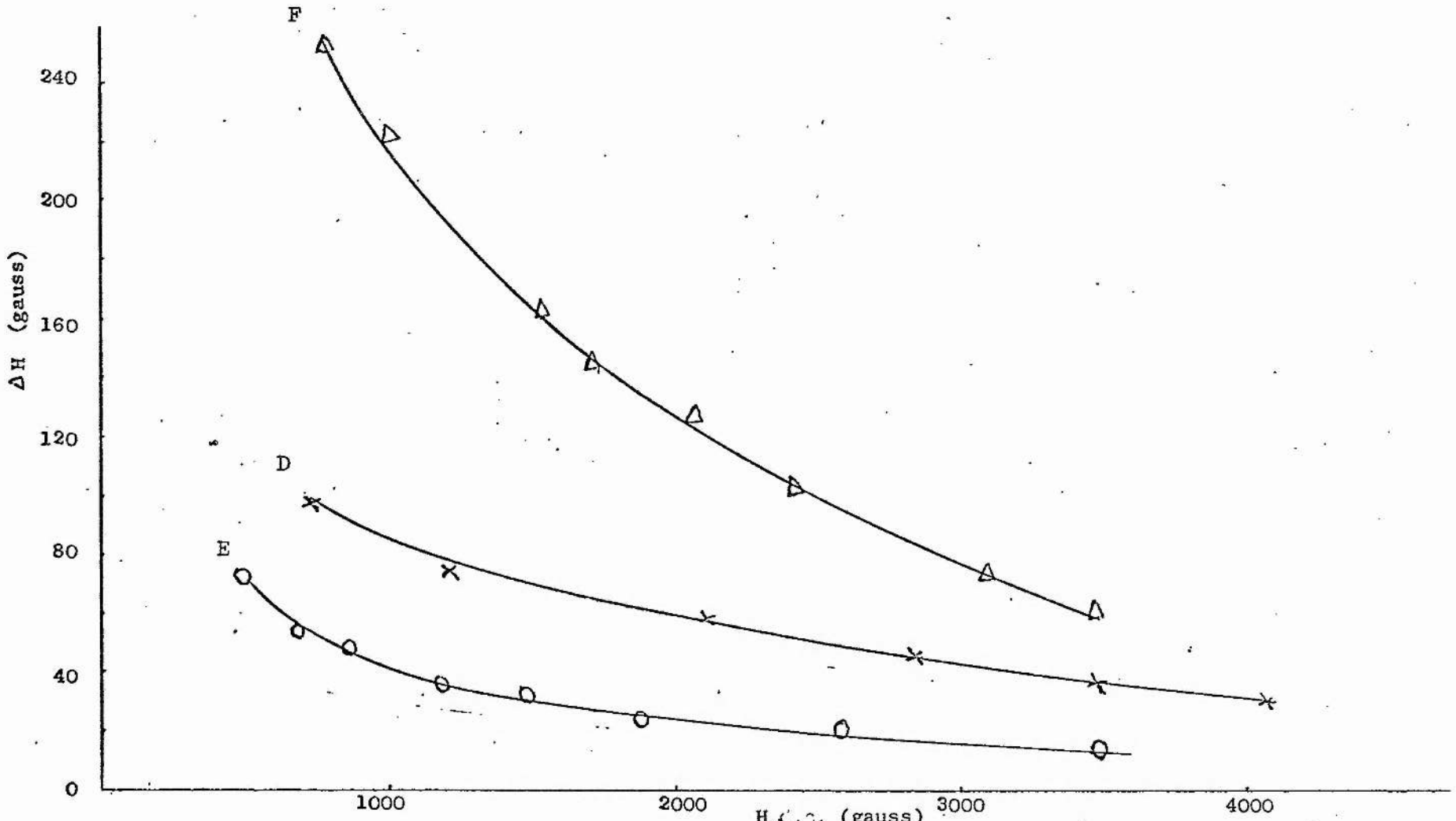

Figure VI.20

The shielding field ΔH plotted against the applied magnetic field, for polycrystalline niobium.

CHAPTER VII

SUMMARY

This study has been done mainly to show the effect of surface conditions on the ac losses in cylindrical rods of niobium.

It has been found that the outgassing treatment in polycrystalline Nb is effective in considerably decreasing the first critical magnetic field H_{c_1}. Electropolishing the surface of this sample has made it rougher. It appears that the electropolishing treatment in both single crystal and polycrystalline Nb adds a new thin surface, which is different from the original surface of the superconducting sample. Mechanical polishing of both samples has removed the roughness left behind by the electropolishing treatment, so that the surfaces of both samples have become very smooth.

It has been shown from our magnetization measurements in Section III that the first critical magnetic field H_{c_1} is greatly influenced by the surface properties and not controlled by pinning of flux vortices in the bulk of the sample. The state of the surface has two different effects; firstly, Bean and Livingston's surface barrier where the surface forms a barrier for moving flux lines, because of an image force and a force depending on the gradient of magnetic field near the surface act on them. A second surface effect is that hysteretic magnetization may be present, caused by induced surface currents and also attributed to flux trapping at surface defects.

The first critical field H_{c_1} observed in both samples with smooth surfaces is higher than than observed in the same samples with rough surfaces. This is in agreement with results found from ac loss measurements Section VI. AC power losses in the niobium samples here

measured with a wattmeter technique gives a higher sensitivity than previously reported. (The minimum detectable loss was 4×10^{-9} w/cm^2/cycle.

The power losses in our samples have been reduced to very low levels by smoothing the surfaces of the samples. The power loss in single crystal niobium with smooth surface is less than that for any of the other samples studied at magnetic field less than 1550 gauss. Surface roughness and trapped flux appear to be the main factors responsible for ac losses.

Losses at small value of the ac magnetic field $H_m \geq H_{c_1}$, where the magnetic field is varying can be explained in terms of flux motion.

Quantitative comparisons between the measured ac losses above H_{c_1} using the wattmeter technique with those calculated from the modified critical state theory has been made. Measured losses for samples with smooth surfaces are higher than rough surfaces of the sample. These results appear contrary with those calculated from the modified critical state theory, but this discrepancy has been resolved by considering also the value of J_c measured.

The critical current density calculated from the power loss in the sample using Bean's formula (Equation V.6) above H_{c_1} which assuming that a thin surface layer has the ability to support a high critical current density is found to give therefore only an estimation of the bulk critical current. This has been altered in our measurements by the surface conditions. Samples with smooth surfaces have higher critical current densities than the same samples with rough surfaces. The shielding surface field ΔH (occuring above H_{c_1}) has been found to be affected in both samples by the surface properties, where the sample with smooth surface has a higher ΔH than the same sample with rough surface.

We conclude that outgassing polycrystalline Nb decreases the pinning centres in the sample which reduces the lower critical magnetic field H_{c_1}, and increases the losses at low applied fields. In this case outgassing

is not advisable for use in superconducting transmission line if a polycrystalline material is used. Electropolishing the samples makes the surfaces rougher particularily in polycrystalline sample. Mechanically polishing is the best method in smoothing the surface of the sample, and is the best surface condition for minimum loss in applied ac fields.

The fact of the matter is that, the superconductors used for transmission of electric power must have lower losses, higher current densities (higher H_{c_1}) and higher working temperature.

Niobium with very smooth surface is the most suitable superconductin element for use as superconducting transmission line, since it can carry larger surface currents, with very little power loss, than any other superconducting element. In superconducting cables there would appear to be no advantage in using superconducting material of thickness greater than can be conveniently handled, since the currents at zero or negligible loss are surface currents.

References

1. Bean C, J.Appl.Phys. 33, 3334 (1962), 36, 31 (1964).
2. London H, Phys.Lett. 6, 162 (1963).
3. Buchhold T, Cryogenics 3, 141 (1963).
4. Beall W.T., and Meyerhoff R.W., J.Appl.Phys., 40, 2052 (1969).
5. Buchhold T and Molenda P.T., Cryogenics 2, 344 (1962).
6. Wisseman W.R., Boutner L.A., and Low F.J.J., J.Appl.Phys., 35, 2649 (1964).
7. Rocher Y.A., and Steptfonds J., Cryogenics 7, 46, 1967.
8. Easson R.M. and Hlawiczka P., Phys.Stat.Sol. K129, 23 (1967).
9. Brankin P.R., and Rhodes R.G., Brit.J.Appl.Phys 2, 1775 (1970)..
10. Male J.C., Cryogenics, 10, 381 (1970).
11. Kamper R., Phys.Lett. 2, 290 (1962).
12. Figgins B.F. and Shepherd T.A., Nature 202, 890 (1964).
13. Hart H.R. and Swartz P.S., Bulletin of the American Physical Society, 9, 252 (1964).
14. Nakyamy Y., and Takano N., Proc. First Cryogenics Engineering Conference 186 (1967).
15. Finnemore D.K., Stromberg T.F., and Swenson C.A., Phys.Rev., 149, 231 (1966).
16. Rogers E.C., Redmonds B.C., and Chan G.D., Cryogenics 9, 431 (1969).
17. Buchhold R.A. and Rhodenizer R.L., IEEE Tran on Mag, 5, 429 (1969).
18. Grigsby R and Slaughter R.J., Bri.J.Appl.Phys. 3, 898 (1970).
19. Easson R.M. and Hlawiczka P., Bri.J.Appl.Physics., 18, 1237 (1967).
20. Tanako N, Proc.First Cryo.Engn.Conf., 184 (1967).
21. Easson R.M., and Hlawiczka P., Phys.Lett., 207, 333 (1966).
22. Linford R.M.F. and Rhodes R.G., J.Appl.Physics.42,10 (1971)
23. Pech T., and Fournet G., Cryogenics 7, 26 (1967).
24. Heinzel W., Phys.Lett. 20, 260 (1966).

25. Jones C.H. and Schenk H.L., Advances in Cryogenic Engineering 579, K-2 (1963).

26. Zar L.J., J.Appl.Phys., 35, 1610 (1964).

27. Rhodes R.G., Rogers E.C. and Siebold R.J., Cryogenics 4, 206 (1964).

28. Grenier, C and Elschner B., Philips Res.Repts 20, 235 (1965).

29. Easson R.M. and Hlawiczka P., Bri.J.Appl.Phys., 18, 1237 (1967).

30. Pech T., Duffot J.P. and Fourent G., Phys.Lett. 16, 201 (1965).

31. Montgomery H., Proc.Roy.Soc. 85, A244 (1958).

32. Hirshfeld A.T., Leupold H.A., and Boorse H.A., Phys.Rev. 127, 1501 (1962); and also Leupold A.T. and Boorse H.A., Phys.Rev., 134, 1322 (1964).

33. Corck W.S. and Garfunkel M.P., Phys.Rev., 98, 1699 (1955).

34. Grasmehr T.W. and Finsi L.A. IEEE Tran. on Mag. 2, 334 (1966).

35. Dammann C., Santamaria E., Maldy J., and Donadieu, L. Phys.Lett 24A, 574 (1967).

36. Rinderer L., Rüferacht J. and Susini A., Phys.Lett. 2, 119, (1962); Hartwig W. Electronics, Page 43, Feb. 22, (1963); Haden C.R., Hartwig W.H., and Victor J.M., IEEE Tran. on Mag. 2, 331 (1966).

37. Meyerhoff R.W., J.Appl.Phys. 40, 2011 (1969).

38. Linford, R.M.F. and Rhodes R.G. Phys.Stat.Sol. K68, 28, (1968).

39. Wipf S.L., Proc. of the 1968 Summer Study on Superconducting Devices and Accelerators, Brookhaven.

40. Love G.R., J.Appl.Phys. 37, 3361 (1966).

41. Ullmaier H.A., Phys.Stat.Sol. 17, 631 (1966).

42. Dunn W.I., and H lawiczka P., .Brit.J.Appl. Phys., 1469, Ser 2, Vol 1 (1968).

43. Ullmaier H.A. and Causter W.F., J.Appl.Phys., 37, 4519 (1966).

44. Ullmaier H.A., Phys.Lett. 21, 507 (1966).

45. Hanox R., PROC IEE, 113, No. 7, 1221 (1966).